

RAILROAD TRACK FASTENING SYSTEM DEMANDS AND RESPONSE:
IMPLICATIONS FOR MECHANISTIC DESIGN

BY

MARCUS SCOTT DERSCH

DISSERTATION

Submitted in partial fulfillment of the requirements
for the degree of Doctor of Philosophy in Civil Engineering
in the Graduate College of the
University of Illinois Urbana-Champaign, 2022

Urbana, Illinois

Doctoral Committee:

Dr. J. Riley Edwards, Chair and Director of Research
Professor Christopher P.L. Barkan, Co-Chair
Professor Erol Tutumluer
Professor John Popovics
Dr. Stephan Freudenstein, Technical University of Munich

ABSTRACT

Rail fastening systems, in conjunction with the crosstie, secure the rail to maintain gauge, transmit thermal and service loads, and anchor the rail-crosstie structure against lateral and longitudinal movements. In doing so, fastening systems must transmit vertical, lateral, and longitudinal loads. Fastening systems have evolved iteratively, through a trial-and-error design approach aimed at addressing conditions symptomatic of track strength and force transfer deficiencies. These deficiencies have led to a variety of track component failures that have, in turn, caused derailments. Many of these failures were a result of an excessive combination of applied vertical, lateral, and longitudinal loads.

Because fastening systems developed using a trial-and-error design process are failing due to force-transfer deficiencies, there is an opportunity to develop and apply the principles of mechanistic-empirical (M-E) analysis and design to fastening systems. Therefore, this dissertation advances the M-E analysis and design of fastening systems through the deployment of field instrumentation, execution of experiments in the laboratory, and development and validation of multiple analytical models.

Deployment of vertical, lateral, and longitudinal wheel-rail load instrumentation in track with a history of broken spikes identified that friction is critical at the plate-crosstie interface and balanced operations have an impact on a component's failure threshold. A novel spike-in-timber 3D analytical model was validated and found a longitudinally applied load is more detrimental than an equivalent magnitude lateral load.

A novel 2D analytical model leveraging beam on elastic foundation (BOEF) principles and a novel 3D fastening system in tie-block model were developed, validated, and used to establish methods to accurately and economically analyze fastening system design variable's effect on

component stress in an effort to reduce spike fatigue failures. The most feasible finding to implement was to develop friction at the plate-tie interface via a vertical plate hold-down force using screw spikes and spring washers. The model and associated laboratory work found that applying 1,000 lb./spike of hold-down force reduced spike stress by 70%.

Finally, a novel 3D nonlinear parametric track model was developed, validated, and used to quantify the effect of various fastening system and track conditions on the longitudinal fastening system load demand. In one example, it was found that when a railroad changes from timber crossties with anchors to elastic fastening systems, the longitudinal rail seat load increases by 24%, due to the direct logarithmic relationship between track stiffness and longitudinal load.

The novel field and laboratory data and validated analytical methods described in this dissertation directly contribute to advancing the M-E analysis and design of railroad fastening systems as they provide direct inputs required for design and methods to quantify component response required for analysis.

ACKNOWLEDGMENTS

I first and foremost acknowledge God the Father, Jesus Christ his son, and the Holy Spirit, who, though powerful enough to create the universe and all that is in it, are relatable enough to know me, and everyone, by name. I thank God for His knowing me, challenging me, and taking me on this amazing journey. I have thoroughly enjoyed learning about railroad fasteners in the preparation of this dissertation and have also enjoyed experiencing God's grace first-hand (Ephesians 2:8,9) and seizing on the amazing opportunities He prepared for me in advance (Ephesians 2:10). I believe that this journey would not have started and would have been tougher to complete, without God and the supporting cast that He blessed me with; the following are only a few of those individuals.

To J. Riley Edwards, saying thank you is not sufficient. God provided you when I was willing to accept less than what He intended. You walked, pushed, and supported me in every aspect of life. I am thankful for you supporting my PhD pursuit while working. I am thankful for your questions that challenge me in work and life. Without your support, belief-in-me, constant-encouragement, questions, and friendship, I can honestly say I would not completing this PhD. Thank you.

To my wife Kristen, I once again must admit that I would not be completing this PhD without your unwavering support. You put up with many nights of me coming to bed late while I studied for classes, prepared for exams, or authored papers. You actively listened to me verbally processing about the challenges I faced with my models or the broken fastening systems I was researching - and for that, I am very thankful. You have supported me emotionally (active listening), physically (providing me with hot tea, water, food, etc. when I needed it), and spiritually (constantly in prayer with and for me) all the while being the best friend I needed, a

mother to our children, and working a full-time job yourself. I pray that obtaining this degree has helped me grow into a more well-rounded husband, friend, father, and engineer and will serve you and our family for years to come.

I know it has been said, but successful and meaningful research cannot be completed by an individual – at least not sustainably. As mentioned above, God has provided me with the right co-worker or student at every step of the way to help me obtain data, prepare figures, or run models. First, I want to thank Yu Qian, who without his encouragement to pursue learning Abaqus on my own, this dissertation would be completely different. Next, I must thank and acknowledge Arthur de Oliveira Lima, who has been an amazing friend in the work-place and has travelled to remote locations (with or without me) to install instrumentation, collect data, and turn sites on. Arthur is always willing to brainstorm with me how to structure a paper, run a test, or collect data. Again, without Arthur, this dissertation would have taken significantly longer to prepare, would have required more sacrificed sleep, or would not have the same chapters – especially Chapter 2.

Many more students have helped me than I can list here. But I must thank Tom Roadcap for providing an amazing “spike-failure” foundation for me to build-upon. Tom’s passion and enthusiasm was contagious, and I loved partnering with him to think about fastening systems – Chapter 1 wouldn’t be possible without him. Thank you to Jae-Yoon Kim for helping me implement the Abaqus code used in multiple Chapters as well as running the models and pulling the data. Without Jae-Yoon, I might still be stuck in Chapter 3, let alone being able to get the data for mitigation methods in Chapter 5! Though these students were critical, I owe even more thanks to Matheus Trizotto. Matheus was an awesome student who challenged me to think about fasteners and longitudinal load transfer in new ways. He stepped up and assisted with an

excellent field experiment on Horseshoe Curve which provided the data for Chapter 2. Matheus was brilliant analytically and was able to build multiple analytical models himself and help me think about the analytical models I present in this dissertation. He not only published his own work but supported the non-linear analytical model in Chapter 6; without him, his conversations, questions, and support, this dissertation would lack the depth required to fulfill the requirements to pass. Last, but not least, I must thank Christian Khachaturian, who walked along side me and helped prepare figures and papers that make up this dissertation – as well as already advancing upon the work that I present in this dissertation.

And finally, I know even with all these amazing people, this work would not be possible without the proper research environment or funding. To Chris Barkan, I say thanks. Chris has assembled an amazing team tackling infrastructure, safety, and systems related railroad engineering challenges. He has encouraged and fostered a team mentality through group lunch meetings and a family atmosphere through weekly happy hours, end-of-semester gatherings and graduation celebrations. He supports all of us to attend and present at conferences and to grow as well-rounded engineers, in part by hosting the William W. Hay Railway Engineering Seminar's that bring in experts from all over the country and world. I also must say thank you to Chris who introduced me to Mr. Dave Connell (retired VP of Engineering from the Union Pacific Railroad) who offered me a summer internship at UP after one of these Hay Seminars which further jump-started my interest in the rail industry. Chris continues to set a high bar for all his students which has significantly impacted me and many others.

Special appreciation goes to Cam Stuart of the Federal Railroad Administration (FRA). There isn't a single chapter that didn't leverage FRA support (e.g. direct funding, data, or resources). Cam challenged my figures and pushed for clearer ways to present the information

contained in the data. I am grateful not only for the funding, but the many meetings we've had over the past four years. I also want to thank Robert Wilson of the FRA for providing additional funds that helped finalize the non-linear analytical model. And finally, thanks to the National University Rail Center (NURail) for providing supplementary funds for the activities presented in this dissertation.

And thank you to my other committee members; for taking time out of your busy schedules to review my documents and to assess and provide feedback on my work. Thanks to my M.S. advisor, Erol Tutumluer, who saw something in me and supported me while I pursued my Masters. Professor Tutumluer has provided timely thoughts and support related to the Mechanistic-Empirical design and analysis approach. Thanks to John Popovics for his consistent encouragement and feedback. Professor Popovics spurred me on as an instructor in my 3rd year of pursuing my undergraduate degree by seeking feedback. The encouragement I continue to receive today reminds me of his consistent character that has been appreciated throughout this process. And finally, but by no means least, thank you to Stephan Freudenstein. I was humbled when Professor Freudenstein agreed to sit on my committee, as I have looked up to him and his knowledge of rail fasteners since I met him in Munich in 2011. I appreciate his willingness to share his experience and provide his expertise as it relates, not just to the content in this dissertation, but also to other railway fastener and crosstie related topics.

Though many in the industry helped me along the way, I want to thank Brad Kerchof who hosted me on field visits, supported field activity, and has continued to be a wealth of information. To the other graduate (e.g. Josue Bastos) and undergraduate students (e.g. Liam Bots) who helped prepare figures, colleagues at Illinois (e.g. Marshall Thompson and David Lange) who provided encouragement and a smiling face, and academic colleagues around the

world (e.g. Ozgur Bezgin, Carmen Sandhaas) who provided insight, asked thoughtful questions, and spurred me on, thank you.

*To the King of the ages, immortal, invisible, the only God, be honor and glory forever and ever.
Amen.*

1 Timothy 1:17

And to my family

Kristen, Kinsie, Madison, and Isaac Dersch

TABLE OF CONTENTS

1	INTRODUCTION	1
1.1	Objective	1
1.2	Background and Motivation.....	1
1.3	Research Methods	6
1.4	Research Scope	7
1.5	Dissertation Organization.....	8
2	QUANTIFICATION OF VERTICAL, LATERAL, AND LONGITUDINAL FASTENER DEMAND IN BROKEN SPIKE TRACK: INPUTS TO MECHANISTIC-EMPIRICAL ANALYSIS AND DESIGN	11
2.1	Motivation	11
2.2	Field Experimentation.....	12
2.3	Instrumentation and Data Collection.....	14
2.4	Data Interpretation.....	17
2.5	Results	21
2.6	Conclusions	37
3	3D FINITE ELEMENT MODELING OF THE EFFECT OF LOAD MAGNITUDE, LOAD DIRECTION, AND TIMBER SPECIES ON SPIKE STRESS	40
3.1	Background	40
3.2	Methodology	42
3.3	Model Properties, Simplifications, and Assumptions	43
3.4	Lateral and Longitudinal Load Magnitudes	48
3.5	Model Validation.....	49
3.6	Results and Discussion.....	51
3.7	Conclusions	56
4	ANALYTICAL METHOD FOR DETERMINING SPIKE STRESS.....	58
4.1	Motivation	58
4.2	Technical Approach	59
4.3	Model Validation, Results, and Discussion	70
4.4	Case Studies	72
4.5	Conclusions	78
5	INVESTIGATION OF METHODS TO MITIGATE RAILWAY SPIKE FATIGUE FAILURES USING FINITE ELEMENT ANALYSIS	81
5.1	Introduction	81

5.2	Methods Theory	82
5.3	Methodology and Model Details.....	89
5.4	Results and Discussion.....	92
5.5	Conclusions	103
6	ANALYTICAL NON-LINEAR MODELING OF RAIL AND FASTENER LONGITUDINAL RESPONSE	105
6.1	Introduction	105
6.2	Previous Models	106
6.3	Model Overview and Validation	113
6.4	Model Application, Results, and Discussion	119
6.5	Conclusions	125
7	CONCLUSIONS.....	127
7.1	Conclusions	128
7.2	Future Research.....	136
	REFERENCES	138

1 INTRODUCTION

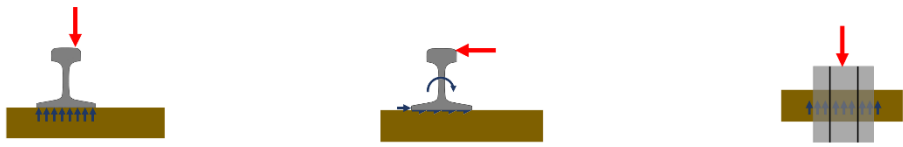
1.1 Objective

The objective of my dissertation is to advance the concept of mechanistic-empirical (M-E) analysis and design of railway track through the quantification of demands placed on track fastening systems and their resulting response. I conducted field experiments and developed and used validated analytical models that leveraged laboratory experimental data. I used these data and methods to relate the fastening system demands to specific failure modes and failure thresholds, thereby contributing to the empirical component of M-E design.

1.2 Background and Motivation

Approximately 94% of railroad track infrastructure worldwide is supported by ballast (Matias and Ferreira, 2020). A ballasted track system consists of the rail, fastening systems, cross-ties, ballast, sub-ballast, and subgrade (Hay, 1982). Rail fastening systems, in conjunction with the cross-tie, secure the rail to maintain gauge, transmit thermal and service loads, and anchor the rail-cross-tie structure against lateral and longitudinal movements (Hay, 1982). In doing so, fastening systems must transmit vertical, lateral, and longitudinal loads. As wheel loads and resulting forces transferred to the track structure have increased, and/or geometric tolerances become more stringent, fastening systems are required to perform more rigorous tasks (maintain tighter tolerances, provide creep resistance, etc.). Table 1.1 provides an overview of fastening system requirements in response to vertical, lateral, and longitudinal forces.

Table 1.1: Requirements of track fastening systems as a function of increasing demands



Increasing track class or tolerance requirement	load			noise & vibration	improved rail		creep resistance
	Crosstie	distribution	attenuation	mitigation	gage restraint	rollover restraint	
Timber		plate			spike & plate		EOTA* or E3TA**
Timber		plate			spike & plate		ETA***
Timber		plate			spike & plate	elastic fastener	elastic fastener
Concrete		pad	pad		elastic fastener	elastic fastener	elastic fastener
Slab		pad	pad	pad	elastic fastener	elastic fastener	elastic fastener

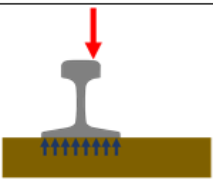
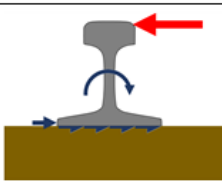
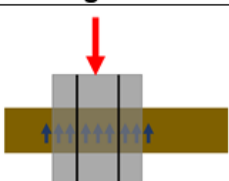
* EOTA is every other tie anchored
 ** E3TA is every third tie anchored
 *** ETA is every tie anchored

As the demands on timber crosstie track increase, so do the number of fastening system components. Timber crossties, plates, and spikes provide sufficient gauge restraint and load distribution when demands are low and creep resistance is less important as is the case with typical track constructed using jointed rail. Use of continuously welded rail (CWR) requires anchors for creep resistance. Higher loading demands, as is the case with sharper curves and higher speeds, commonly require elastic fasteners given their improved rail rollover restraint. When stringent gauge tolerances are required due to loading demands or higher speeds, track strength must be further increased. To provide increased strength, concrete crossties with elastic fasteners or slab track with elastic fasteners are commonly used.

Fastening systems, like many of the components in the rail infrastructure, have evolved iteratively over time, through a trial-and-error design approach aimed at addressing conditions symptomatic of track strength and force transfer deficiencies (e.g. plate cutting, rail seat deterioration (RSD), rail rollover, rail pad movement) (Kerr, 2003a). These deficiencies have

also led to various track component failures (e.g. broken spikes, broken shoulders, broken threaded rods, etc.) that have caused derailments (Choros et al., 2007; Wolf, 2014; Wu and Kerchof, 2014; McHenry and LoPresti, 2015; Edwards et al., 2018a; Roadcap et al., 2019b). Between 1999 and 2018 there were 250 Federal Railroad Administration (FRA) reportable derailments on mainlines and sidings in the United States caused by “defective or missing spikes or rail fasteners” [FRA Rail Equipment Accident or Incident Report (REAIR) 6180.54 database as discussed by Wang et al. (2020)]. Fastening system failure modes can be classified by the different rail loading directions that contribute to failure (Table 1.2).

Table 1.2: Fastening system failure modes and related driving loads

	Vertical	Lateral	Longitudinal
Fastening System Failure Mode			
rail seat deterioration	x	x	x
plate cutting	x	x	x
spike pullout	x	x	
rail rollover		x	
anchor disengagement			x
missing clip			x
broken clip		x	x
plate wear	x	x	x
broken spikes	x	x	x
missing pad	x		x
burnt pad	x	x	x
broken shoulder		x	
broken plate	x		
broken rod		x	x
excessive noise/vibration	x		

Most fastening system failures are not caused by loads acting from a single direction (vertical, lateral, or longitudinal). Instead, failures often result from a combination of these

loads, thus demonstrating a disconnect between the loading demands placed on the track and strength of critical track components. Additionally, as indicated indirectly (Table 1.2), fastener failures are not isolated to a single method of track construction (i.e. ballasted vs. ballastless track), nor can they be solely attributed to rolling stock with the highest wheel loads. Force-transfer fastener failures have been observed in both timber and concrete crosstie track on heavy axle load (HAL) freight railroads as well as ballastless, direct-fixation (DF) track systems (Tutten III and Daniels, 2005; Lima et al., 2021).

Despite recent increases in analytical modelling and laboratory testing of fastening system components, the development and adoption of new fasteners continues to rely heavily on practical experience and monitoring of revenue service field performance. This iterative approach has led to inefficient designs and insufficient understanding of the underlying mechanisms that govern the track system's response to changing conditions (e.g. input loads, component wear, support conditions). At times, this lack of understanding has manifested itself in maintenance and safety problems as is evident from review of track-caused derailment data in the FRA REAIR database.

RSD and plate cutting are examples of failures that have occurred due to inadequate force transfer on different track types (concrete vs. timber crossties) and demonstrate how failures are driven through a combination of load directions. RSD can be caused by multiple mechanisms (Zeman, 2010; Greve et al., 2016) but is driven by abrasion (lateral and longitudinal movement of the rail pad relative to the concrete) (Kernes, 2013; Shurpali et al., 2017). Similarly, plate cutting, is largely driven by the abrasive motion of plates that have insufficient lateral and longitudinal restraint (Kerr, 2003a), though it is exacerbated by vertical loads (e.g. use of smaller plates and/or high pressures) that exceed timber's compressive strength. These examples of

failures point to the critical role of friction in the track fastening system. The importance of friction has been demonstrated in previous finite element (FE) modeling of concrete crosstie track (Chen et al., 2014; Chen et al., 2016; Edwards et al., 2017a).

Recently, there has been increased interest in applying the principles of M-E design to rail infrastructure component and system design. The underlying principles were developed for, and are now used in, the field of pavement design (AASHTO, 2008). Initial suggestions for the application of a M-E design approach in the rail domain were presented by Van Dyk et al. (2013), Csenge et al. (2015), and Edwards et al. (2017b). These were further advanced by Quirós-Orozco (2018) and Edwards (2019), leading to development a proposed framework for mechanistic-empirical design of railway track and its components (Edwards et al., 2021) (Figure 1.1).

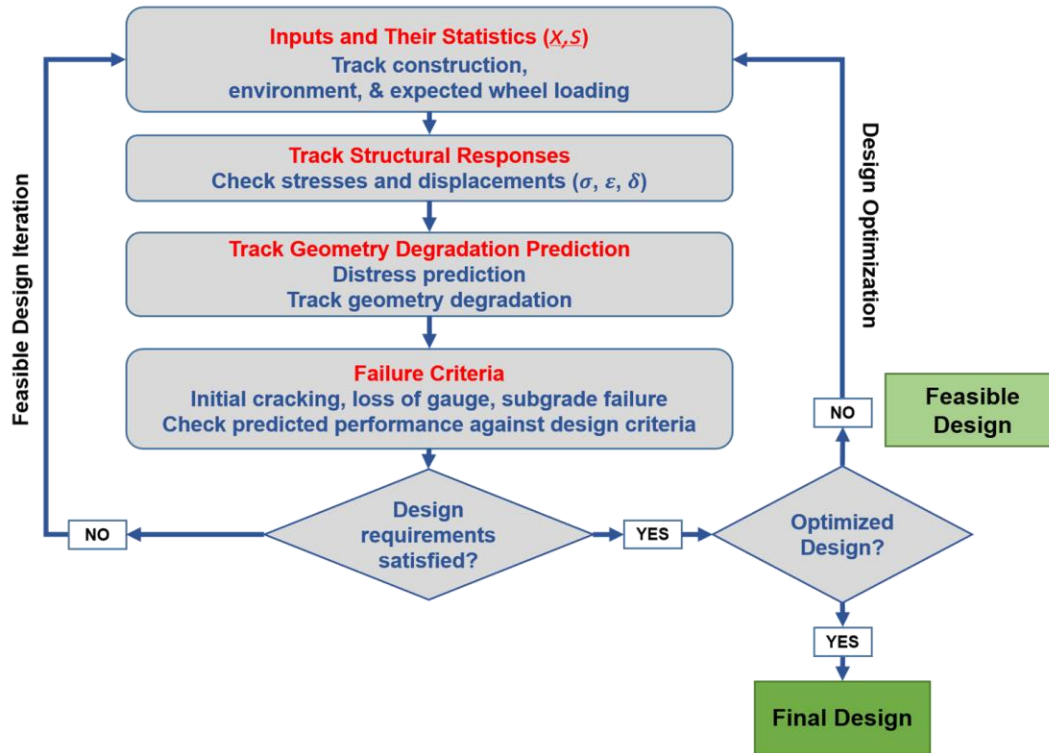


Figure 1.1: Proposed mechanistic-empirical railroad track design procedure (Edwards et al., 2021)

The mechanistic components of this procedure are the quantification of inputs (track construction, loading, etc.) and response (component stress and displacement). The empirical component of M-E design is advanced by establishing relationships between the design inputs and response to failure criteria and degradation rates. My proposed research will advance both the mechanistic and empirical components of the M-E design paradigm as it relates to fastener design, but I will primarily focus on the mechanistic component.

1.3 Research Methods

My research methods included revenue service field experimentation, laboratory experimentation to supplement field data and validate models, and the development and use of validated analytical models. These, in combination with a thorough review of international

literature on this subject, provided the basis for fulfilling the objectives of this research. These methods helped ensure that I achieved the overarching research theme of quantifying fastening system demand and response and development of fastening system M-E design procedures.

1.4 Research Scope

The primary objective of my research was to improve the fundamental understanding of the M-E analysis and design of fastening system components and quantify critical parameters that affect load magnitude and component response (i.e. stress). More specifically, my research answers the following questions:

- What are the magnitudes of the vertical, lateral, and longitudinal fastening system loads in tracks with failed components and how does friction influence load transfer within the fastening system?
- How do lateral and longitudinal loads, timber species, and timber grain direction affect spike stress and the location of maximum stress along the spike?
- Can an analytical model based on beam on elastic foundation (BOEF) principles be developed and validated to provide accurate spike stress values for future use in improved spike design?
- What is the effect of fastening system design parameters (spike cross sectional area, spike type, spike loading location, plate-to-crosstie friction, spike engagement with the plate, and number of spikes) on spike stress magnitude?
- How do track ballast and fastener stiffness and slip affect the magnitude of longitudinal fastener load placed on the fasteners?

My research is applicable to general fastening system design for HAL freight, intercity and high-speed passenger rail, and rail transit operations. Some of the questions are directly related to the failure of broken spikes in elastic fastening systems that have led to at least eleven derailments on HAL freight lines over the past 20 years. Recent research also demonstrated that North American railroads consider these spike failures a moderate to serious safety concern (Roadcap et al., in review). Field interviews and industry surveys indicated that inspection for broken spikes is time and labor intensive requiring experienced personnel to walk track using manual inspection methods. Given that the spike fracture surfaces are below the crosstie surface, the scope of inspections and their resulting accuracy is limited.

1.5 Dissertation Organization

I begin my dissertation with an introductory chapter, in which I present background information, review previous research findings, and demonstrate the relevance of my proposed research theme. The introduction is followed by five body chapters, each one dedicated to one of the questions posed in Section 1.4. I conclude my dissertation with a discussion of the principal findings and future research needs. A short summary description of each of the five body chapters follows.

In Chapter 2 I present vertical, lateral, and longitudinal rail seat load data from revenue service field testing conducted at a demanding field location that has experienced numerous spike fatigue failures. Instrumentation was deployed on the high and low rails of two tracks. The high rail of the track carrying empty trains experienced the most spike failures. This chapter also documents the role of vertical rail seat loads and friction on the threshold for spike-fatigue

failures. This chapter advances the M-E analysis and design approach by describing and quantifying the input loads fastening systems must withstand under high-demand circumstances.

In Chapter 3 I describe the development, validation, and use of a 3D finite element model (FEM), of a single spike installed in a timber block. This chapter also documents the effect of timber grain (parallel or perpendicular to grain), load magnitude, and timber species on the magnitude and location of maximum spike stress. This chapter advances the M-E analysis and design approach by documenting the component response in relation to common variables (timber species, load magnitude, etc.).

In Chapter 4 I present the development, validation, and use of an analytical approach for spike-stress estimation based on BOEF theory. This chapter documents the effect of spike cross-sectional area, timber type, and applied load magnitude on the maximum spike stress and relates these data to the spike's endurance limit to predict possible fatigue failures. This chapter advances the M-E analysis and design approach by presenting a computationally economic and accurate tool to investigate the effect of critical design variables on component response.

In Chapter 5 I describe further enhancement of the validated 3D FEM developed in Chapter 3. This chapter documents the use of the model to quantify the effect of important fastening system variables (e.g. spike type, number of spikes, and plate-to-crosstie friction) on spike stress. This chapter advances the M-E analysis and design approach by providing spike response data and providing an analytical tool that can be used to investigate the effect of a variety of input variables on fastening system response.

In Chapter 6 I present the development, validation, and use of a FEM of the complete track structure. This novel 3D track model builds upon prior approaches found in the literature by leveraging bi-linear springs at the ballast – crosstie and crosstie – fastener interfaces and

quantifies the effect of important variables (e.g. ballast and fastener stiffness and slip limits) on fastener loads. This chapter advances the M-E analysis and design approach by describing and quantifying the input loads fastening systems must withstand in various track configurations.

In Chapter 7 I summarize the conclusions from my research, its contributions and introduce ideas for future research.

2 QUANTIFICATION OF VERTICAL, LATERAL, AND LONGITUDINAL FASTENER DEMAND IN BROKEN SPIKE TRACK: INPUTS TO MECHANISTIC-EMPIRICAL ANALYSIS AND DESIGN

In this chapter I describe the design and execution of revenue-service field tests on a major Class I railroad mainline that characterized the loading environment for curved track that had experienced many spike-fatigue failures. The tests were designed to quantify the vertical, lateral, and longitudinal rail seat loads and the role of friction in fastener failures. A paper related to this chapter was published in the *Journal of Rail and Rapid Transit (JRRT)*¹ in 2021.

2.1 Motivation

Fastening systems developed using a trial-and-error design process are failing due to force-transfer deficiencies. This challenge presents an opportunity to develop and apply the principles of mechanistic-empirical (M-E) analysis and design to fastening systems. One of the first steps in the proposed M-E approach is to quantify system inputs such as type of track construction (e.g. track components, ballast health, etc.), substructure depths, loading environment, and other factors.

Recent research has focused on quantifying vertical and lateral wheel loads on heavy axle load (HAL) freight, intercity passenger, and rail transit infrastructure (Van Dyk, 2014; Van Dyk et al., 2014; Lin et al., 2018; Edwards et al., 2018b; Quirós-Orozco et al., 2018). Additionally, there has been significant research focused on development of analytical models describing the track's ability to distribute vertical wheel loads (Eisenmann, 1970; Hay, 1982; Kerr, 2003b; Hasan, 2015), and to a lesser extent the distribution of lateral loads (Shenton III, 1997; Kerr,

¹ Dersch, M., M. Trizotto Silva, J.R. Edwards and A. de O. Lima. 2021. Quantification of vertical, lateral, and longitudinal fastener demand in broken spike track: Inputs to mechanistic-empirical design. *Proceedings of the Institution of Mechanical Engineers, Part F: Journal of Rail and Rapid Transit*. DOI 10.1177/09544097211030736

2003b; Kish, 2011; Williams et al., 2016; Deshimaru et al., 2017; Holder et al., 2017a; Holder et al., 2017b). Finally, while longitudinal forces and displacements have been quantified (Kish and Samavedam, 1987; El-Sibaie and Anderson, 1994; Harrison et al., 1999; Otter et al., 2001; Kerokoski, 2010; Ahmad et al., 2011; Bose et al., 2018), most studies have focused on quantifying absolute forces on bridge structures or inputs to rail neutral temperature (RNT) models but not transient loads on fastening systems or rail seats due to passing trains.

Although the vertical wheel-rail interface load may be a sufficient input for the analysis of the overall track structure (e.g. subgrade pressure, ballast depth, etc.), when determining the stresses and/or displacements of fastening system components, it is important to quantify rail seat loads. While methods and models exist to estimate the distribution of the vertical wheel load to the rail seats (Talbot, 1918; Kerr, 2003b), there are few methods to quantify the magnitude and distribution of lateral and longitudinal rail seat loads.

Instrumentation was deployed on a North American HAL freight railroad mainline to collect data to quantify the vertical, lateral, and longitudinal loading demands. These data address the problem of failed spikes in premium elastic fastening systems and contribute to the M-E design foundation for future fastening system components. Loading data are unavailable in track locations that have experienced fastening system failures further revealing the need to quantify the loading environment in the field before pursuing fastener design changes.

2.2 Field Experimentation

Instrumentation was installed and revenue service data were collected on Tracks 1 and 3 within the full body of a 9.2 degree (623 ft (190 m) radius) curve on a 1.76% grade on Norfolk Southern's (NS) Pittsburgh Line near Altoona, PA. The curve has three ballasted tracks

constructed using timber cross-ties and elastic fasteners with cut spikes. A visual walking-inspection identified one broken spike prior to installation of instrumentation and tracks that appeared to be in a state-of-good-repair with properly-maintained cross-tie support and track components. Figure 2.1 shows an overview of the field site, primary directions of traffic, generalized (expected) loading (empty vs. loaded trains), and other relevant site information as well as the specific instrumentation deployed.

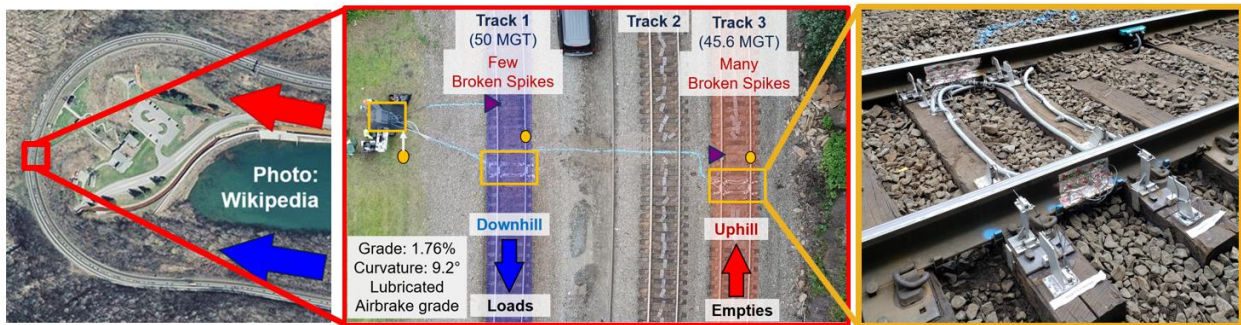


Figure 2.1: Aerial views of HAL field site with relevant track geometry and operations information (left and middle) and completed instrumentation on Track 3 (right)

HAL freight and Amtrak intercity passenger trains operate on all three tracks, but traffic direction and train type composition vary. Tracks 1 and 2 are primarily used by loaded freight trains operating downgrade (railroad east) while empty trains primarily operate upgrade (railroad west) on Track 3. Though tracks 1 and 3 each accumulate approximately 50 MGT annually, spike-fatigue failures primarily occur on the high rail of Track 3 (Roadcap et al., in review; Roadcap et al., 2019a).

This field site was selected because it provided an opportunity to quantify the forces on each track while controlling for other differences in track geometry (e.g. grade, superelevation,

and curvature), climate, and weather. This facilitated isolation of the variables and their magnitudes that led to increased spike failures on Track 3.

2.3 Instrumentation and Data Collection

Instrumentation was installed on the high and low rails of Tracks 1 and 3 (Figure 2.1). Surface strain gauges were installed on the rail using, industry-standard circuits as described by Harrison et al. (1999) and Edwards et al. (2017a). These gauges were subsequently calibrated using a loading frame, relating strains to vertical, lateral, and longitudinal wheel-rail loads. Additional instrumentation (Figure 2.1) was deployed as a part of broader research program that included quantifying displacements. Data analysis followed industry best practices and is described in more detail in the following sub-sections.

2.3.1 Vertical and Lateral Load Circuits

Using the vertical load circuit, the voltages captured under passing wheels were transformed into vertical wheel forces using the calibration factors that were previously obtained. Next, peaks in the data were identified, extracted, and compared to on-site data from a commercially available RSR110 wheel sensor manufactured by Frauscher, to ensure all peaks (wheels) were identified. Train speeds were estimated using the time between peaks and known locomotive axle spacing. To align with industry best practices, the maximum lateral load was quantified as the output from the lateral load circuit at the same timestamp as the application of maximum vertical wheel load. This is important because the lateral load signals are less consistent than vertical load signals and are most reliably quantified when the wheel is directly over the center of the crib. Lateral forces were considered positive or negative when acting in the direction of the field or gauge,

respectively. An example distance and time history of vertical and lateral load signals (Figure 2.2) demonstrates the cleanliness of the data recorded.

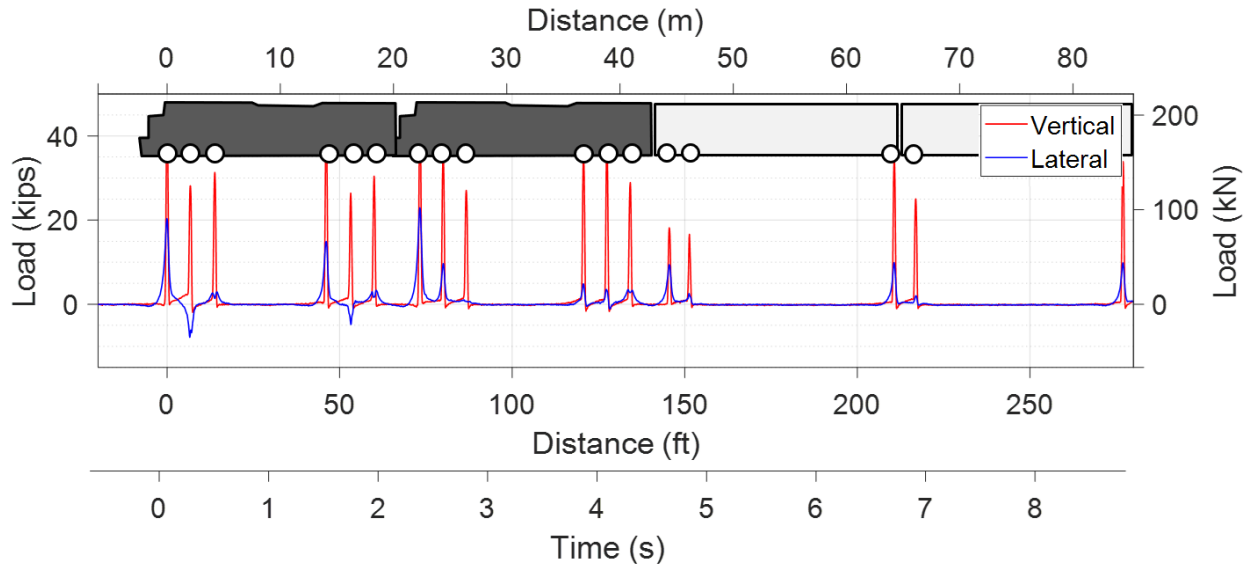


Figure 2.2: Example time, space history of vertical and lateral wheel loads

2.3.2 Longitudinal Circuits

Longitudinal rail forces were quantified using a circuit proposed by Harrison et al. (1999) that includes gauges on both sides of the web of the rail at the neutral axis. To quantify the longitudinal rail force, the strains from the circuit are multiplied by the Young's modulus and cross-sectional area of the rail. This method does not allow for the identification of absolute rail axial loads since RNT is unknown but does facilitate the quantification of changes in rail load over time due to temperature changes and passing trains. The longitudinal load circuit does not show peaks for each wheel in the same way as the vertical and lateral circuits and requires additional insight to correctly interpret the results. Specifically, longitudinal strain from the bending of the rail under vertical and lateral loads overpower longitudinal strains under wheels,

making readings inaccurate at those locations. Nevertheless, the theory leads me to believe the method produces accurate measurements before the train's arrival, between the lead and trailing trucks of each railcar, and after the passage of the train. Longitudinal rail loads were taken at approximately 10-20 ft (3-6 m) in advance of the first wheel. To compensate for the offset, the measured rail loads are increased using an exponential function described by Kerr (2003b) for a single wheel and more recently confirmed by Trizotto, et al. (2021) for multiple wheels. The superposition of multiple wheels was demonstrated to generate a median longitudinal load increase of 16%. Finally, results indicated that the longitudinal influence zone is significantly longer than what is observed from vertical and lateral load circuits (i.e. greater than 100 ft (30.5 m) as compared to approximately 10 ft (3.05 m)) (Figure 2.3).

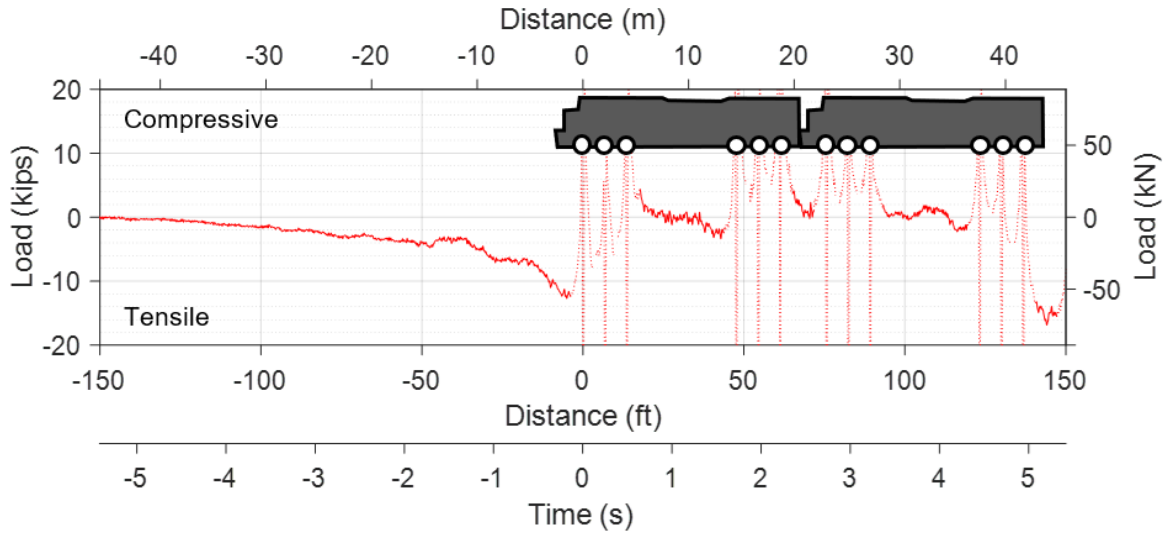


Figure 2.3: Example space history of longitudinal rail axial loads

2.4 Data Interpretation

A variety of methods were employed to quantify the demands placed on the rail seats using wheel-rail forces obtained via the rail-mounted strain gauge circuits. The following sub-sections detail the methods and assumptions used to transform the wheel-rail interface force data to rail seat loading data.

2.4.1 Vertical and Lateral Rail Seat Loads

Analytical techniques relying on beam on elastic foundation (BOEF) fundamentals have been developed by Winkler (1867), Talbot (1918), and Zimmerman (1941) to quantify vertical load distribution from multiple wheels to the supporting rail seats. Winkler initially proposed a method based on BOEF theory that the reaction at longitudinal supports (i.e each crosstie rail seat) was proportional to rail deflection. Talbot and Zimmerman advanced this theory and validated its approach by comparing analytical results to field data (Talbot, 1918; Zimmermann, 1941). While additional research on this topic has been conducted, this BOEF method has been

widely accepted since the 1940s (Kerr, 2003b), and is considered accurate for quantifying vertical rail seat forces. Therefore, applying BOEF theory and assuming the following: timber crosstie track modulus of 3,500 lb./in./in. (24,270 kN/m/m), crosstie spacing of 19.5 in. (49.5 cm), axle spacing of 81.5 in. (207 cm), 136 RE rail (approximately UIC 60), and 36 in. (91 cm) wheel diameters, and superposition of adjacent wheels, the rail seat load would be 26% of the wheel load.

Vertical rail loads are influenced by multiple variables (e.g. speed of the train (Van Dyk et al., 2017), track modulus (Van Dyk et al., 2016), and wheel health). In this chapter, the applied vertical rail loads are quantified by the instrumentation on the rail that accounts for these effects. Rail seat loads are also influenced by multiple variables (e.g. crosstie type, fastening system type, and crosstie support). Extensive field inspections confirm that spike failures are not isolated to poorly supported crossties. During one field inspection, up to 10 crossties in a row were found to have failed spikes. In another instance, 121 failed cut spikes were identified in a span of 150 crossties on the high rail of a single curve (i.e. 20% of potential spikes)). Given that crossties and most of the fastening systems at the instrumented field site appeared to be in good health, I assumed uniform support of the crossties at this location. Thus, the relationship between the wheel-rail interface loads and rail seats loads was assumed to be a fixed value.

Compared to vertical loads, there has been relatively little research assessing the distribution of lateral loads to the fastening system. The limited field observations and laboratory studies conducted to date have consistently indicated that lateral loads are distributed over fewer crossties than vertical loads (AREMA, 2017b), thereby increasing the maximum force transferred to the center crosstie's rail seat. More specifically, studies on concrete crossties have found that lateral rail seat loads range between 35% and 60% of the applied wheel load

(Williams et al., 2016; Holder et al., 2017a). Given that timber crossties are less stiff than concrete crossties, although this is partially offset through use of premium fastening systems, 35% lateral load transfer to the center crosstie was assumed in this study.

2.4.2 Longitudinal Rail Seat Loads

Although the magnitude and distribution of longitudinal rail loads has been studied with respect to RNT, no research has quantified their distribution to the rail seats. Kerr (2003b) used analytical modeling to describe longitudinal rail load and displacement due to a single longitudinal wheel load. This model uses a bar resting on a longitudinally elastic foundation, analogous to the BOEF method used for vertical load distribution. More elaborate, nonlinear finite element (FE) models have been developed (Cho et al., 2020) and are available in commercial software (Icke and Paice, 2014). Despite these advancements, quantification of rail seat load distribution and its demands on fastening system components has not been undertaken.

Kerr's (2003b) analytical method has been expanded by Trizotto et al. (2021). This method enables the quantification of longitudinal rail seat loads by assuming they are proportional to longitudinal rail displacement (Equation 2.1) and no slip occurs at the rail-fastener interface. A parametric study identified the effect of the superposition of multiple wheel loads and of varying track stiffness. Findings from the study indicate that, in the elastic region, higher track stiffness (combined ballast and fastener stiffness) reduces the range of distribution of fastener and rail loads but increases individual fastener loads. Moreover, the effect of superposition was found to be substantial when multiple wheels were present. Regardless, increasing track stiffness resulted in increased maximum fastener loading and reduced rail

longitudinal loading. The approach developed by Trizotto et al. (2021) was used to quantify the rail seat loads in this study.

$$\underbrace{u(x) = \frac{R}{2\kappa EA} e^{-\kappa|x|}}_{\text{Rail Displacement}} \rightarrow \underbrace{F_r(x) = \frac{k_a}{2} u_r(x) = \frac{\kappa R}{2} e^{-\kappa|x|}}_{\text{Fastener Force per Unit Length}} \text{ with } \kappa^2 = \frac{k_a/2}{EA} \quad \text{Eq. 2.1}$$

where,

x is the location, in relation to the wheel load.

$u(x)$ is the rail section displacement at location x .

$F_r(x)$ is the fastener force per unit length at location x .

R is the longitudinal wheel load, per rail.

$k_a/2$ is the longitudinal track stiffness, per rail.

E is the Young's modulus of the rail.

A is the cross-sectional area of the rail.

Longitudinal track stiffness varies due to variation in ballast condition, crosstie type, fastening system, and magnitude of vertical loads (Van, 1997). Since the longitudinal stiffness of the tracks studied is unknown, a representative (and conservative) stiffness of 3,000 lb./in./in. (20,800 kN/m/m) was selected for both tracks. This value is comparable to measured longitudinal stiffness of vertically-loaded ballasted track sections (Kerokoski, 2010) and is expected to bound actual field conditions. Further, Trizotto et al. (2021) found that while there is a direct non-linear relationship between longitudinal track modulus and fastener loads, a quadrupling of modulus was required for a 30% increase in fastener load. Therefore, it is

reasonable to assume that any small changes in longitudinal track modulus will have a small effect on the longitudinal fastener loads.

The method used in this chapter involves estimating the rail and fastener load distribution for the assumed longitudinal track stiffness, uniform wheel loads, and approximate wheel configuration for each train. It considers lead locomotives for both uphill and downhill trains and additional cars following the locomotives for downhill trains (to simulate the contribution of all braking axles). I assumed that loads are in the elastic region, so these distributions are linearly proportional to the applied wheel loads. Therefore, the distributions were scaled to match the rail longitudinal loads at the first passing wheel and the maximum rail seat load was recorded.

2.5 Results

The following sub-sections document the vertical, lateral, and longitudinal wheel-rail and fastener forces and the role they play in spike fatigue failures. Data were recorded on both tracks for a period of nine days. Over 50 trains were recorded on each track during this period. Only freight trains were considered in the analysis. Due to the directionality of traffic a comparison was made between trains on Track 1 going downhill and trains on Track 3 going uphill; representing the dominant directions for traffic.

The trains operated at median speeds of 18 and 17 mph (29 and 27 kph) on Tracks 1 and 3, respectively (Figure 2.4). The balance speed for both tracks was calculated to be 25.5 mph (41 kph) given the design superelevation was 4" (10.2 cm) and curvature was 9.2 degree (623 ft (190 m)). Therefore, most trains were operating below balance speed. Furthermore, over this

range of speeds, the impact on dynamic loading would be minimal as shown by Sadeghi (2010) and Van Dyk (2017).

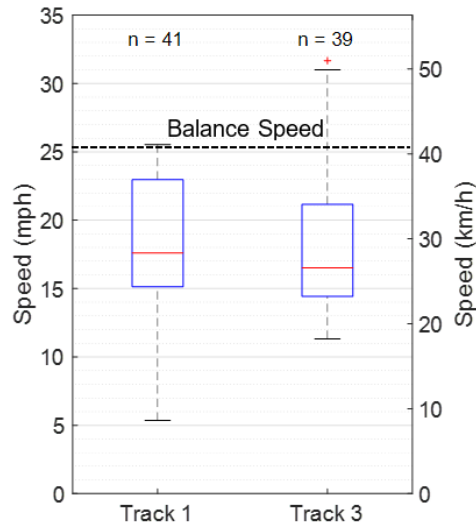


Figure 2.4: Box-plot of measured train speeds on Tracks 1 and 3 in July 2019

2.5.1 Vertical Loading

I used the methods described in Section 2.4.1 to quantify the vertical rail loads and corresponding rail seat loads (Figure 2.5). As expected, the vertical demands on Track 1 were greater than Track 3. Median vertical rail seat loads were 7.5 and 7.8 kips (33.4 and 34.7 kN) (high and low rails, respectively) on Track 1 and 2.8 and 4.3 kips (12.5 and 19.1 kN) (high and low rails, respectively) on Track 3.

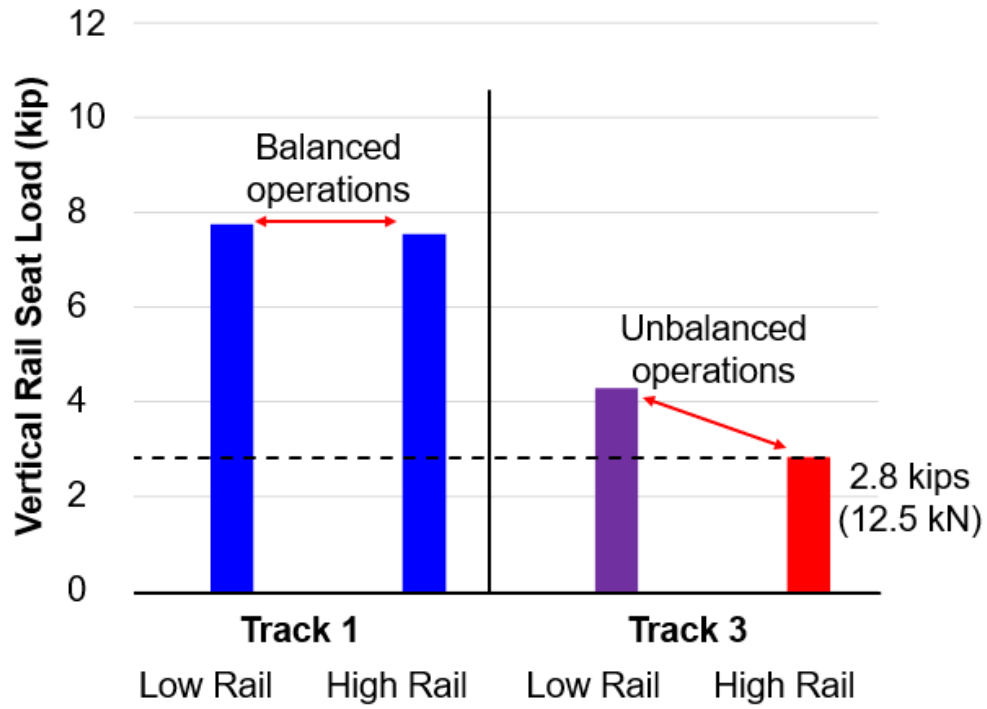


Figure 2.5: 50th percentile vertical rail seat loads for both tracks

Analysis of the complete field dataset (Figures 2.6 and 2.7 and Tables 2.1 and 2.2) indicates a convergence of vertical loading between both rails on Track 1 and the low rail of Track 3 at higher percentiles (i.e. greater than 90%).

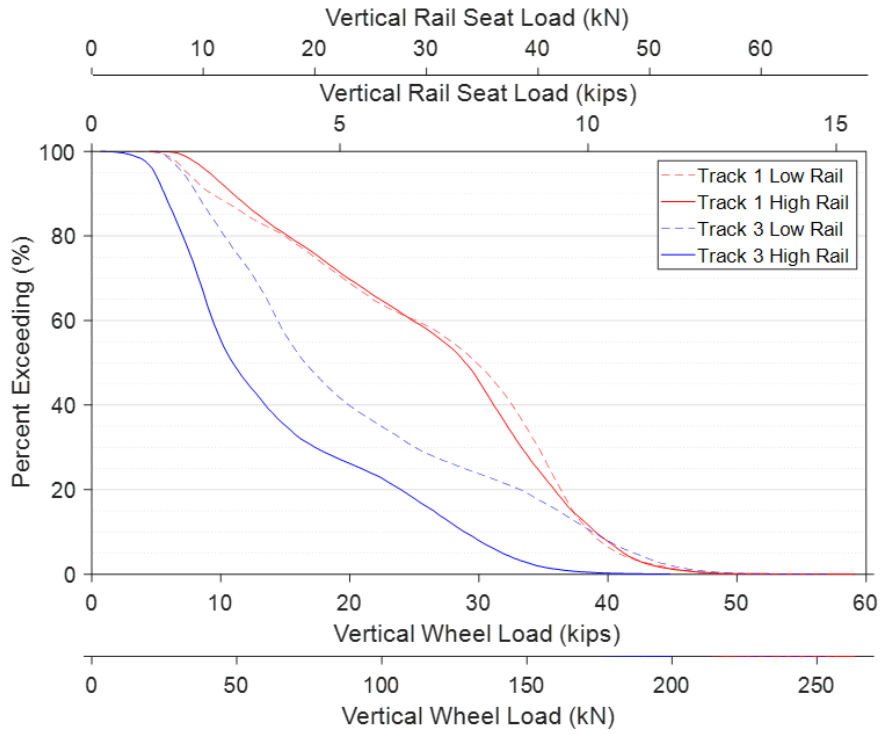


Figure 2.6: Vertical wheel and rail seat load percent exceedance for both high and low rails of both tracks

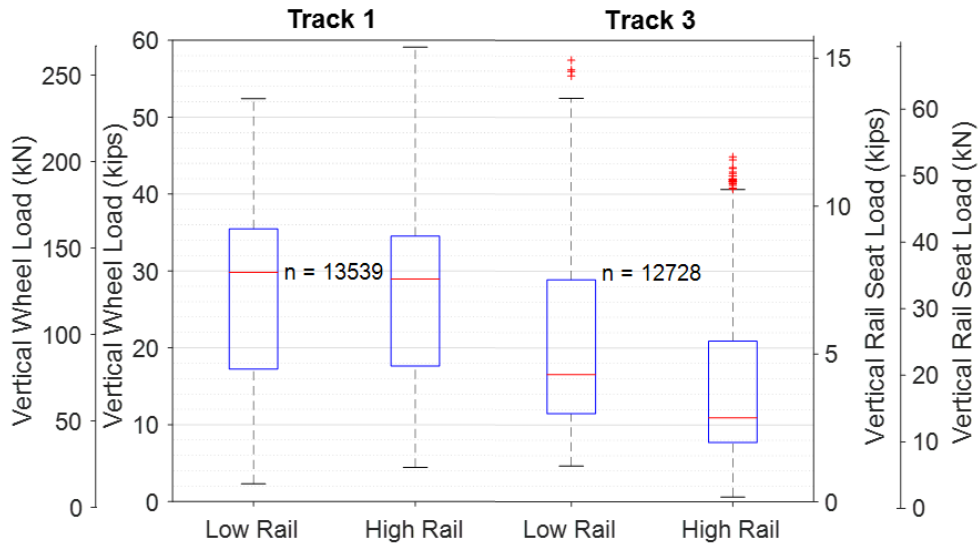


Figure 2.7: Vertical wheel and rail seat load box plots for both high and low rails of both tracks

Table 2.1: Vertical wheel loads at select percentiles for high and low rails of both tracks

Vertical Wheel Load - kips (kN)				
%	Track 1		Track 3	
	Low Rail	High Rail	Low Rail	High Rail
99	45.9 (204)	45.5 (202)	46.7 (208)	36.4 (162)
95	40.8 (181)	41.2 (183)	42.0 (187)	31.8 (142)
90	38.6 (172)	39.0 (174)	38.8 (173)	28.9 (128)
50	29.8 (133)	29.0 (129)	16.5 (74)	10.9 (49)

Table 2.2: Vertical rail seat loads at select percentiles for high and low rails of both tracks

Vertical Rail Seat Load* - kips (kN)				
%	Track 1		Track 3	
	Low Rail	High Rail	Low Rail	High Rail
99	11.9 (53)	11.8 (53)	12.1 (54)	9.5 (42)
95	10.6 (47)	10.7 (48)	10.9 (49)	8.3 (37)
90	10.0 (45)	10.1 (45)	10.1 (45)	7.5 (33)
50	7.8 (34)	7.5 (33)	4.3 (19)	2.8 (13)

This convergence of loads on the low rail of Track 3 is a result of the locomotives and railcars on occasional loaded trains. The data also show a consistently lower vertical loading on the high rail of Track 3. This imbalance in loads between the high and low rails is consistent with operations below balanced speed (Dick and Ruppert Jr., 2019). Underbalanced operations on Track 3 lead to lower vertical rail seat loads (median value of 2.8 kips (13 kN)) on the high rail, and a corresponding reduction in frictional capacity at the tie-plate-to-cross-tie interface. This reduction in frictional capacity plays a role in the increased number of spike failures given lower longitudinal or lateral loads would be required to exceed the frictional resistance and thus greater loads would be transferred to the spikes. This, in turn, would lead to an increase in spike stress.

2.5.2 Lateral Loading and L/V Ratios

I then used the methods described in Section 2.4.1 to quantify the lateral rail loads and corresponding rail seat loads (Figure 2.8 and 2.9 and Table 2.3 and 2.4). As expected, the lateral demands on Track 1 are significantly greater than Track 3. Median lateral rail seat loads were 1.61 and 1.98 kips (7.2 and 8.8 kN, respectively) (high and low rails, respectively) on Track 1 and 0.11 and 0.53 kips (0.5 and 2.5 kN, respectively) (high and low rails, respectively) on Track 3. Therefore, the high and low rails of Track 1 are subjected to 1.50 and 1.45 kips (6.7 and 6.5 kN, respectively) more lateral force than Track 3, respectively. However, the high rail of Track 3 is an outlier in that loads generated from trailing axles are most often oriented inward toward the track centerline as opposed to the more common outward loading direction toward the field. Therefore, it is the only rail that would regularly be subjected to reverse lateral loads (i.e. alternating field and gauge facing). This reversal of load would lead to increased movement of the fastening system and greater fastener component stress ranges. Additionally, when considering fatigue, load reversals lead to a decrease in fatigue life (Norton, 2006).

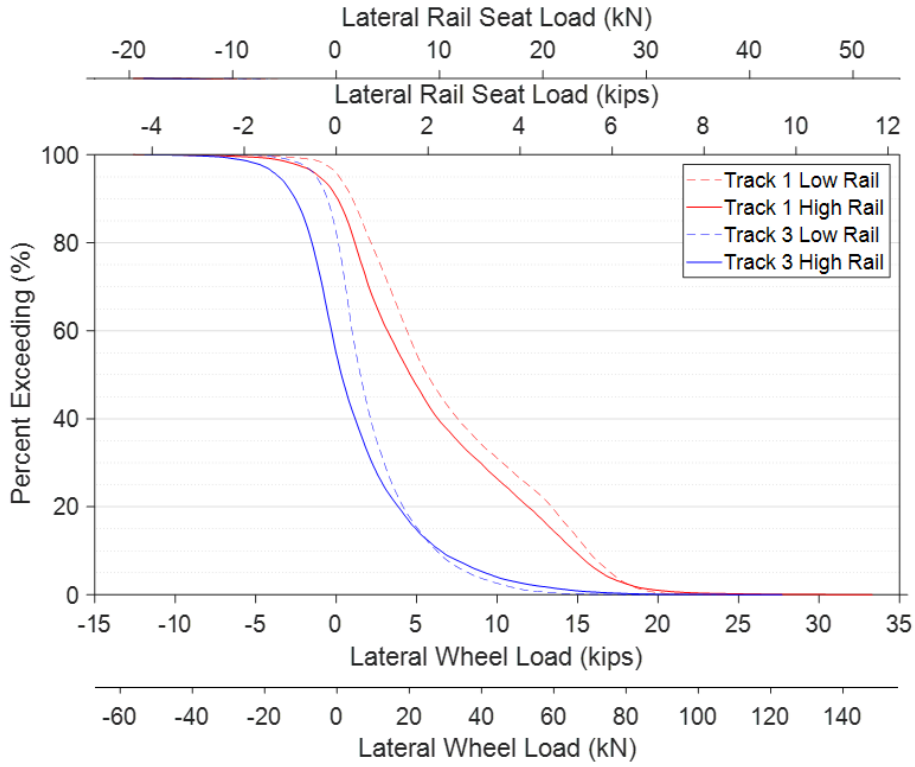


Figure 2.8: Lateral wheel and rail seat load percent exceedance for high and low rails of both tracks

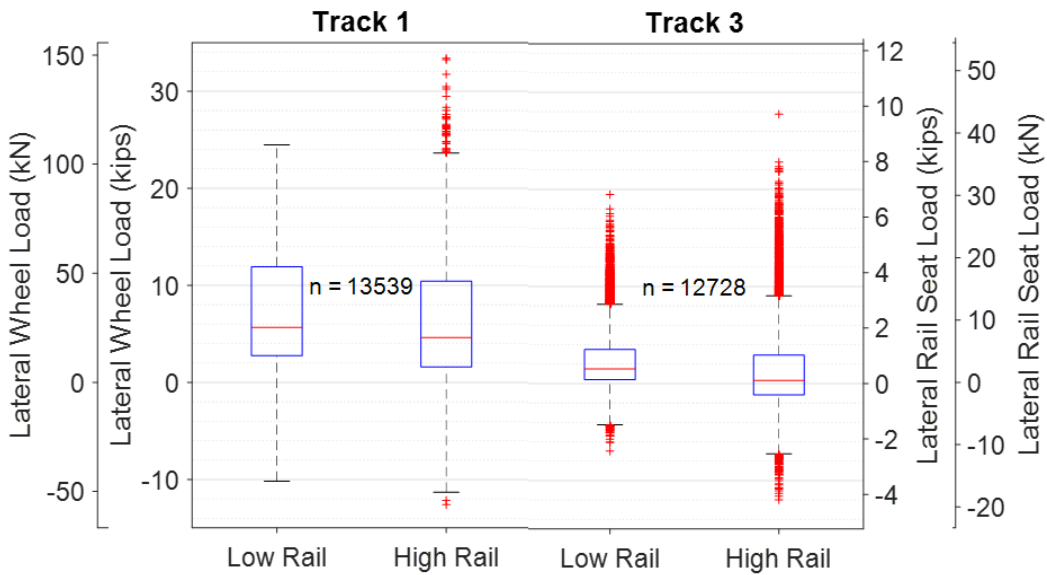


Figure 2.9: Lateral wheel and rail seat load box plots for high and low rails of both tracks

Table 2.3: Lateral wheel loads at select percentiles for high and low rails of both tracks

Lateral Wheel Load - kips (kN)				
%	Track 1		Track 3	
	Low Rail	High Rail	Low Rail	High Rail
99	19.2 (85)	20.0 (89)	11.8 (53)	14.7 (65)
95	17.1 (76)	16.5 (73)	8.2 (37)	9.3 (41)
90	15.6 (70)	14.8 (66)	6.2 (28)	6.5 (29)
50	5.7 (25)	4.6 (20)	1.5 (7)	0.3 (1)

Table 2.4: Lateral rail seat loads at select percentiles for high and low rails of both tracks

Lateral Rail Seat Load* - kips (kN)				
%	Track 1		Track 3	
	Low Rail	High Rail	Low Rail	High Rail
99	6.71 (29.9)	7.02 (31.2)	4.14 (18.4)	5.14 (22.9)
95	5.97 (26.6)	5.77 (25.7)	2.88 (12.8)	3.24 (14.4)
90	5.47 (24.3)	5.18 (23.0)	2.19 (9.7)	2.27 (10.1)
50	1.98 (8.8)	1.61 (7.2)	0.53 (2.3)	0.11 (0.5)

The applied lateral to vertical (L/V) load ratio is a numerical ratio of lateral and vertical load applied at a point on the rail (FRA, 2011). Though commonly used as a metric for determining derailment risk (e.g. wheel-climb or rail-rollover), the L/V ratio is commonly increased during laboratory testing to represent more severe loading environments (CEN, 2002; AREMA, 2017b). Hay (1982) indicates that 0.68 is the threshold where the rail becomes unstable due to the resultant lateral and vertical force passing outside the rail base. Although the metric represents the loads applied at the wheel-rail interface, a rail seat L/V load ratio (i.e. representing the loads applied at the rail seat) could be more representative of what the fastener would be subjected while also aligning more closely with the American Railway Engineering and Maintenance-of-Way Association (AREMA) (2017b) recommendation that considers L/V ratios above 0.52 to be “severe service.” The rail seat L/V would be 35% higher

than what is seen at the wheel-rail interface, accounting for the parameters previously discussed in this chapter (i.e. the vertical and lateral load percentages transferred to the rail seat beneath the point of load application are 26% and 35%, respectively). To further investigate the fastening system demands at this location, I calculated the wheel-rail and rail seat L/V ratios for the leading axles of Tracks 1 and 3 (Table 2.5).

Table 2.5: Wheel-rail and rail seat L/V ratios of leading axles of the high and low rails on tracks 1 and 3

Percentile	Wheel Rail L/V				Percentile	Rail Seat Rail L/V			
	Track 1		Track 3			Track 1		Track 3	
	Low	High	Low	High		Low	High	Low	High
99	0.54	0.56	0.48	0.72	99	0.73	0.75	0.65	0.97
95	0.50	0.50	0.39	0.58	95	0.67	0.67	0.53	0.78
90	0.48	0.46	0.34	0.49	90	0.64	0.63	0.46	0.65
50	0.36	0.34	0.12	0.17	50	0.48	0.46	0.17	0.23
10	0.15	0.21	0.03	-0.19	10	0.21	0.28	0.04	-0.25
5	0.11	0.17	0.00	-0.27	5	0.15	0.23	0.00	-0.36
1	-0.01	0.08	-0.05	-0.44	1	-0.01	0.11	-0.07	-0.59

The wheel-rail L/V ratios were greatest on the high rail of Track 3 and ranged from -0.44 to 0.72 (1st percentile to 99th percentile, respectively). The field side L/V of 0.72 exceeds the 0.68 threshold proposed by Hay (1982) indicating that the high rail of Track 3 could be unstable. The 95th percentile rail seat L/V ratios of all rails exceeded the 0.52 threshold classified by the AREMA in Chapter 30 (Ties) for design qualification testing (AREMA, 2017b) as severe-service loading. Track 3 was subjected to rail seat L/V magnitudes that were 50% greater at the 95th percentile (0.78) and 87% greater at the 99th percentile (0.97) as compared to the 0.52 AREMA threshold. Previous research by Kerchof (2016) showed that excess superelevation leads to increased L/V load ratios on the high rail and increased gauge widening. Therefore,

reducing the elevation of the curve and balancing the forces has already been shown to improve track health (Kerchof, 2016) and thus could also be expected to mitigate spike failures.

2.5.3 Longitudinal Loading

I used the methods described in Section 2.4.2 to quantify the longitudinal rail loads and corresponding rail seat loads (Figures 2.10, 2.11, and 2.12 and Tables 2.6 and 2.7). The mean tensile rail loads were greater on Track 3 than Track 1 and the longitudinal rail seat loads are at least an order of magnitude lower than the longitudinal wheel loads (i.e. rail seat longitudinal loads were less than 10% the axial rail loads). Therefore, the longitudinal loading demands on Track 3 are greater than Track 1. The median longitudinal rail seat loads were 0.97 and 0.84 kip (4.3 and 3.7 kN, respectively) (high and low rails, respectively) on Track 1 and 1.29 and 1.39 kips (5.7 and 6.2, respectively) (high and low rails, respectively) on Track 3. Therefore, the high and low rails of Track 1 are subjected to 0.32 and 0.55 kips (1.4 and 2.4 kN, respectively) lower longitudinal force than Track 3, respectively.

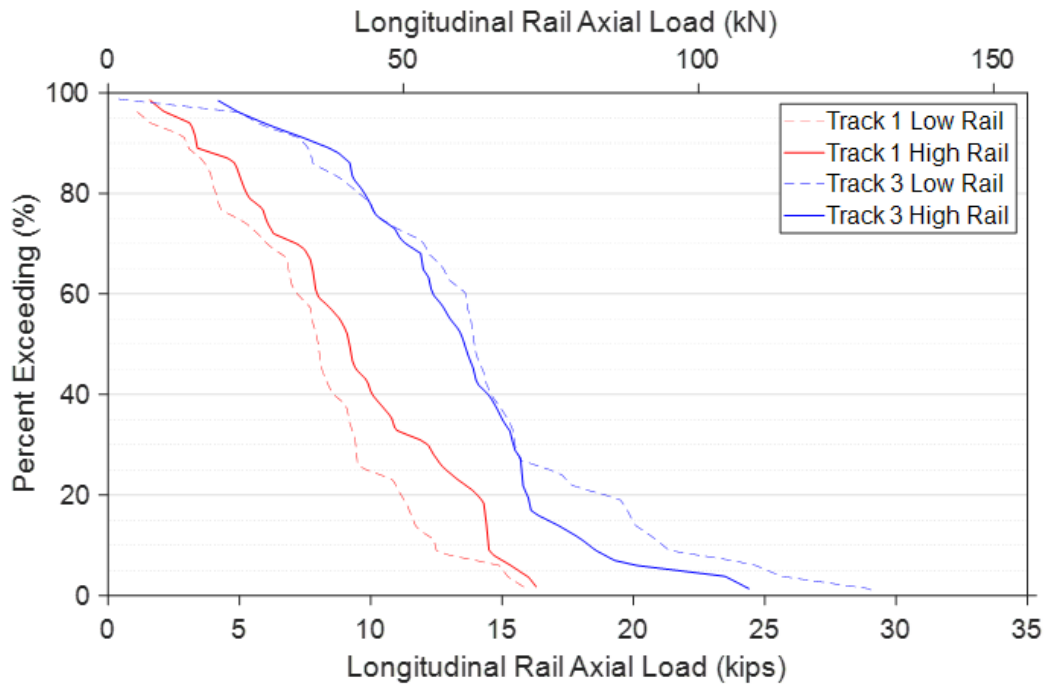


Figure 2.10: Longitudinal rail axial load percent exceedance for high and low rails of both tracks

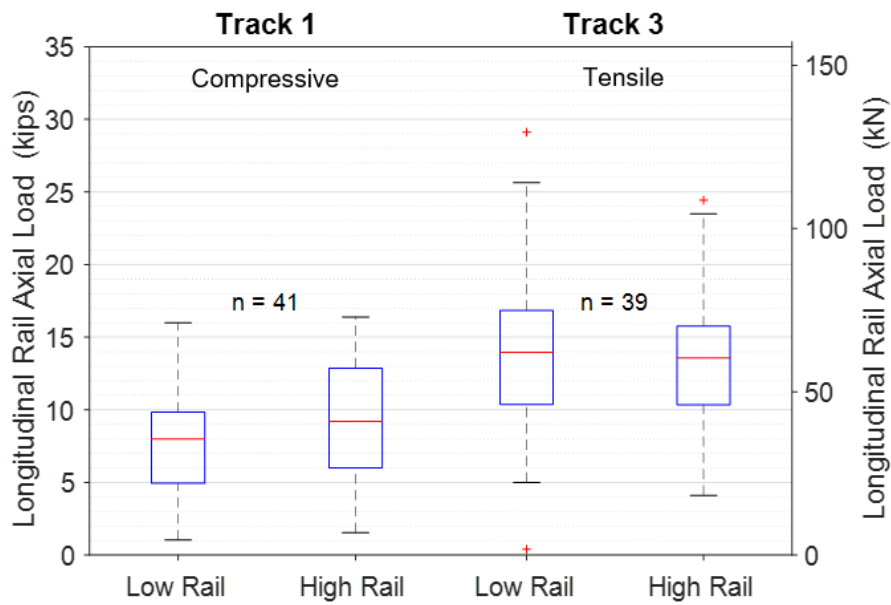


Figure 2.11: Longitudinal rail axial load box plots for high and low rails of both tracks

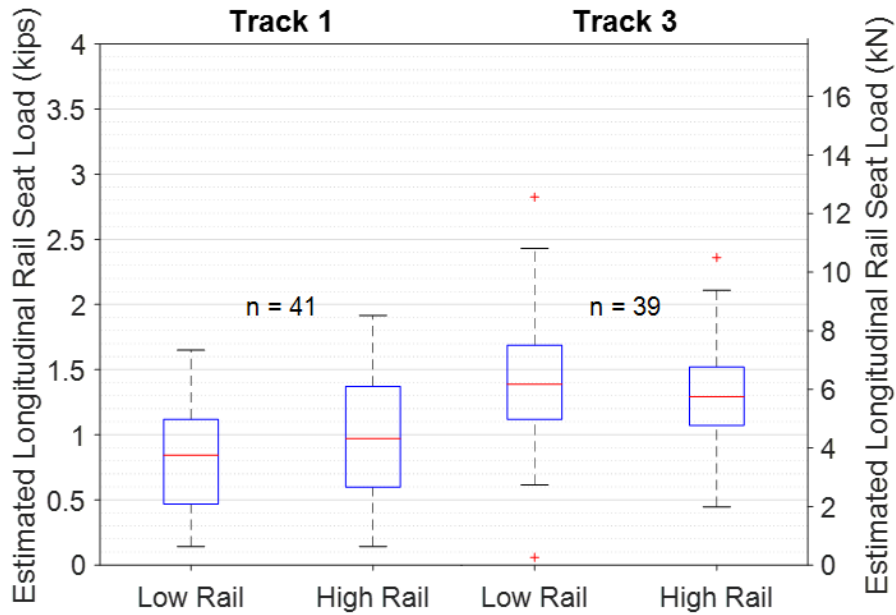


Figure 2.12: Longitudinal rail seat load box plots for high and low rails of both tracks

Table 2.6: Longitudinal rail axial loads at select percentiles for high and low rails of both tracks (kips (kN))

%	Track 1		Track 3	
	Low Rail	High Rail	Low Rail	High Rail
99	16.0 (71)	16.4 (73)	29.1 (129)	24.4 (109)
95	15.0 (67)	15.6 (69)	25.1 (112)	21.7 (97)
90	12.5 (55)	14.5 (64)	21.1 (94)	18.3 (81)
50	8.0 (36)	9.2 (41)	14.0 (62)	13.6 (60)

Table 2.7: Longitudinal rail seat loads at select percentiles for high and low rails of both tracks (kips (kN))

%	Track 1		Track 3	
	Low Rail	High Rail	Low Rail	High Rail
99	1.65 (7.3)	1.92 (8.5)	2.82 (12.6)	2.36 (10.5)
95	1.51 (6.7)	1.64 (7.3)	2.40 (10.7)	1.96 (8.7)
90	1.25 (5.5)	1.55 (6.9)	2.09 (9.3)	1.73 (7.7)
50	0.84 (3.8)	0.97 (4.3)	1.39 (6.2)	1.29 (5.7)

2.5.4 Total Spike Demands Considering Timing of Load Application and Frictional Effects

Because spike fatigue failures are a result of bending stresses, I used the lateral and longitudinal forces to calculate the total resultant force imparted on the spike (Equation 2.2 and Figure 2.13). A simplified fatigue failure threshold of 2.3 kips (10.2 kN) was set, based on model data I will describe in Chapter 3,

$$Resultant = \sqrt{Lateral^2 + Longitudinal^2} \quad \text{Eq. 2.2}$$

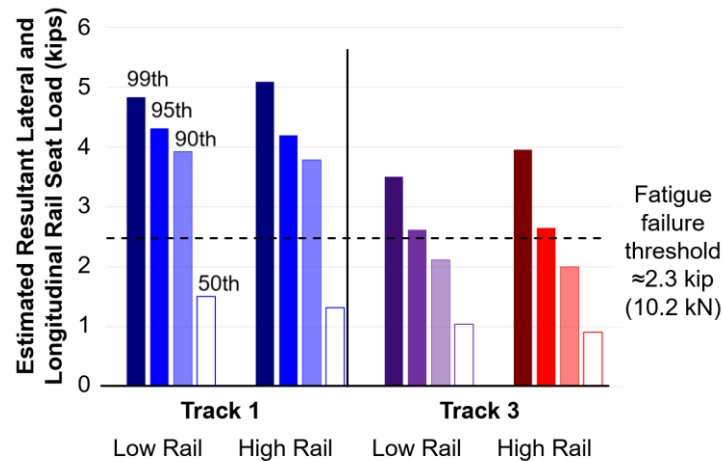


Figure 2.13: Resultant longitudinal and lateral rail seat loads with fatigue failure threshold indicated

My analysis indicates that if friction and vertical rail seat loads are not accounted for, failures would be expected on all four rails. This analysis also indicated that the high rail of Track 3 is subjected to lower forces than both rails of Track 1, thus I focused my investigation on the effect of friction and vertical load on the high rail of Track 3.

Additionally, a single spike would not be expected to transfer 100% of the rail seat load. Instead, Gao and LoPresti (2020) and Dersch et al. (2020b) showed that a single spike is

subjected to 70% of the applied rail seat load given non-uniform distribution among the spikes within a single rail seat.

When considering the combined effect of longitudinal and lateral loads, the timing of load application and quantification of the friction at the plate-crosstie interface is critical. The zone of longitudinal loading influence is greater than either the vertical or lateral. Furthermore, the wave action of the rail ahead of a wheel produces rail uplift (Talbot, 1918), as predicted by BOEF models (Kerr, 2003b). It is therefore reasonable to assume that the longitudinal loads are applied when there is rail uplift, directly bearing on the spikes (e.g. not carried by friction) (Figure 2.14, a). Based on the sequence of load application, the lateral loads would be resisted by friction and spike bearing given that the loads are applied when there is contact at the plate-crosstie interface (Figure 2.14, a).

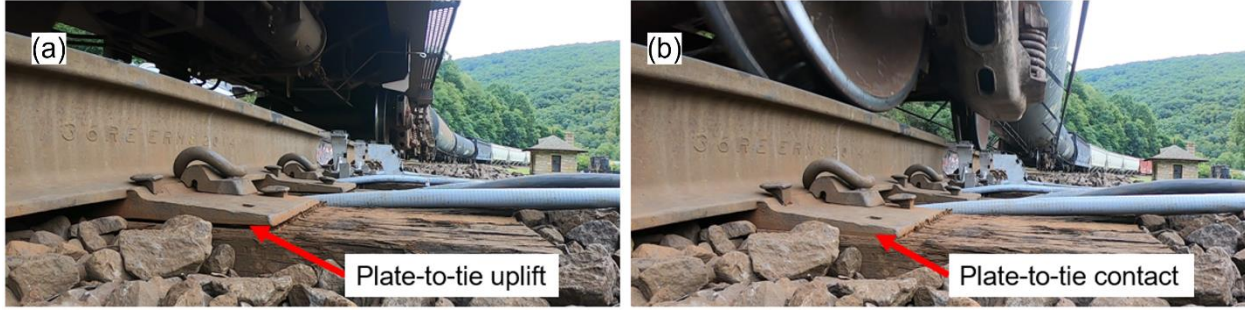


Figure 2.14: Plate-to-tie uplift at center of locomotive (a) and plate-to-tie contact directly under wheel (b)

For a more realistic analysis of total demand placed on the spike as well as the failure threshold that accounts for the orthotropic nature of the timber crosstie, the median, 90th, 95th, and 99th lateral and longitudinal rail seat loads from all rails were transformed into spike loads (Equations 2.3 and 2.4).

$$P_{Spike,Long} = 0.7 \cdot F_{Long} \quad \text{Eq. 2.3}$$

$$P_{Spike,Lat} = \begin{cases} 0.7(F_{Lat} - \mu \cdot F_{Vert}) & \text{if } |F_{Lat}| > \mu \cdot F_{Vert} \\ 0 & \text{if } |F_{Lat}| \leq \mu \cdot F_{Vert} \end{cases} \quad \text{Eq. 2.4}$$

where,

F_{Vert} is the Fastener vertical load (≥ 0).

F_{Lat} is the Fastener lateral load.

F_{Long} is the Fastener longitudinal load.

$P_{Spike,Lat}$ is the Spike lateral load.

$P_{Spike,Long}$ is the Spike longitudinal load.

This is similar to the load severity calculation the Federal Railroad Administration (FRA) includes in 49 CFR Part 213 – Track Safety Standards (FRA, 2011). Additionally, considering that coefficients of friction (CoF) (μ) between timber and steel can vary from 0.3 to 0.7 depending on moisture content of the timber, surface treatment, or roughness of the plate (Forest Products Laboratory, 2010), the role of the CoF was also investigated. The resulting lateral and longitudinal spike loads are plotted, as are the spike endurance limit thresholds for the given rail seat vertical load (V) and CoF (Figure 2.15).

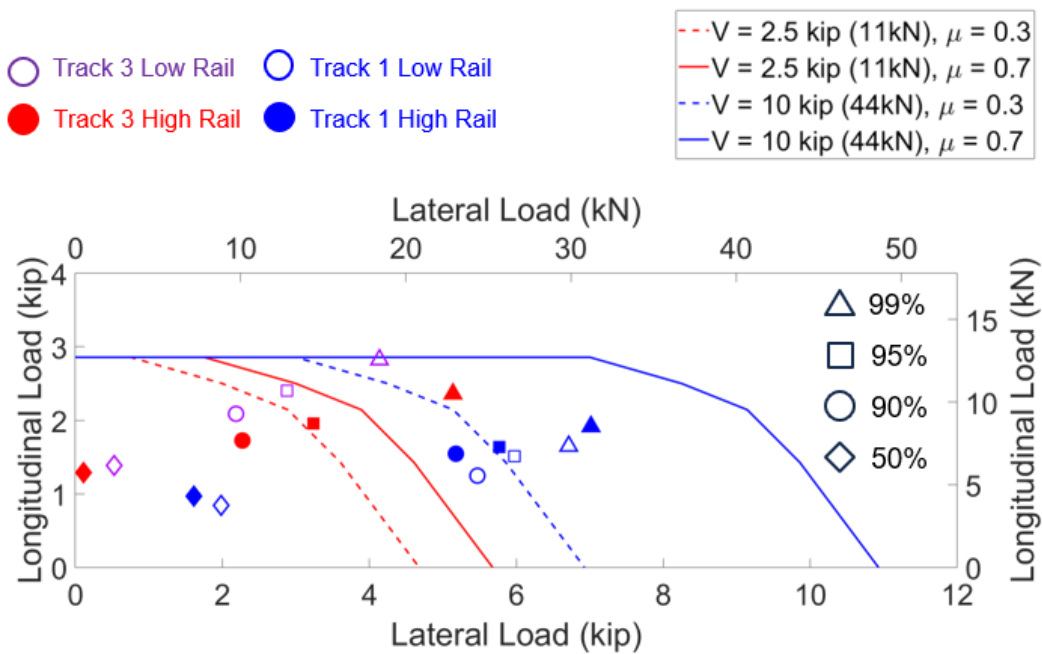


Figure 2.15: Effect of rail seat vertical load (V) and plate-to-cross-tie friction (μ) on total spike load for various lateral and longitudinal rail seat load combinations with failure thresholds identified

Field data indicate that fatigue failures could be expected on either track when friction is low. However, as friction increases, fewer failures would be expected given the load required to exceed the failure threshold increases. Considering vertical load data from the field site, the high rail of Track 3 (median vertical rail seat load of 2.8 kips (12.5 kN)) is closest to the lower-bound,

vertical applied load (2.5 kips (11.1 kN)), as presented. However, the low rail of Track 3 and both rails of Track 1 would have failure thresholds closer to the upper-bound, vertical load (10 kips (44.5 kN)) (Figure 2.15). Therefore, these data indicate that while the magnitude of lateral and longitudinal applied loads on the high rail of Track 3 is the lowest, the threshold for failure is also the lowest. At reasonable friction levels, more failures would be expected on the high rail of Track 3, which is consistent with observed field performance.

2.6 Conclusions

In this chapter I quantify the vertical, lateral, and longitudinal fastening system demands in locations with failed elastic fastening system components and illustrate the impact of friction in fastening system load transfer. These data and insights regarding the importance of friction can be used to inform future fastening system design for high demand track. Additionally, this research identifies the relationship between design values for track superelevation, operation, and failures and how these parameters affect the stress state of track components.

In summary, the revenue service field data that I collected at a curved location that has experienced broken spikes, showed that the failure threshold was affected by the applied vertical load. That is, while the magnitude of the applied vertical load was the lowest on the high rail of Track 3 (the location of most failures), the threshold for failure is also the lowest given that the lower magnitude vertical rail seat load reduced the frictional load capacity to a level that was exceeded more often than on Track 1. Additionally, the high rail of Track 3 was subjected to the highest L/V load ratios and was an outlier in that it experienced lateral load reversals that are expected to create a shorter fatigue life.

A summary of additional findings from this investigation include:

- For a given wheel, the maximum vertical, lateral, and longitudinal load percentage transferred to the fastening system was approximately 26%, 35%, and <10%, respectively.
- Underbalance operations led to a median rail seat vertical load of 2.8 kips (12.5 kN) on the high rail of Track 3 and thus the lowest friction capacity of all rail seats.
 - The higher magnitude vertical loads on both rails of Track 1 and the low rail of Track 3 provide greater frictional resistance as compared to the high rail on Track 3, likely reducing the amount of load transferred into the spikes.
- Longitudinal fastener loads ranged from 1.29 to 2.40 kips (5.8 to 10.7 kN) for Track 3 and 0.84 and 1.64 kips (3.7 to 7.3 kN) for Track 1 for the nominal and 95% loads, respectively.
- Lateral fastener loads ranged from 0.11 to 2.88 kips (0.5 to 12.8 kN) for Track 3 and 1.61 and 5.97 kips (7.1 to 26.6 kN) for Track 1 for the nominal and 95% loads, respectively.
- The 95th percentile rail seat L/V ratio of 0.78 on the high rail of Track 3 is 50% greater than the 0.52 values fastening systems are subjected to during severe service testing as recommended by AREMA.
- Spike fatigue failures are driven by a combination of both lateral and longitudinal loading.
 - The longitudinal load magnitudes, which are present even when vertical and lateral loads are not applied, are insufficient to independently cause fatigue failures.

To mitigate spike failures at this location, as well as similar failures in other track types (e.g. rail seat deterioration, etc.), railroads should ensure trains operate at speeds that are close to the balance speed of curves. Balanced operation would increase the vertical force on the high rail of Track 3 while reducing the L/V ratios and lateral load reversal. Finally, encouraging contact (friction) between the tie plate and crosstie is critical for reducing the forces transferred to the spike.

3 3D FINITE ELEMENT MODELING OF THE EFFECT OF LOAD MAGNITUDE, LOAD DIRECTION, AND TIMBER SPECIES ON SPIKE STRESS

In this chapter, I present the development, validation, and application of a 3D finite element model (FEM) of the interaction between the spike and timber crosstie. The FEM accounts for the orthotropic nature of the timber. The FEM also quantifies the effect of timber grain direction and load magnitude on the depths and corresponding levels of maximum spike stress. A paper related to this chapter was published in *Engineering Failure Analysis*² in 2019.

3.1 Background

Several recent derailments (TSB Canada, 2012; FRA, 2016; Kerchof, 2017) have occurred due to wide gauge in track constructed using premium fastening systems and investigations found that the wide gauge was caused by broken spikes. These derailments occurred on three different railroads and in all cases the track met applicable track-class-based geometric standards and had no visually-detectable broken spikes. Each derailment also occurred in track with different elastic fastening system designs installed using both screw and cut spikes. Investigations found the depth at which the spike failure occurred ranged from 1 – 2 in. (25 – 50 mm) with a typical depth to failure at approximately 1.5 in. (38 mm) below the top of the crosstie surface (Figure 3.1). Further investigations revealed that spike fracture surfaces were consistent with fatigue failures resulting from loading in the lateral and longitudinal directions (Kerchof, 2017).

² Dersch, M., T. Roadcap, J.R. Edwards, Y. Qian, J.-Y. Kim and M. Trizotto. 2019. Investigation into the effect of lateral and longitudinal loads on railroad spike stress magnitude and location using finite element analysis. *Engineering Failure Analysis*, 104: 388–398. doi:10.1016/j.engfailanal.2019.06.009



Figure 3.1: (a) A premium fastening system with two broken spikes. (b) Example fracture surface of a broken spike. (c) Examples of broken spikes with varying depths of failure

While problems with broken spikes in elastic fastening systems were noted as early as 1982 (Dean, 1982) there has been limited research focusing on their root causes. Previous research on spike fatigue failures has included basic FEM (Dick et al., 2007), limited field experimentation (Gao et al., 2018), and an industry-wide survey and field visits to heavy axle load (HAL) railroads to learn about the performance of both cut and screw spikes in revenue service (Roadcap et al., in review).

The primary motivation to use elastic fasteners is to improve track stability, reliability, and reduce maintenance through greater rail rollover resistance and plate restraint. Recent derailments and the need for walking inspections indicate that these elastic fastening systems are not fulfilling these objectives. Thus, there is a need to characterize the failure mechanism of the spikes and develop a solution. The objectives of this chapter are to quantify the effect of timber grain direction and load magnitude on the depth and corresponding maximum spike stress

(response), while also developing an analytical tool that can further characterize spike response as a function of these variables.

3.2 Methodology

Commercially available FEM software Abaqus/CAE was selected to perform the simulations for this study because of its recent use studying other rail infrastructure components (Chen et al., 2016; Zhu et al., 2016; Zhu et al., 2017; Chen and Andrawes, 2017). The spike modeled in this study was the standard 6 in. (152mm) long by 0.625 in. (15.9mm) square-shaft cut spike shown in Figure 5-2-1 in Chapter 5 of the AREMA Manual on Railway Engineering (2017b). This type of spike is widely used in HAL and rail transit systems in North America. The numerical model in this study consists of two principal components: a simplified cut spike and a timber crosstie block (Figure 3.2). Both components were modeled as 3D deformable solids. The cut spike was meshed using linear brick, type C3D8R for both the spike shaft, where the stress was of most interest, and the spike tip with a total of 9,936 elements. The simplified timber crosstie block was also modeled using 33,584 linear brick, type C3D8R elements and incorporated reduced integration and hourglass control. The static coefficient of friction (CoF) between the cut spike and timber block was set at 0.7 and the interaction between the spike and timber was modeled as two contact surfaces and did not consider perfect bonding (Gurfinkel, 1981).

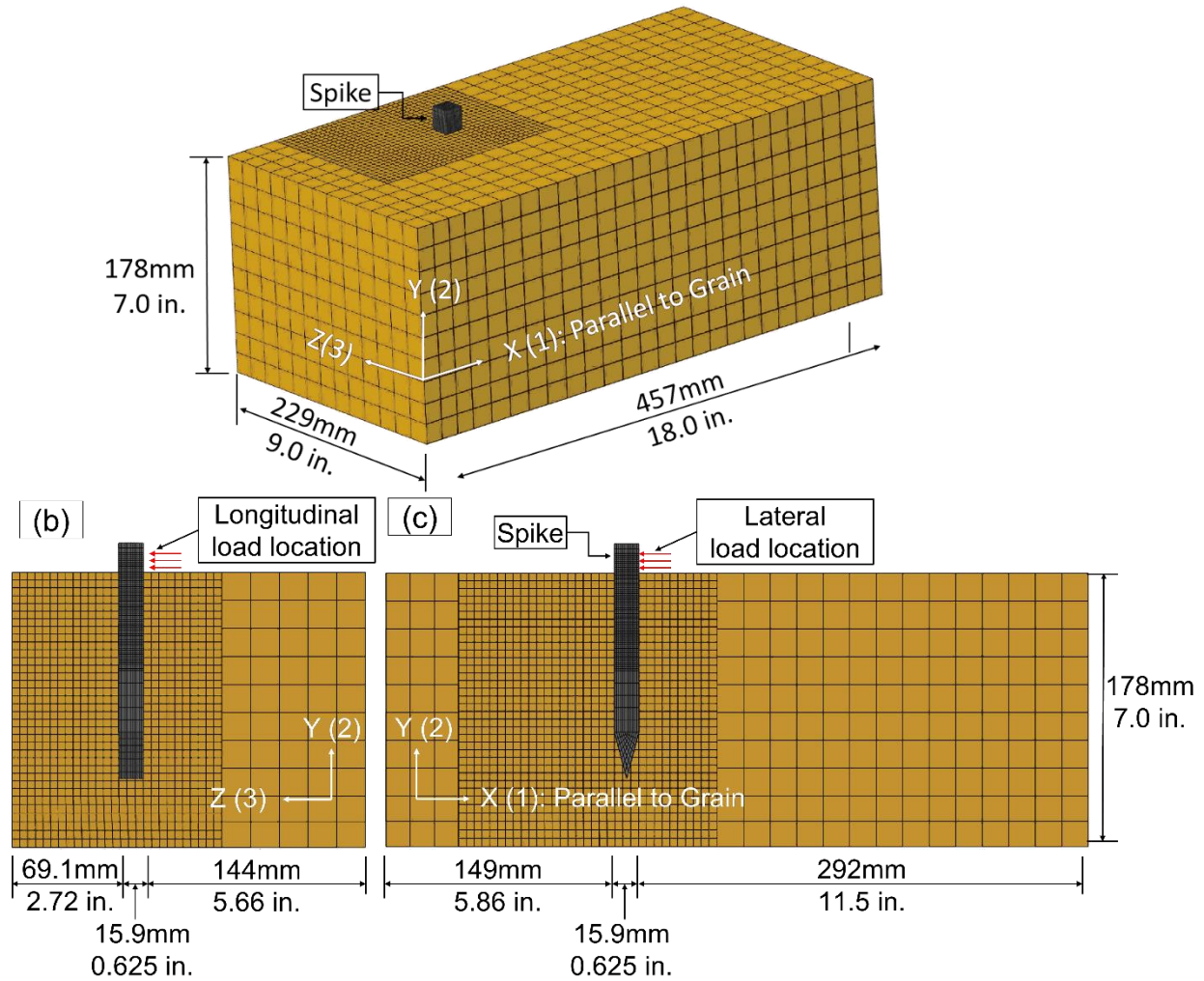


Figure 3.2: (a) isometric view of 3D block and spike model; (b) view x-y cut section of cut spike in timber crosstie block; (c) view z-y cut section of cut spike in timber block

3.3 Model Properties, Simplifications, and Assumptions

To reduce the computational cost for the parametric study, yet maintain representative conditions, simplifications and assumptions were made to the spike and crosstie block models. Given that the scope of this chapter was to investigate the effect of load magnitude and grain direction on spike stress, only a single cut spike and block of the crosstie were modeled because Dick et al. (2007) demonstrated that the load transferred to the spikes varies significantly. Additionally, the cut spike head geometry was simplified because it was not the specific area of

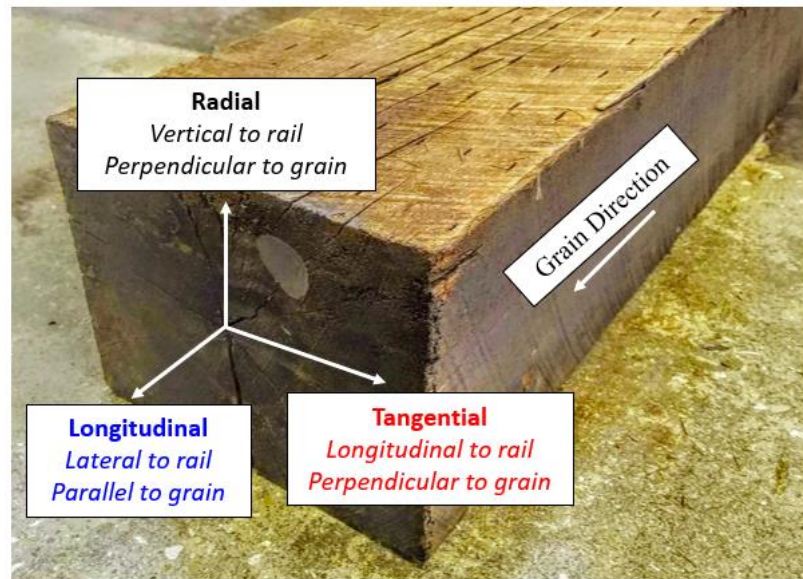
interest and does not play a role in stress distribution. These simplifications allowed the use of a more refined mesh of the spike and timber crosstie block at critical locations to accurately quantify the spike stress and displacement while maintaining computational efficiencies. The spike model represented the hold-down spike and thus the size of the crosstie block and amount of timber material for reaction was modeled to simulate the field side of the tie (Figure 3.2).

An additional timber crosstie block simplification was the placement of a 0.625 in. (15.9 mm) square hole into the timber block at the location where the spike would be installed. This provided clearance for the spike without having to expend computational time inserting the spike into the crosstie and calculating the resulting stresses. This assumption was justified given this study was focused on simulating the working condition of the spike, and not the process of driving the spike into the timber. Therefore, the model sets the spike at a predefined position and defines interaction between the spike and the timber crosstie accordingly. Given that failed spikes can occur at various stages of spike life (e.g. ranging from ca. 3 to >100 million gross tons (MGT)), the detailed spike-crosstie reaction was simplified. That is, given some spikes are known to lift out of the crosstie, the stresses directly after installing a spike are not as relevant as a spike that has been in track and undergone a period of settling.

Unlike previous studies that have investigated spike performance, the timber crosstie block was modeled as an orthotropic material due to timber's unique and independent mechanical properties in the three mutually perpendicular axes: longitudinal (parallel to the direction of the timber fibers), tangential (perpendicular to the direction of the timber fibers and tangent to growth rings), and radial (perpendicular to the direction of the timber fibers and growth rings) (Gurfinkel, 1981; Green et al., 1999) (Figure 3.3). To account for this behavior, I used a validated, timber, user-defined material model (UMAT) that has been used previously to

investigate the mechanical behavior of timber joints with slotted-in steel plates (Sandhaas, 2011; Sandhaas, 2012)

I use the following nomenclature to refer to principal axes of timber and grain direction in this chapter (Figure 3.3). The parallel timber grains align with the length of the crosstie and will be the primary reaction direction for lateral loads. The tangential and radial directions primarily run perpendicular to the timber grain, align with the width and depth of the crosstie, and will be the primary reaction direction for longitudinal and vertical loads.



Grain Direction	Loading Definition	Model Direction
Longitudinal	Lateral	1
Tangential	Longitudinal	3
Radial	Vertical	2

Figure 3.3: Principal axes of timber with respect to grain direction, growth rings, and wheel loading

The material properties used for the timber models (Table 3.1) fall within the expected ranges found in the literature when accounting for expected variability and/or strength reductions

(Green et al., 1999; American Wood Council, 2017). All species selected are regularly treated with preservatives and used by North American Class I HAL railroads according to the Railway Tie Association (RTA) . Material properties, were either calibrated using laboratory data or were found in the literature (Green et al., 1999; Sandhaas, 2012; American Wood Council, 2017; Stanzl-Tschegg, et al., 1995; Ehrhart, et al., 2015).

The Young's Modulus, tensile strength, and yield strength of the cut spike properties were found through laboratory tests to be 30,850,000 psi (212,700 MPa), 85,000 psi (585 MPa), and 56,265 psi (390 MPa), respectively. I set the endurance limit at 33,800 psi (233 MPa) based on the assumption that it is approximately 40% of the ultimate strength. This falls between the 35 – 60% range for endurance limits found in the literature (Campbell, 2008). Finally, I assumed the spike had a Poisson's ratio of 0.3 and a density of 0.029 lb./in.³ (8,050 kg/m³).

Table 3.1: Engineering properties of select hardwood timber

Property	Direction	Timber Type			
		Calibrated Model	White Oak	Silver Maple	Northern White Cedar
		psi (Mpa)	psi (Mpa)	psi (Mpa)	psi (Mpa)
Modulus of Elasticity	E1	1,650,000	1,780,000	1,140,000	800,000
		11,376	12,273	7,860	5,516
	E2 = E3	194,000	209,150	115,710	54,400
		1,338	1,442	798	375
Shear Modulus	G12 = G13	163,493	153,080	137,940	168,000
		1,127	1,055	951	1,158
	G23	41,118	93,450	50,730	80,800
		283	644	350	557
Compressive Strength	Perpendicular to Grain	235	1,070	740	310
		1.6	7.4	5.1	2.1
Tensile Strength		270	800	500	240
		1.9	5.5	3.4	1.7
Compressive Strength	Parallel to Grain	3,000	7,440	5,220	3,960
		20.7	51.3	36.0	27.3
Tensile Strength		7,161	12,000	8,900	6,500
		49.4	82.7	61.4	44.8
Longitudinal Shear Strength		1,000	2,000	1,480	850
		6.9	13.8	10.2	5.9
Rolling Shear Strength		800	800	444	255
		5.5	5.5	3.1	1.8

- Sandhass (2012), chose Poisson's ratio values incorporating damage at the beginning of the model and thus some improvement could be made in future models incorporating linear degradation

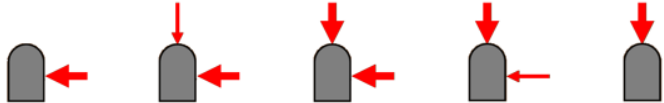
- Given the limited values within the literature, and the limited affect they have on the current model, the fracture energy values were treated as constants as 3 (0.53), 36 (6.30), 60 (10.50), & 60 (10.50) (lb/in. (N/mm)) for the tension perpendicular to grain, tension parallel to grain, longitudinal shear, and rolling shear respectively

3.4 Lateral and Longitudinal Load Magnitudes

Lateral and longitudinal loads were applied to the spike shaft over a 0.3125 in.² (201 mm²) area that is representative of the tie-plate to spike contact patch. Five load cases (Table 3.2) were considered in which the magnitude of the lateral and longitudinal loads ranged from 0 to 5,000 lb. (0 to 22.2 kN). The load levels were in agreement with the literature (Dean, 1982; Dick et al., 2007; AREMA, 2017b) and are discussed in more detail below.

Table 3.2: Five cases varying lateral and longitudinal load

Load	Units	Load Case				
		1	2	3	4	5
Longitudinal	kN	22.2	22.2	22.2	11.1	0
	lb	5,000	5,000	5,000	2,500	0
Lateral	kN	0	11.1	22.2	22.2	22.2
	lb	0	2,500	5,000	5,000	5,000



The American Railway Engineering and Maintenance-of-Way Association (AREMA) Chapter 30 recommends applying a lateral load of 16,900 lb. (75.2 kN) to a single rail seat fastening system for the Tie and Fastener System Wear/Deterioration Test (AREMA, 2017b). If this lateral load were evenly distributed among four spikes, the load in each spike would be 4,225 lb. (18.8 kN). Dick et al. (2007) measured a 5,000 lb. (22.2 kN) lateral spike load from temperature changes alone and measured a maximum lateral load of 14,800 lb. (65.8 kN). This maximum load was not considered in the model because it would not be representative of the spikes that are not permanently deformed in track and would cause unnecessary model instability. Additionally, I demonstrated in Chapter 2 that plate-to-cross-tie friction would resist

lateral applied loads. Dick et al. (2007) also found that one of the four spikes carried 63% of the total load indicating a non-uniform distribution in a given plate.

AREMA specifies that a fastening system resist a 2,400 lb. (10.7 kN) longitudinal load before rail slip occurs (AREMA, 2017b). Elastic fastening systems tested by (Dean, 1982) endured more force than this before the rail slipped; the strongest system tested was the German K-Type system that took 6,310 lb. (28.1 kN) of longitudinal load per rail seat before rail slip occurred. In 1977, the South-African Railways used new e-clips to increase their rail seat longitudinal restraint to 6,300 lb. (28 kN) to combat rail creep problems on concrete crossties in HAL service (Lombard and Wildenboer, 1981). Therefore, I assumed that a single spike could be subjected to a 5,000 lb. (22.2 kN) longitudinal load given the non-uniform distribution of forces in the rail as found by Dick et al. (2007).

3.5 Model Validation

To validate the model, I collected laboratory data while a load was applied to an instrumented spike in a direction that was perpendicular to the grain (simulating a longitudinal load) (Figure 3.4a). A strain gauge was attached to a spike approximately 2.44 in. (62 mm) from the top of the spike (as measured in the model) (Figure 3.4b). This corresponds to the strain gauge being approximately 1.69 in. (43 mm) below the top of the crosstie. Additionally, the longitudinal displacement of the spike head was measured approximately 0.50 in. (13 mm) from the top of the spike. These strains and displacements were measured for the duration of the test in which load was applied up to approximately 2,300 lb. (10.2 kN) (Figure 3.5).

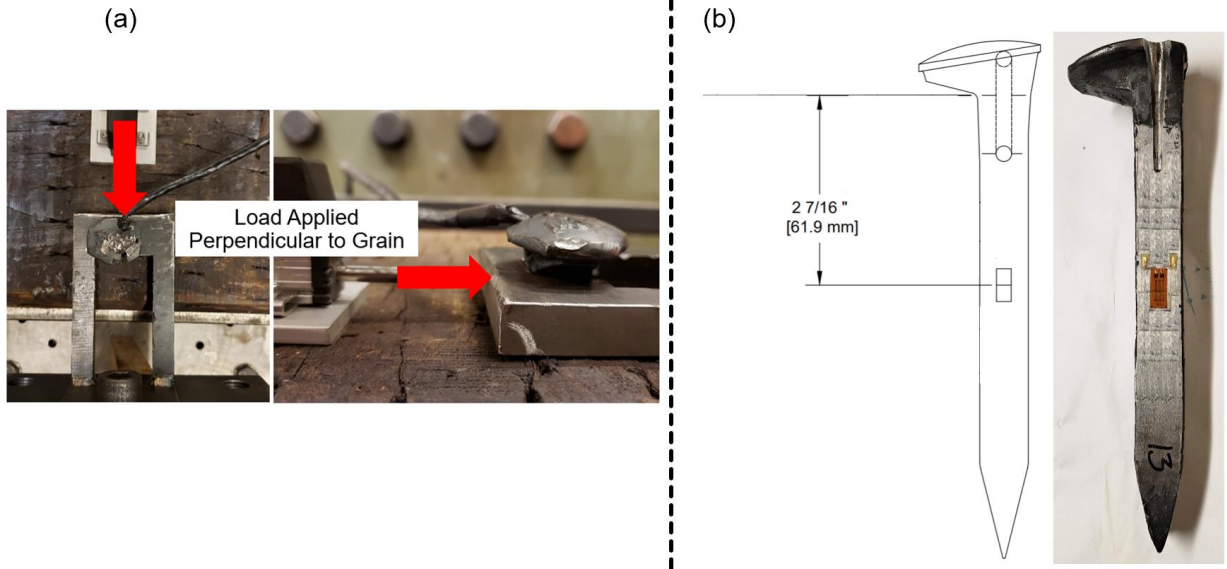


Figure 3.4: (a) Longitudinal load application to instrumented spike installed in the crosstie and (b) unprotected instrumented spike

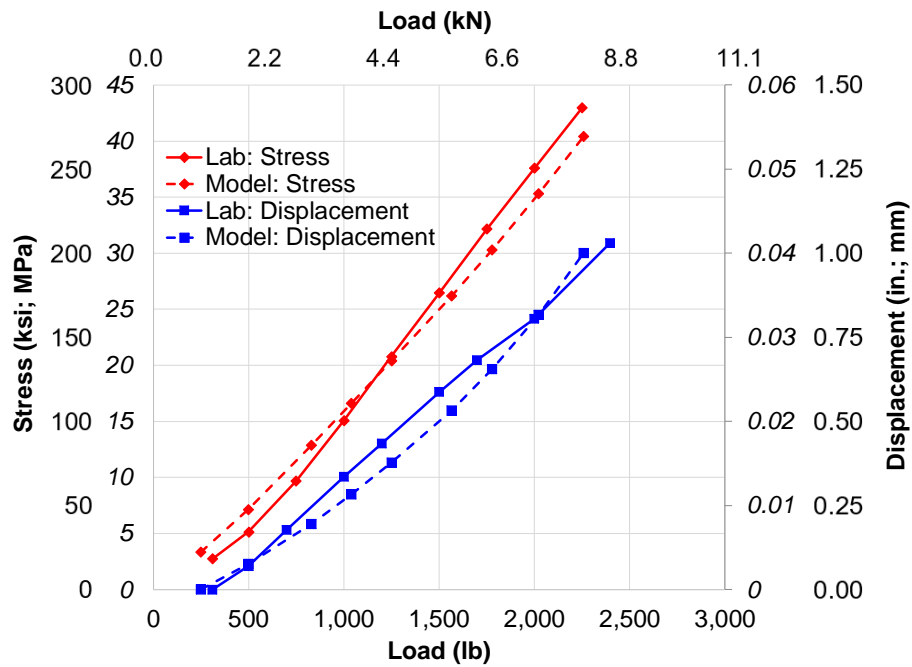


Figure 3.5: Comparison of laboratory measurements and stress and displacement calculated by the model

The model showed good agreement with the spike response at 1.69 in. (43 mm) below the top of crosstie, which is the critical stress location given that it corresponds with the approximate depth that spike breakage is observed in the field. Furthermore, the model accurately represents the displacement behavior of the spike as recorded in the laboratory test. These results validate use of the model to quantify the effect of load magnitude and direction on spike stress.

3.6 Results and Discussion

Maximum stress increases with load magnitude (Figure 3.6). The results indicate that longitudinal load is more detrimental to spikes than lateral load, which can be attributed to the orthotropic characteristics of timber. Not only is the modulus of the timber perpendicular to the grain approximately 10% of the modulus parallel to the grain, the compressive, tensile, and shear strengths are also weaker in that direction. These lower strength values allow timber damage to occur at lower load magnitudes. These, in turn, lead to greater spike deflections and stresses when longitudinal loads are applied. This leads to stresses in exceedance of the endurance limit at a lower load magnitude when longitudinal loads alone were applied as compared to the application of lateral loads alone (i.e. Case 1 compared to Case 5).

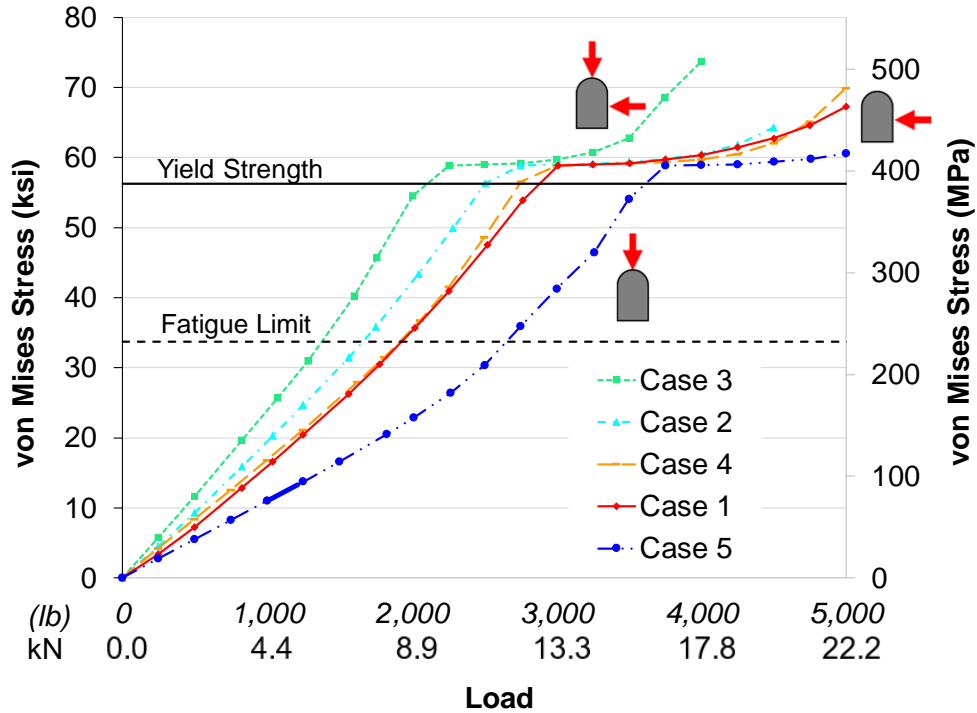


Figure 3.6: Effect of various lateral and longitudinal loads on maximum spike stress

To quantify this effect, when a lateral load is applied with no longitudinal load (Case 5), a cyclic load of approximately 2,750 lb. (12.2 kN) would be required to result in fatigue failure of the spike. However, a longitudinal load of only 2,000 lb. (8.9 kN) would be required to produce the same failure, or an approximately 30% reduction in magnitude when considering Case 1.

I also qualitatively assessed the spike stress distribution when subjected to the combinations of lateral and longitudinal loads (Figure 3.7). When longitudinal or lateral loads are applied individually (Case 1 and Case 5; (a) and (b)), the stress is distributed uniformly across the loaded face. The stress is distributed over a larger area of spike when longitudinal loading is applied to the spike (Case 1) compared to the lateral load (Case 5). This is logical given that there is greater deflection in the weak direction of the timber due to increased timber

near the surface of the tie. When lateral and longitudinal loads are applied simultaneously (Case 3; (c)), the stress is concentrated on a corner of the spike. The location of the stress concentration in the model aligned with actual spike failures observed in the field.

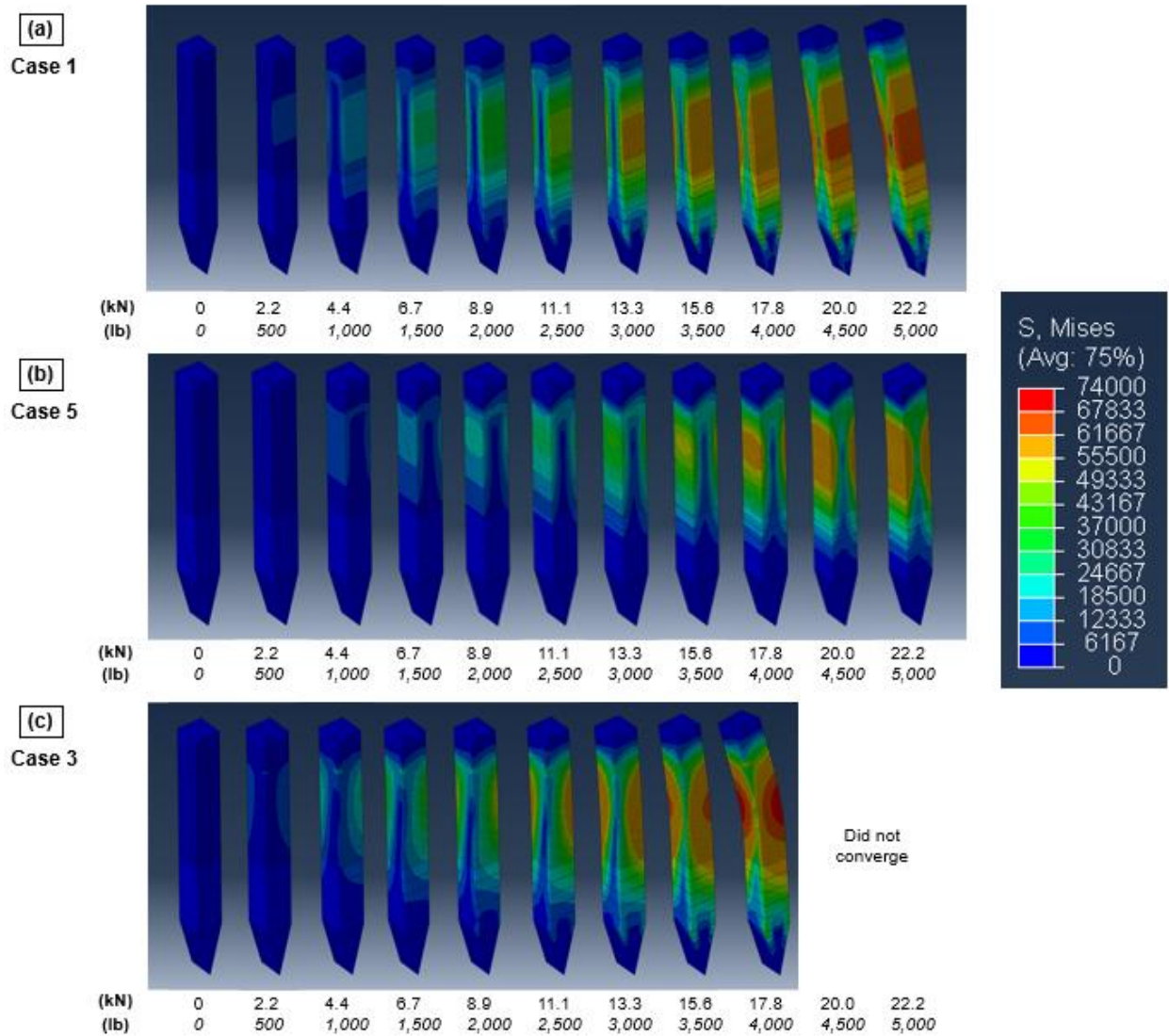


Figure 3.7: Effect of lateral and longitudinal load on cut spike stress distribution for Load Case 1 – Longitudinal Only (a), Load Case 5 – Lateral Only (b), and Load Case 3 – Lateral and Longitudinal Load (c)

I modeled and quantified the effect of three different species of timber (i.e. White Oak, Silver Maple, and Northern White Cedar) on the maximum spike stress to determine if my earlier findings were representative (Figure 3.8).

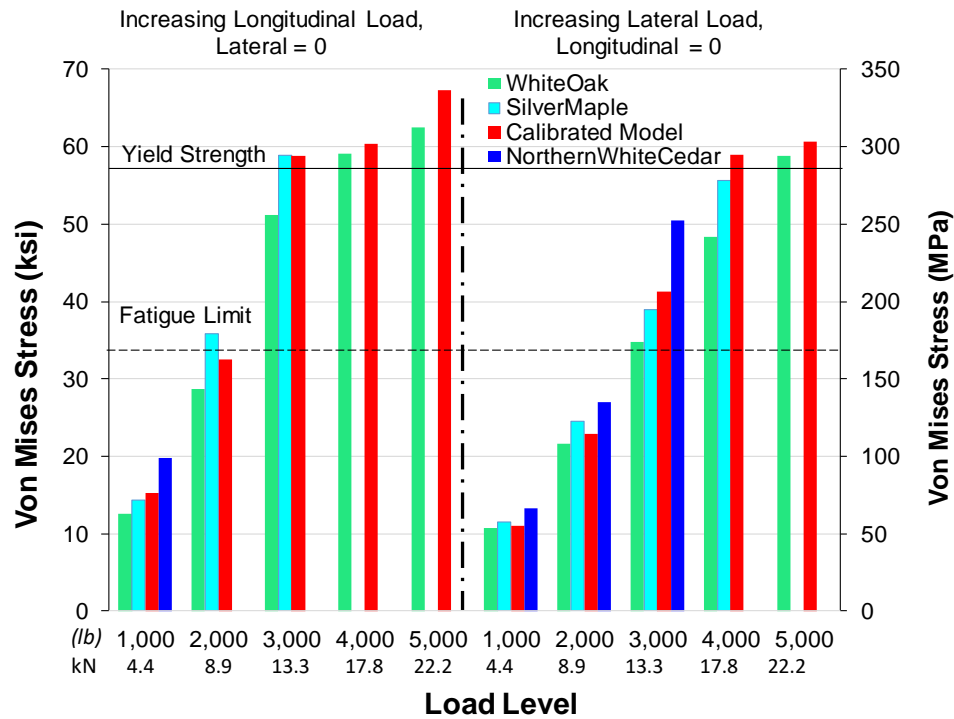


Figure 3.8: Effect of load level and timber type on maximum Von Mises stress

The Northern White Cedar model stopped converging at the lowest applied load due to significant timber damage and excessive spike displacements. Spikes in the softwood (i.e. Northern White Cedar) experienced higher stresses at lower applied loads because the timber experienced more damage, which allowed for greater spike bending. As expected (Gurfinkel, 1981) the stress data from the White Oak and Silver Maple indicate that not all hardwood species behave the same and thus railroads must consider this as a part of their purchasing and maintenance decisions.

Because field failure of spikes has typically been found to range between 1 – 2 in. (25 – 50 mm), it is necessary to understand what factors affect the depth of the maximum stress. Therefore, I quantified the effect of load magnitude, direction, and timber type on maximum spike stress depth (Figure 3.9).

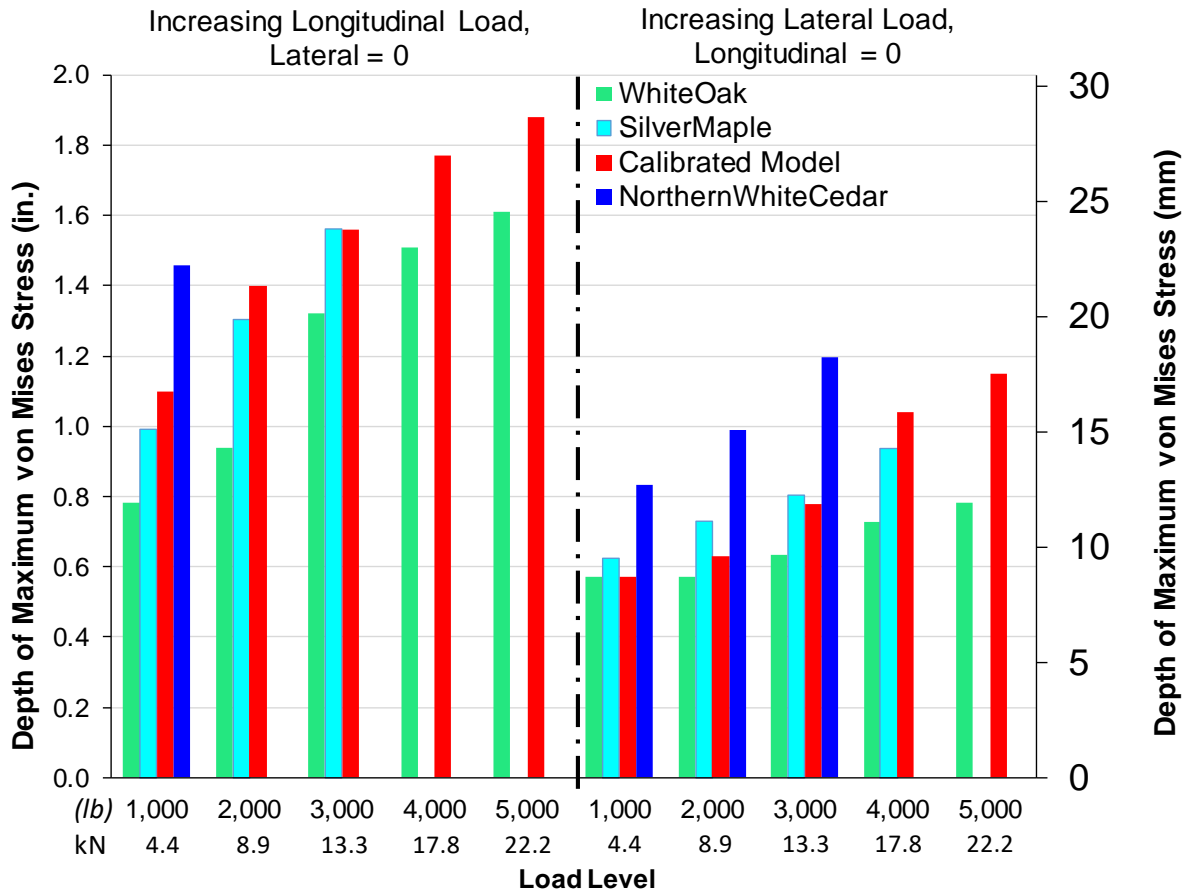


Figure 3.9: Effect of load magnitude, direction, and timber type on the depth of the maximum Von Mises stress

The depths to maximum stress fell within the typical range found in the field and the maximum depth where failure would occur was 1.9 in. (48 mm) at 5,000 lb. (22.2 kN) of force applied with the calibrated model. The data also indicated that the depth of maximum stress was greater when longitudinal loads were applied as compared to lateral loads, regardless of timber

species. Furthermore, as the timber mechanical properties (modulus, compressive, tensile, and shear strengths) were reduced, the depth to maximum stress increased. The shallowest depth recorded was 15.3 mm (0.6 in.) below the top of crosstie and occurred when a lateral load of 1,000 lb. (4.4. kN) was applied; a load that would not lead to fatigue failures. These data demonstrate that the maximum stress depth is dependent on the load magnitude, load direction, and timber species.

Timber species had a substantial effect on the maximum stress magnitude and location (Figure 3.6 - 3.9). Therefore, timber selection used in conjunction with elastic fastening systems is critical. Additionally, as has been indicated within the industry, not all hardwoods are equivalent; and therefore, simply specifying a “hardwood” will not ensure acceptable results. As the value of critical mechanical properties of the timber increase, the spike stress will decrease and the depth to maximum stress will become shallower.

When used in conjunction with premium fastening systems, railroads should specify hardwood timber with compressive, tensile, and shear strength properties that are as high as is feasible given sourcing options and economic considerations. This will help delay premature failure of the timber which in turn leads to excessive deflections and spike stresses.

3.7 Conclusions

In this chapter I developed and validated a 3D FEM consisting of a single cut-spike fastener and timber crosstie block. The model was validated using laboratory data and the outputs were representative of field performance, with the depth to maximum stress consistent with broken spikes observed in the field.

The results from the study also indicate that timber species affects the maximum stress magnitude and location. Consequently, use of premium fastening systems should include consideration of the effect of timber species on possible spike fatigue failure. Additionally, hardwood species differ in key characteristics, therefore, simply specifying a hardwood will not ensure acceptable results. Thus, the value of critical mechanical properties of the timber are increased, spike stress will decrease and the depth to maximum stress will be reduced. Hardwood timber used in conjunction with premium fastening systems should ensure that the compressive, tensile, and shear strength properties are as high as is feasible given source options and economic considerations. This will help delay premature failure of the timber, which in turn leads to excessive deflections and spike stresses. Additional research is needed to quantify recommended values. Additional findings from this study include:

- When longitudinal and lateral loads are applied at equal magnitudes, the fatigue strength of the spike can be exceeded with a load of only 1,500 lb. (6.7 kN) in each direction.
- Longitudinal load had a more detrimental effect on spike stress state than lateral load.
 - To exceed the fatigue strength of the cut spike, a longitudinal load 30% lower than a lateral load (2,000 lb. (8.9 kN) vs. 2,750 lb. (12.2 kN)) is required.
- Loading direction had a significant effect on maximum stress depth.
 - When only longitudinal load was applied, the depth of maximum stress could be up to two times deeper than when lateral load only was applied.
- Timber species had a substantial effect on the magnitude and depth of maximum stress.
 - It is hypothesized that the timber mechanical properties driving this are compressive, tensile, shear, and rolling shear strengths.

4 ANALYTICAL METHOD FOR DETERMINING SPIKE STRESS

In this chapter I present the development and validation of an analytical model based on beam on elastic foundation (BOEF) principles for accurate and economical quantification of spike stress magnitude. This model can be used as both an analysis and design tool, informing and improving future design decisions. A paper related to this chapter was published in *Transportation Research Record (TRR)*³ in 2020.

4.1 Motivation

As stated in previous chapters, spikes have experienced fatigue failures resulting in at least 12 derailments since 2000. To improve safety and the state of good repair, tools are needed to analyze and understand how various design changes could mitigate or prevent such failures. Multiple approaches should be pursued to quantify the magnitude and distribution of stress in spikes driven into timber cross-ties. The methods commonly used by the rail industry to analyze and quantify the spike stress state, or test the adequacy of new fastening system components include: finite element modeling (FEM) (Chen et al., 2014; Chen et al., 2016; Chen and Andrawes, 2017; Edwards et al., 2018a; Dersch et al., 2019), standardized laboratory testing (AREMA, 2017b), or field-experimentation and testing programs (Akhtar et al., 2012; McHenry and LoPresti, 2015; McHenry and LoPresti, 2016; Edwards et al., 2017a; LoPresti, 2018). These methods can be costly in terms of both time and expense, especially full-scale field-testing programs and laboratory test programs that include many replicates. Given the complexities and time required for prototyping, a limited number of design solutions can be tested in the

³ Dersch, M.S., M. Trizotto Silva, J.R. Edwards, A. de O Lima and T. Roadcap. 2020. Analytical method to estimate railroad spike fastener stress. *Transportation Research Record (TRR): Journal of the Transportation Research Board*. doi:10.1177/0361198120949259

laboratory, and even fewer can be tested in the field. Consequently, a common approach employed by researchers is to develop FEMs to perform an analysis of the key input variables affecting a given result (output). Despite their benefits, the development, execution, and validation of FEMs require special care and expertise, the absence of which can lead to inaccurate results (Kaewunruen et al., 2016).

4.2 Technical Approach

The analysis of laterally loaded, driven piles is rooted in BOEF mechanics as proposed by Winkler (1867). The methodology I propose in this chapter uses a similar approach as presented by Long (2011). Though not used in foundation design, Kerr (2003) leverages mechanics principles in his methods for analytically assessing the track structure and its response to load. Using the analysis method I propose in this chapter, the resulting displacement, shear, bending moment, and/or slope of a beam (pile or spike) subjected to lateral loading can be quantified. Applying these to a spike, the lateral loading is analogous to a force generated by a wheel load that passes through the rail and tie plate and into the top of the spike. This analysis must consider that the surrounding medium (soil or timber) reaction (resistance) is dependent on the beam's movement. In turn, the beam's movement is dependent on the response of the surrounding medium. As such, it is an interaction problem between the beam and medium; and in the specific case of my research, the steel spike and timber. The following sections will describe the development of equations to analyze the spike behavior and then detail the equations for analyzing the timber's response.

The solution to the interaction problem of a spike loaded perpendicular to a given timber face (laterally or longitudinally) follows the p-y method commonly used by engineers to quantify

the deflection of a laterally loaded pile in soil (FHWA, 2006). Unless otherwise referenced, and regardless of the direction of the load application (lateral or longitudinal), I will assume the general loading case to be a laterally loaded spike. A visual representation of the interaction between the spike and timber used to develop the analytical solution is like the BOEF approach proposed by Winkler (Figure 4.1). The timber is continuous and a deformation at any point will cause a deformation at all other points. I assume that the interaction is a set of discrete, independent springs and my results will demonstrate that this assumption is sufficient for this analysis.

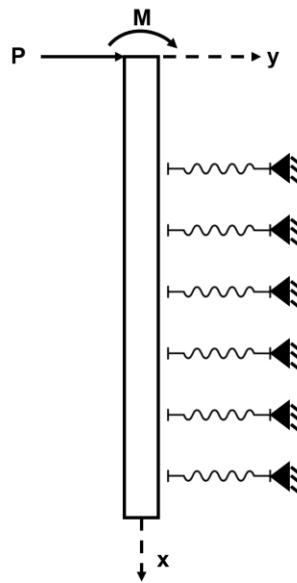


Figure 4.1: Visual representation of mathematical setup to model interaction of spike with surrounding timber medium when subjected to lateral loading from tie plate

The resulting behavior of a laterally loaded spike can be solved using differential equations that describe the relationship between bending moments and curvature. The problem can be solved assuming the spike and timber remain in equilibrium and are compatible via appropriate boundary condition assumptions. If all assumptions can be maintained, then a solution for the

spike response can be developed along the entire length of the spike. If assumptions are not met (e.g. permanent deformation of the timber occurs, spike experiences yielding, etc.), then the closed form solution will no longer be applicable. Therefore, care must be taken when applying this analytical approach to various problems.

For this analysis, the following assumptions must be satisfied:

- The spike is straight and has a uniform cross section
- The spike has a longitudinal plane of symmetry and loads and reactions are in that plane
- The spike material is homogeneous
- The proportional limit of the spike material is not exceeded
- The modulus of elasticity of the spike is the same for tension and compression
- Transverse deflections of the spike are small
- The spike is not subjected to dynamic loads
- Deflections due to shearing stresses are negligible

In this analysis I assumed that plane sections remain plane as the spike is loaded and the slope, dy/dx , is very small. The relationship between moment, M , and curvature, ϕ , (Equation 4.1) can be applied and an expression for ϕ in terms of x and y (Equation 4.2) where the x -axis is the axis of the unloaded spike, the y -axis is the lateral deflection of the spike, E is the modulus of elasticity, and I is the area moment of inertia.

$$\phi = \frac{M}{EI} \quad \text{Eq. 4.1}$$

$$\phi = \frac{d^2y}{dx^2} \quad \text{Eq. 4.2}$$

When combining Equations 4.1 and 4.2, I arrive at the desired differential equation considering the spike moment, M , (Equation 4.3). Next, equations for spike shear, V , (Equation 4.4) and timber reaction, p , (Equation 4.5) can be developed.

$$\frac{M}{EI} = \frac{d^2y}{dx^2} \quad \text{Eq. 4.3}$$

$$\frac{V}{EI} = \frac{d^3y}{dx^3} \quad \text{Eq. 4.4}$$

$$\frac{p}{EI} = \frac{d^4y}{dx^4} \quad \text{Eq. 4.5}$$

A spike's response to lateral loads using a full analysis that considers a simply supported beam with uniform loading can be summarized visually (Figure 4.2). A complete derivation of the equations is provided by Hetenyi (1946).

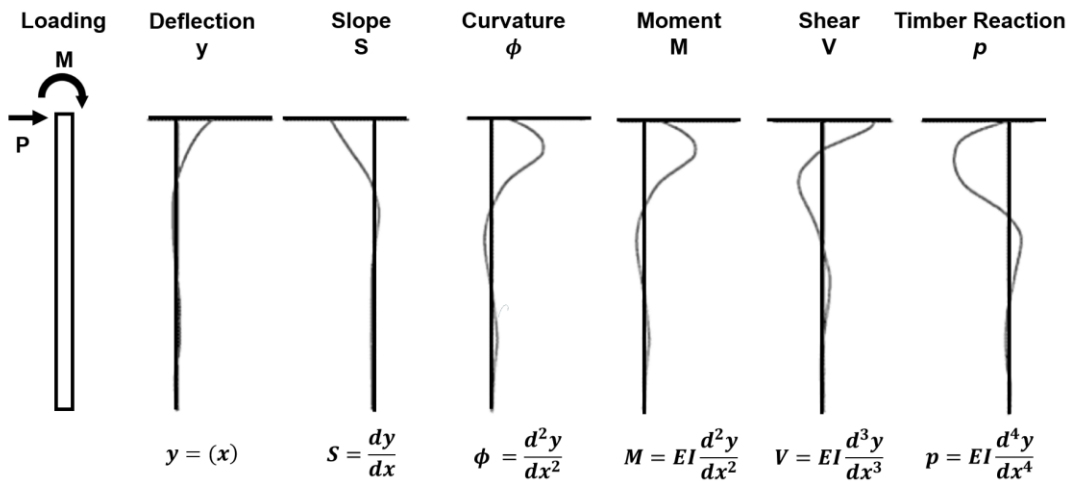


Figure 4.2: Visual representation of spike response to loading, with accompanying equations to calculate parameters

Understanding timber's response to load is critical to developing an accurate method to analyze spike response. The timber's response can be characterized as a set of discrete springs as suggested by Winkler (1867). A spike inserted into a wood crosstie (Figure 4.3a) will initially have a uniform stress distribution before any lateral load is applied (Figure 4.3b). If a lateral load is applied, the stress distribution will be altered (Figure 4.3c). Integration of this altered stress distribution produces a force per unit length along the spike (p). The variable p is defined as the timber reaction and acts in the opposite direction to the spike deflection, y ; hence the naming convention for p - y curves.

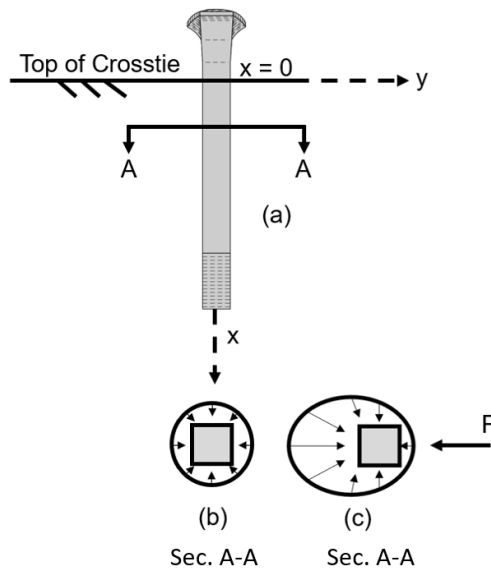


Figure 4.3: View of a spike after installation (a), with representations of forces on the spike in the unloaded condition (b), and the condition with a lateral or longitudinal load (c)

To apply these methods, no shear stress can be present at the surface of the spike acting parallel to the y -axis. Additionally, spike lateral resistance and moment can be accounted for by a p - y curve on the side near the timber crosstie surface. No adjustment is made for the effects of the spike installation. I assumed that the effects of spike installation are principally confined to

an area close to the spike whereas the timber reacting against the spike is several spike diameters greater in size. I considered the errors due to violation of these assumptions to be minimal and reasonable. Some spikes can be pulled out by hand, indicating that the reaction from installation is not permanent (Dersch et al., 2019).

I developed experimental moment curves using data recorded by strain gauges installed on spikes that were subsequently driven into timber crossties and loaded laterally. Timber is orthotropic (Green et al., 1999) thus loading direction is a critical parameter. Perpendicular to the grain (Figure 3.3), timber strength and modulus are approximately ten percent of the same values parallel to grain (Green et al., 1999). Therefore, the lateral load was applied perpendicular to the grain because this results in higher magnitude spike stresses (Dersch et al., 2019).

The computation of the timber's reaction along the length of the spike involves two differentiations of a bending moment curve. Matlock (1970) performed this differentiation for piles driven in soil. p - y curves can then be plotted when multiple curves representing the distribution of deflection and soil reaction are obtained.

Once the differential equations are developed and the timber's reaction is understood, the full derivation of the solution to the differential equations can be completed. The solution can consider the spike length as either an "infinite" or "finite" beam. In either case, I made the following assumptions:

- the spike is supported along its entire length;
- the timber's reaction, p , per unit length of spike is related to the deflection, y , by the timber modulus, E_t ,

- uniform timber modulus (Figure 4.4);
- the spike modulus, E, and cross-section are consistent.

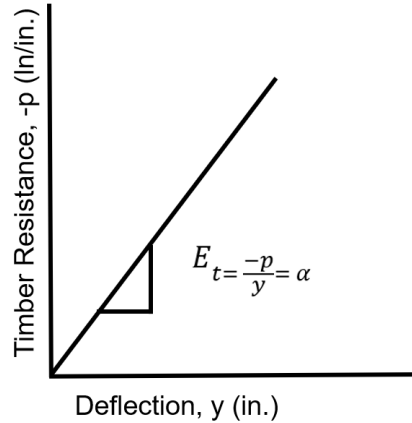


Figure 4.4: Constant timber modulus results from relationship between reaction and deflection, and constant, uniform cross-section assumptions

Considering the relationship between the timber reaction, p, and spike deflection, y, and using basic identities, Equation 4.6 was derived.

$$\frac{d^4y}{dx^4} + 4\beta^4y = 0 \quad \text{Eq. 4.6}$$

where β is the relative stiffness factor. Manipulation of Equation 4.6, while employing Equations 4.3 – 4.5, produces the basic differential equations for slope, moment, shear, and timber reaction (Equations 4.7 – 4.10).

$$\begin{aligned} \frac{dy}{dx} = & \beta e^{\beta x}(\overline{C}_1 \cos(\beta x) + \overline{C}_2 \sin(\beta x) - \overline{C}_1 \sin(\beta x) + \overline{C}_2 \cos(\beta x)) \\ & + \beta e^{-\beta x}(-\overline{C}_3 \cos(\beta x) - \overline{C}_4 \sin(\beta x) - \overline{C}_3 \sin(\beta x) + \overline{C}_4 \cos(\beta x)) \end{aligned} \quad \text{Eq. 4.7}$$

$$\frac{d^2y}{dx^2} = 2\beta^2 e^{\beta x} (\overline{C}_2 \cos(\beta x) - \overline{C}_1 \sin(\beta x)) + 2\beta^2 e^{-\beta x} (\overline{C}_3 \sin(\beta x) - \overline{C}_4 \cos(\beta x)) \quad \text{Eq. 4.8}$$

$$\frac{d^3y}{dx^3} = 2\beta^3 e^{\beta x} (\overline{C}_2 \cos(\beta x) - \overline{C}_1 \sin(\beta x) - \overline{C}_2 \sin(\beta x) - \overline{C}_1 \cos(\beta x)) + 2\beta^3 e^{-\beta x} (-\overline{C}_3 \sin(\beta x) + \overline{C}_4 \cos(\beta x) + \overline{C}_3 \cos(\beta x) + \overline{C}_4 \sin(\beta x)) \quad \text{Eq. 4.9}$$

$$\frac{d^4y}{dx^4} = 4\beta^4 e^{\beta x} (-\overline{C}_2 \sin(\beta x) - \overline{C}_1 \cos(\beta x)) + 4\beta^4 e^{-\beta x} (-\overline{C}_3 \cos(\beta x) - \overline{C}_4 \sin(\beta x)) \quad \text{Eq. 4.10}$$

where;

$C_1, C_2, C_3,$ and C_4 are the coefficients to be evaluated at the given boundary conditions.

To solve for these coefficients, the spike length must be classified as either finite or infinite relative to the timber. For the spike to be considered infinite in length, the relationship in Equation 4.11 must be satisfied, which requires Equation 4.12.

$$\beta L \geq 4 \quad \text{Eq. 4.11}$$

$$\beta = \sqrt[4]{\frac{\alpha}{4EI}} \quad \text{Eq. 4.12}$$

where,

β is the relative stiffness factor.

L is the length of spike in the timber crosstie.

E is the elastic modulus of the spike.

I is the area moment of inertia of the spike.

α is the modulus of the timber, E_t .

Rearranging these equations results in Equation 4.13, that quantifies the timber modulus, E_t , threshold for determining what spike embedment length, L, would be infinite or finite. This is possible when assuming the spike modulus, E, cross-section, and length of the spike driven into the crosstie, are constant and dependent on spike position (i.e. hold-down or line spikes).

$$E_t \geq \left(\frac{4}{L}\right)^4 \times 4EI ; \text{infinite} \quad \text{Eq. 4.13}$$

For a spike with a length of 6.0 in. (152.4 mm), L will be approximately 5.00 in. (127.0 mm) for hold-down spikes, or 4.20 in. (106.7 mm) for line spikes (AREMA, 2017a). I assumed that the E and I for the steel used to manufacture the standard 0.625 x 0.625 in. (15.9 x 15.9 mm) spike was 29,000 ksi (200 GPa) and 0.0127 in.⁴ (5,300 mm⁴), respectively. Therefore, the timber modulus must be greater than or equal to approximately 604 ksi (4.16 GPa) for hold-down spikes and approximately 1,213 ksi (8.36 GPa) for line spikes to be considered infinite. According to Green et al. (1999) the modulus of timber perpendicular to grain ranges from 50 – 250 ksi (0.345 – 1.72 GPa) and parallel to grain ranges from 800 – 2,300 ksi (5.52 – 15.9 GPa), so a standard 6 in. (152 mm) spike will be classified as finite when the loading is applied perpendicular to the grain. If the spike length were increased such that the allowable timber modulus was satisfactory (Equation 4.13) (i.e. 7 in. (178 mm) spike), then an “infinite” analysis could be considered.

The key differences between the solutions for a finite and infinite beam are traceable to the assumptions that are made when preparing the solutions to the differential equations. Table 4.1 lists the boundary conditions for each condition.

Table 4.1: Spike in elastic medium governing differential equations and boundary conditions

		Boundary Conditions	
		x = 0	x = L
Finite	$\frac{dy^2}{dx^2} = \frac{M}{EI}$		$\frac{dy^2}{dx^2} = 0$
	$\frac{dy^3}{dx^3} = \frac{P}{EI}$		$\frac{dy^3}{dx^3} = 0$
Infinite	$\frac{dy^2}{dx^2} = \frac{M}{EI}$		n/a
	$\frac{dy^3}{dx^3} = \frac{P}{EI}$		n/a

With these boundary conditions, the coefficients of the differential equations listed previously for deflection, slope, moment, shear, and timber reaction can be determined for both finite and infinite beams. The equations for infinite beams are comparatively simple and are presented as Equations 4.14 – 4.18 below.

$$y = \frac{e^{-\beta x}}{2\beta^2 EI} \left[\frac{P_t}{\beta} \cos(\beta x) + M_t (\cos(\beta x) - \sin(\beta x)) \right] \quad \text{Eq. 4.14}$$

$$S = -e^{-\beta x} \left[\frac{2P_t \beta^2}{E_s} (\cos(\beta x) + \sin(\beta x)) + \frac{M_t}{EI\beta} \cos(\beta x) \right] \quad \text{Eq. 4.15}$$

$$M = e^{-\beta x} \left[\frac{P_t}{\beta} \sin(\beta x) + M_t (\cos(\beta x) + \sin(\beta x)) \right] \quad \text{Eq. 4.16}$$

$$V = e^{-\beta x} [P_t (\cos(\beta x) - \sin(\beta x)) - 2M_t \beta \sin(\beta x)] \quad \text{Eq. 4.17}$$

$$p = 2\beta e^{-\beta x} [-P_t \cos(\beta x) - M_t \beta (\cos(\beta x) - \sin(\beta x))] \quad \text{Eq. 4.18}$$

The equations for finite beams, however, are non-trivial to derive because the methods to solve for the coefficients are more complex (Table 4.2).

Table 4.2: Equations to solve for coefficients for finite beams

$C_1 = 2C_2 + C_3 - A_{15}$	$C_2 = \frac{A_{22}}{A_{20}} - \frac{A_{21}}{A_{20}} C_3$	$C_3 = \frac{A_{26}}{A_{27}}$	$C_4 = C_2 - A_1$
$A_1 = \frac{M_t}{2\beta^2 EI}$	$A_2 = \frac{V_t}{2\beta^2 EI}$	$A_3 = 2\beta^2 e^{\beta L} \cos(\beta L)$	$A_4 = 2\beta^2 e^{\beta L} \sin(\beta L)$
$A_5 = 2\beta^2 e^{-\beta L} \cos(\beta L)$	$A_6 = 2\beta^2 e^{-\beta L} \sin(\beta L)$	$A_7 = \beta A_3$	$A_8 = \beta A_4$
$A_9 = \beta A_5$	$A_{10} = \beta A_6$	$A_{11} = A_7 + A_8$	$A_{12} = A_7 - A_8$
$A_{13} = A_9 - A_{10}$	$A_{14} = A_9 - A_{10}$	$A_{15} = A_1 + A_2$	$A_{16} = A_3 - A_5$
$A_{17} = A_1 A_5$	$A_{18} = A_{12} + A_{14}$	$A_{19} = A_1 A_{14}$	$A_{20} = A_{16} - 2A_4$
$A_{21} = A_6 - A_4$	$A_{22} = A_{17} - A_4 A_{15}$	$A_{23} = A_{13} - 2A_{11}$	$A_{24} = A_{13} - A_{11}$
$A_{25} = A_{19} - A_{11} A_{15}$	$A_{26} = A_{25} - \frac{A_{22} A_{23}}{A_{20}}$	$A_{27} = A_{24} - \frac{A_{21} A_{23}}{A_{20}}$	

4.3 Model Validation, Results, and Discussion

The instrumented spike strain data described in Chapter 3 were used to validate this analytical approach. Moments at each location along the spike were plotted against the moments calculated via the analytical approach presented considering a finite spike for the load applied perpendicular to the grain. A 1,500 lb. (6.67 kN) force was applied over an area of 0.50 in.² (322 mm²) in the analytical model that was representative of the loading fixture and is similar to the contact area of a tie plate for a hold-down spike. The modulus perpendicular to the grain was assumed to be 200 ksi (1.38 GPa), which is consistent with the value used in the validated FEM presented in Chapter 3. I compared the laboratory experimental and analytical model results while considering the spike yield strength and fatigue limit, defined as 50% of the ultimate tensile strength (Figure 4.5).

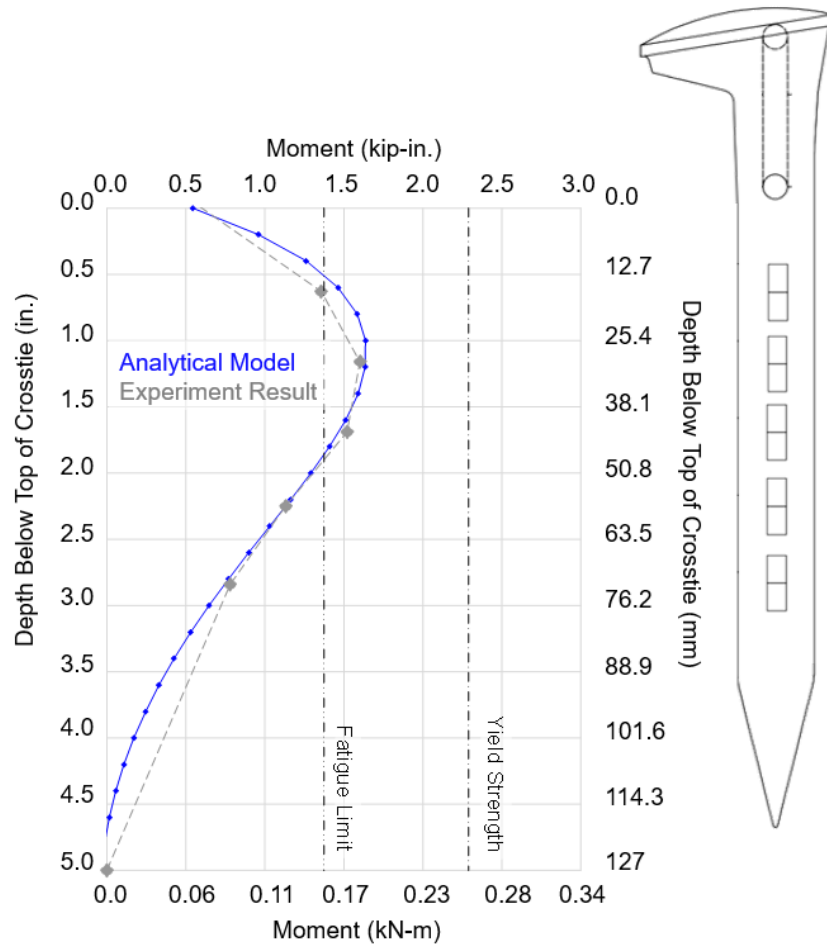


Figure 4.5: Comparison of experimental spike stress (laboratory) data with analytical model results

The results demonstrate good agreement between $x = 0.0$ and $x = 3.0$ in. (76.2 mm) below the top of the crosstie. The difference between the analytical model and the laboratory results is near a minimum at a depth of 1.5 in. (38.1 mm) which I consider to be the most critical depth given that this is where most spike failures are found (Dersch et al., 2019). The moment values beyond approximately 3.0 in. (76.2 mm) below the top of the crosstie do not match as well. This may be due to the assumed location of zero moment established for the laboratory condition. This region is not considered as critical given it is not the area of maximum moment, nor is it where failures are observed in the field. The resulting moments also exceed the fatigue limit

from approximately 0.5 – 1.9 in. (12.7 – 48.3 mm) below the top of the crosstie, which provides additional insight into why the spikes show variation in the depth of failure. This analytical approach provides an accurate means for analyzing the stress along the depth of the spike driven into timber crossties within a reasonable range of loading conditions, and beyond load levels that would likely result in fatigue failures.

4.4 Case Studies

Long (2011) suggests that the three factors having the greatest effect on a p-y curve are timber properties, spike geometry, and the nature of loading. Therefore, the following subsections of this chapter document the effects of timber modulus, spike cross-sectional area, and load magnitude on the magnitude and locations of the maximum bending moment. All data are reported in relation to the spike fatigue limit and yield strength as previously demonstrated by Dersch et al. (2019).

4.4.1 Effect of Timber Modulus

Given that this analytical approach cannot account for permanent deformation of the timber, the elastic modulus was the primary parameter studied, and was used in-lieu of compressive strength. Further, given that the analytical approach was validated at 1,500 lb. (6.67 kN), this loading magnitude was held constant at each modulus value. I investigated modulus values of 100, 200, and 500 ksi (0.689, 1.38, and 3.45 GPa) (Figure 4.6). I selected 100 ksi (0.689 GPa) as a practical lower bound for the modulus of the timber perpendicular to the grain and 500 ksi (3.45 GPa) as the upper bound because this was the level in which spike stresses fell below the fatigue limit. Further, this value aligns with the modulus of glass fiber reinforced

composite (GFRC) crossties (Gao and LoPresti, 2020; Khachaturian et al., in review), which could be used as a substitute for timber. Finally, though 500 ksi (3.45 GPa) is below the 800 ksi (5.52 GPa) lower bound for the modulus of timber parallel to grain, as mentioned previously, general trends can be found using this range.

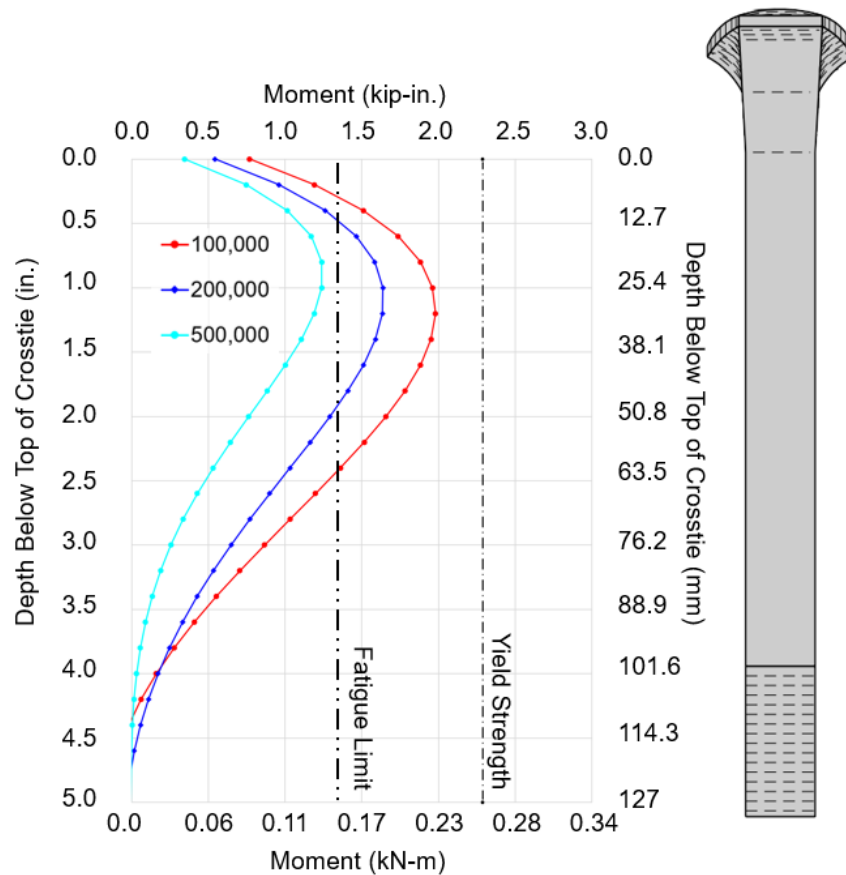


Figure 4.6: Dependency of moment on timber modulus (psi) and depth below top of crosstie

The results indicate an inverse relationship between timber modulus and maximum spike stress (e.g. as timber modulus is decreased, the maximum spike moment increased), as load is held constant. This result aligns with previous findings by Dersch et al. (2019) that loading perpendicular-to-grain (higher modulus) is more detrimental than loading parallel-to-grain. I hypothesize that spikes fail more often in new, stiffer crossties because they take a greater share

of the applied load than older, softer crossties that might not be well-engaged in the load path. Therefore, when there is a differential in crosstie stiffness, fastener loading demands on new crossties would be greater than older crossties. However, if all crossties exhibit a uniform stiffness, as modulus decreases, the spike moment increases.

The moments for the 100 and 200 ksi (0.689 and 1.38 GPa) cases both exceed the fatigue limit, indicating fatigue failures could occur if this load magnitude were regularly experienced in the field. The moment for the 500 ksi (1.38 GPa) case fell below the fatigue limit. Given 500 ksi (1.38 GPa) produces moments below the fatigue limit, and lateral loads applied parallel to grain would be resisted by timber with modulus values greater than 800 ksi (5.52 GPa), fatigue failures would not be expected unless load magnitudes were increased. This provides insight into the lack of spike failures in traditional fastening systems that do not use elastic fasteners.

Also, as the modulus is reduced, the location of maximum moment (i.e. failure location), would become deeper in the crosstie; moving from approximately 1.00 to 1.25 in. (25.4 mm to 31.8 mm) below the crosstie surface. As a spike breaks deeper in a crosstie, there is a greater likelihood it would become harder to detect and a greater risk to the safety of railroad operations. Therefore, specifying a crosstie with a greater modulus increases the likelihood that failure would occur closer to the surface and thus could be more easily identified during track inspection.

4.4.2 Effect of Spike Cross-Sectional Area

I studied the effect of spike cross-sectional area by varying the width, while maintaining a square cross-section. Spike geometry is likely the easiest parameter to change/control in the design of future fastening systems. The timber modulus was held constant at 200 ksi (1.38 GPa)

given that this had been validated in the laboratory. A standard cut spike is 0.625 in. x 0.625 in. (15.9 x 15.9 mm) while the smallest hole in a plate is 0.690 in. (17.5 mm) and the largest is 0.750 in. (19.1 mm). Therefore, to limit the requirement to change every spike hole size, while also attempting to limit the risk of tie splitting, square spikes with widths of 0.500, 0.625, and 0.700 in. (12.7, 15.9, and 17.8 mm) were investigated (Figure 4.7).

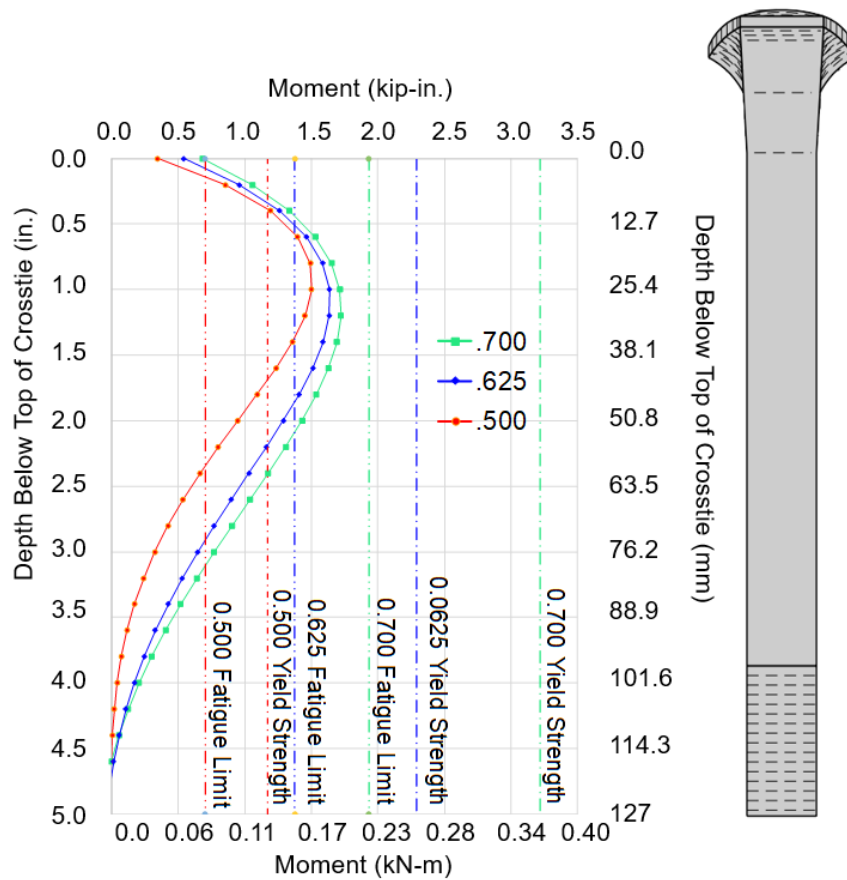


Figure 4.7: Dependency of moment on spike width and with depth, with associated moments required for steel fatigue and yield limits

As spike width increases, the moment also increases from 1.5 kip-in. (0.169 kN-m) to 1.72 kip-in. (0.194 kN-m). This is attributed to the increased reaction from the timber as the width increases from 0.500 to 0.700 in. (12.7 to 17.8 mm). Though the moment increases, the fatigue

limit and yield strength (i.e. capacity) is increasing at a greater rate; 1.17 kip-in. to 1.93 kip-in. (0.132 to 0.218 kN-m) and 3.22 kip-in. (0.364 kN-m), respectively. In the cases considered, the following “reserve” capacities (moment at yield/moment calculated at 1,500 lb. (6.67 kN)) were found to be 0.8, 1.4, and 1.9 for 0.500 in., 0.625”, and 0.700” (12.7, 15.9, and 17.8 mm) widths, respectively. Further, as the width is increased to 0.700 in (17.8 mm), the fatigue limit of the spike is no longer exceeded at this applied load.

Finally, as width is increased, the depth to maximum moment shows a slight increase. That is, as the width increased from 0.500 in. to 0.700 in. (12.7 to 17.8 mm), the depth increased from 1.0” to 1.2” (25.4 to 30.5 mm). This effect was less than timber modulus, and thus not considered as concerning given the safety factor is also increased. Therefore, increasing spike width could increase the resiliency of these fastening systems and reduce the risk of spike failure.

4.4.3 Effect of Load Magnitude

The last parametric study I performed was quantifying the effect of load magnitude. I varied the load from 500 to 2,500 lb. (2.2 to 11.1kN, while maintaining a constant timber modulus of 200 ksi (1.38 GPa) and spike width of 0.625 (15.9 mm) (Figure 4.8). It is intuitive that increasing load magnitude would increase the resulting moment. However, I investigated this parameter to provide additional confidence in this analytical approach by comparing the results to published finite element analysis (FEA) results as well as understanding how the depth of maximum moment changes with load.

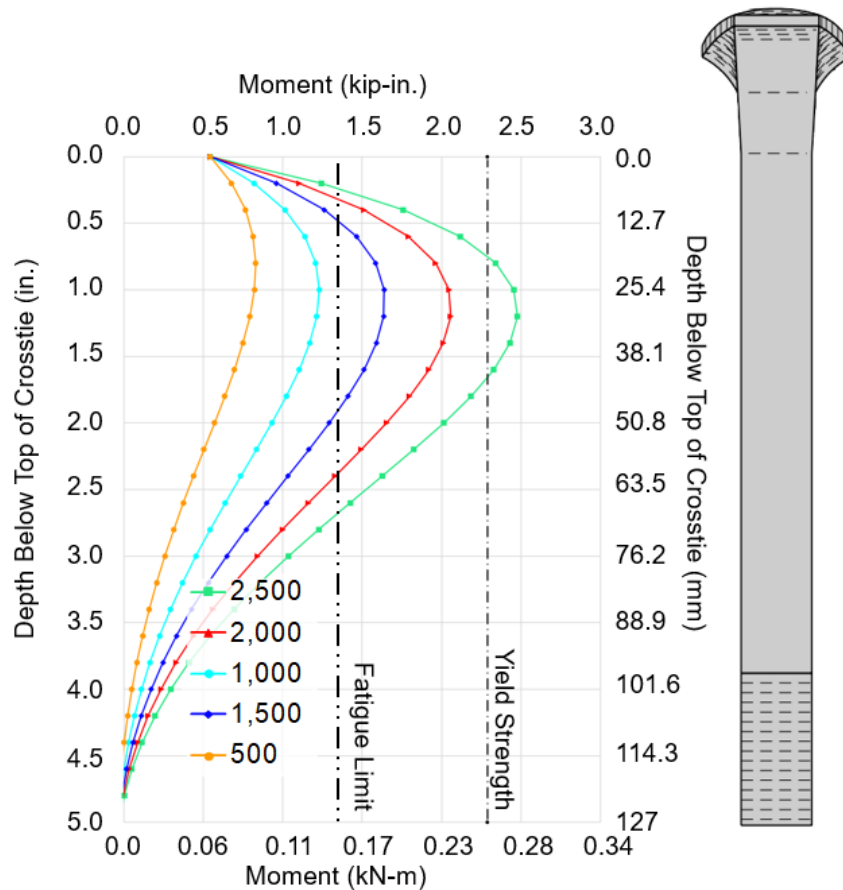


Figure 4.8: Dependency of moment on input force and with depth from the tie plate

As the applied load was increased, the maximum moment also increased. The load at which the spike exceeded the yield stress here is similar to what was reported as a part of more detailed and validated FEA study by Dersch et al. (2019) (i.e. between 2,000 and 3,000 pounds (8.90 and 13.3 kN)). This provides more confidence in the results from the analytical solution. The fatigue limit would be exceeded with a load magnitude between 1,000 and 1,500 pounds (4.45 and 6.65 kN), further indicating the sensitivity of spike stress to loading applied perpendicular to the grain.

The depth to maximum stress also increased from 0.8 in. to 1.2 in. (20.3 to 30.5 mm), respectively. The depth to maximum moment, using this analytical approach, is shallower than

would be expected based upon the field failures and FEA results (i.e. 1.4 and 1.6 in. (35.6 and 40.6 mm) below the top of the crosstie). Therefore, while this model can estimate the demand on the spike to a reasonable range, the depth to maximum demand could be improved. This may be attributed to the fact that this analytical model does not account for timber behavior beyond its elastic limit (i.e. timber crushing).

4.5 Conclusions

In this chapter I presented the development and validation of an analytical model leveraging BOEF principles. This analytical model can accurately and economically analyze the effect of design variables (e.g. timber type and spike size) on component stress thereby providing insight into responses required for a mechanistic-empirical (M-E) design process.

This method was applied in several case studies that were designed to quantify the effect of key variables on spike stress. The results from these studies demonstrate that the model can be used to improve fastener resiliency and railway safety through revised design recommendations. Furthermore, while this study only investigated uni-direction loading, the findings can be generalized to account for bi-directional loading. That is, regardless of loading direction, reduced in modulus, reduced spike size, or increased load, will lead to increased spike demands. The findings from this research and the model generated are summarized as follows:

- A validated analytical model has been developed and used to answer design-related questions that can lead to improved component and track resiliency
- As timber modulus increased (100 to 500 ksi) the:

- induced bending moments decreased (1.98 to 1.24 kip-in. (0.223 to 0.140 kN-m))
- depth to maximum stress decreased (1.2 to 0.8 in. (30.5 to 20.2 mm))
- spike fatigue limit was not exceeded when timber modulus exceeded 500 ksi.
- As spike width is increased (0.500 to 0.700 in. (12.7 to 17.8 mm)), the:
 - factor of safety for spike fatigue failures increased (0.8 to 1.9) at a greater rate than the induced bending moment (1.50 to 1.72 kip-in. (0.169 to 0.194 kN-m)) leading to increased resiliency
 - fatigue limit would no longer be exceeded above 0.700 in. (17.8 mm) for this load case
 - depth to maximum stress does not significantly increase (1.0 to 1.2" (25.4 to 30.5 mm)).
- As loads applied perpendicular to the timber grain increase (500 to 2,500 lbs), the:
 - induced bending moments would increase (0.83 to 2.48 kip-in. (0.093 to 0.280 kN-m))
 - the depth to maximum stress also increases (0.8 to 1.2" (20.2 to 30.5 mm)).

Therefore, to reduce spike stress and fatigue failures, when feasible based on economics, logistics, and other factors, railroads could ensure that timber crossties installed with premium elastic fasteners in demanding locations had higher moduli, could increase the size of spikes installed, and/or, reduce the longitudinal and lateral loads through proven methods (e.g. distributed power and top-of-rail friction modification). Future work could include further model refinement and validation to provide greater applicability to a wider range of problems.

Additionally, this method can be used to conduct additional case studies to further improve upon the recommendations for improved spike resiliency.

5 INVESTIGATION OF METHODS TO MITIGATE RAILWAY SPIKE FATIGUE FAILURES USING FINITE ELEMENT ANALYSIS

In this chapter I present the extension of the 3D finite element model (FEM) developed and introduced in Chapter 3 and used to quantify the relationships between important fastening system design variables and spike stress. This chapter presents data that can be used to develop formal design recommendations based on mechanistic-empirical (M-E) principles to reduce fastener fatigue failures. A paper related to this chapter was published in *Engineering Failure Analysis*⁴ in 2021.

5.1 Introduction

There are many feasible timber crosstie elastic fastening system designs as described in the M-E design framework in Chapter 1 (Figure 1.1). These designs vary in type and geometry of spike used (cut versus screw), quantity of spikes installed per tie plate (four versus five), use of anchors, as well as the type and dimension of the tie plate, shoulder, and elastic fastener (e-clip, tension clamp, etc.) used. Though feasible, none have proven to be an optimal design based on their field performance. Furthermore, given limited research in this area, there are currently no formal recommendations (mechanistic or empirical) for how to mitigate spike fatigue failures.

Therefore, in this chapter I provide data that could be implemented in future fastening system designs to eliminate the fatigue failures through spike stress reductions. I accomplished this by investigating methods to reduce the spike stress state using 3D finite element analysis (FEA) leveraging a validated model I presented in Chapter 3.

Methods to mitigate spike stresses considered within this chapter include:

⁴ Dersch, M., C. Khachaturian and J.R. Edwards. in review. Methods to mitigate railway premium fastening system spike fatigue failures using finite element analysis. *Engineering Failure Analysis*.

- spike cross-sectional area,
- spike type (cut vs. screw),
- spike loading location,
- tie plate normal (vertical) hold-down force, and
- spike engagement with plate and number of spikes in a given fastening system.

5.2 Methods Theory

The methods investigated in this chapter are not exhaustive. For example, recent studies have investigated the effect of crosstie material, loading direction, or fastener stiffness (Yu and Liu, 2019; Dersch et al., 2019; Dersch et al., In Review; Khachaturian et al., In Review; Khachaturian et al., in review), and thus were not the focus of this study. The following subsections provide engineering reason and justification for the fastening system studies considered.

5.2.1 Spike Cross-Sectional Area

As discussed in Chapter 4, given this is a flexural fatigue problem, the maximum bending stress considering Euler-Bernoulli beams is related to both the demand on the spike and its geometry (Equation 5.1). Therefore, reductions in stress would result from decreasing the bending moment, increasing the distance from the outermost surface of the spike to the neutral axis, and/or increasing the moment of inertia of the spike.

$$\sigma = My/I \quad \text{Eq. 5.1}$$

where,

σ is the maximum normal stress.

M is the bending moment.

y is the distance from the neutral axis.

I is the area moment of inertia.


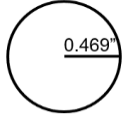

Increasing the cross-sectional area of the spike would reduce the maximum spike stress given it increases the ratio of the distance from the neutral axis to the area moment of inertia. Though this is an obvious solution based on mechanics, the FEA results below quantify the effectiveness of this solution.

5.2.2 Spike Type (Cut vs. Screw)

Although failures of both systems have been observed in the field, multiple Class I heavy axle load (HAL) railroads are transitioning from cut spikes to screw spikes, but conversely at least one railroad has recently switched from screw spikes to cut spikes (Roadcap et al., 2019b). I first performed a preliminary comparison of the geometry and resulting bending stress as a function of moment (M) (Table 5.1). The moment of inertia is largest for the screw spike upper shaft, and smallest at the screw-spike threads. Calculated stresses, given an equivalent applied moment, indicate that the threaded portion of the screw spike would experience stress magnitude more than 25% higher than the standard cut spike. This is consistent with field measurements indicating that cut spikes fail at an average depth of 1.5 in. (38.1 mm) below the top of crosstie

while screw spikes fail near the first two threads of the threaded region, at a depth of approximately 2 in. (50.8 mm) (Dick et al., 2007; Dersch et al., 2019).

Table 5.1: Comparison of geometric characteristics and resulting demands on standard cut and screw spikes

Spike (type/location)	Cut	Screw (Upper Shaft)	Screw (Threads)
Cross Section			
Area Moment of Intertia Formula	$bh^3/12$	$\pi r^4/4$	$\pi r^4/4$
I (in⁴)	0.0127	0.0380	0.0110
y (in.)	0.3125	0.4690	0.3438
Stress (force/in²)	$24.6 \times M^*$	$12.3 \times M^*$	$31.3 \times M^*$

*where M represents the internal moment in force-in.

5.2.3 Plate Normal (Vertical) Hold-down Force

Roadcap et al. (2019b) hypothesized that plate friction, or lack thereof, plays a critical role in determining the magnitude of spike stresses. As friction is lost due to rail and plate uplift, all longitudinal force is transferred to the spike. In the early 20th century, the Tie Committee of American Railway Engineering Association (AREA) (the predecessor organization to the American Railway Engineering and Maintenance-of-Way Association (AREMA)) recommended that there should be no movement between the crosstie and plate and that there should be a firm connection between the crosstie and plate (Kerr, 2003a). While cut spikes are not designed to provide any plate-to-crosstie hold-down force, screw spikes (when properly installed) provide hold-down force to ensure this contact between the plate and crosstie (Kerr, 2003a; Dick et al., 2007). This design encourages transfer of longitudinal loads through friction at the plate-to-crosstie interface in addition to spike bending.

The fundamental equation for quantifying the frictional force considers the normal (vertical) force applied and coefficient of friction (Equation 5.2). To increase force transfer through friction, the coefficient of friction or, normal force must be increased. The nominal coefficient of friction between the plate and crosstie is 0.7 (Gurfinkel, 1981).

$$f = \mu N \quad \text{Eq. 5.2}$$

where,

f is the Friction force.

μ is the Coefficient of friction.

N is the Normal force.

Spring washers have been used to address the problem of screw spikes loosening over time. They maintain the normal force between the plate and crosstie and can apply up to 10,000 lbs. (44.5 kN) of force (Figure 5.1) (Kerr, 2003a). Even when plate cutting or loosening of the screw occurs, a residual normal force is present to ensure that the plate is engaged with the crosstie. Therefore, to quantify the effect of normal plate hold-down force applied by spring washers, two magnitudes of normal force were applied to the plate while holding the longitudinal load constant.

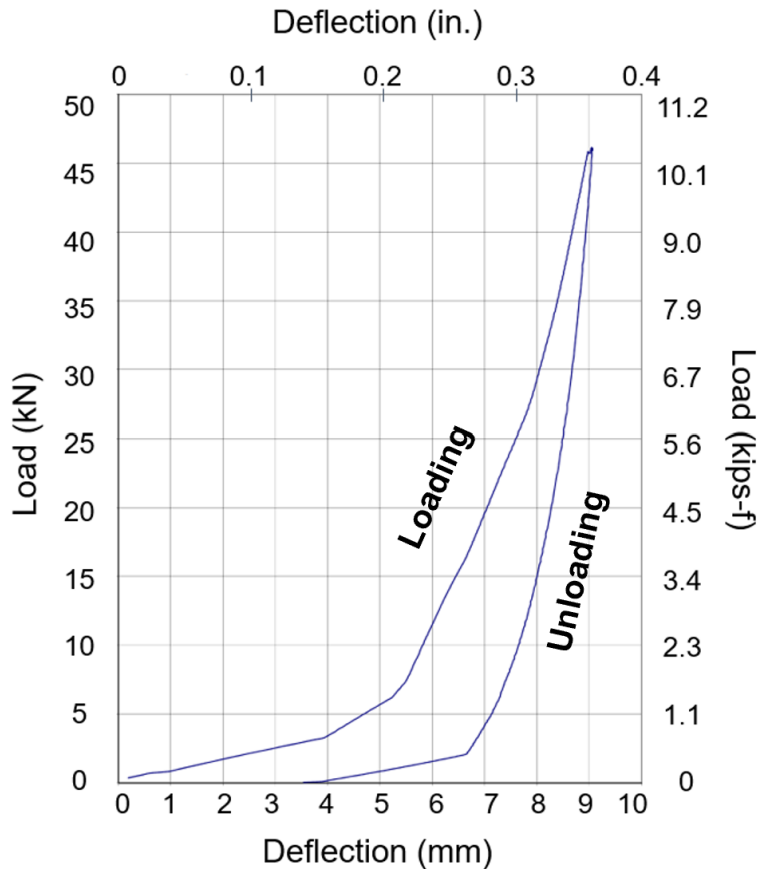


Figure 5.1: Example of typical railroad fastening system spring washer load versus deflection characteristics

5.2.4 Spike Loading Location

The point of spike loading (i.e. plate to spike contact location) will affect spike stress given it would change the distance between the points of load and support (i.e. moment arm) and resulting bending moment. There are several factors affecting the location of load contact (Figure 5.2): (a) the angle of the spike as driven into the crosstie, (b) the non-planar finished surface of the spike or plate, and (c) plate uplift and/or rotation. Therefore, to quantify the effect of plate uplift, while maintaining the depth at which the spike was driven, I varied the location of the applied load centroid.

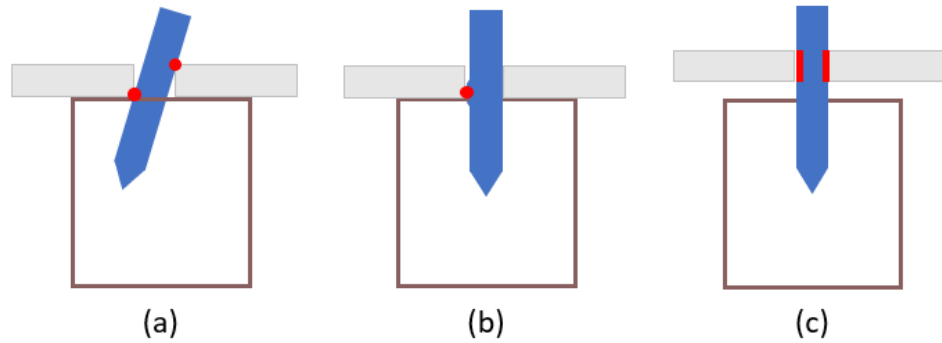


Figure 5.2: Potential mechanisms leading to changes in load contact location (red dots/bars)

5.2.5 Spike Engagement with Plate and Quantity of Spikes within a given Fastening System

When plate uplift occurs, load transfer is only possible when the spike(s) are engaged with the plate (i.e. no friction). The hold-down and line spike holes are 0.065 in. and 0.125 in. (1.65 and 3.18 mm) larger, respectively, than the 0.625 in. (15.88 mm) standard cut spike (Figure 5.3). Given the over-sized holes, in combination with findings by Dersch et al. (2019) demonstrating the displacement of the spike is not expected to exceed 0.04 in. at 2,000 lb. (1.02 mm at 8.90 kN), it is likely that not all spikes will be in contact with the plate simultaneously.

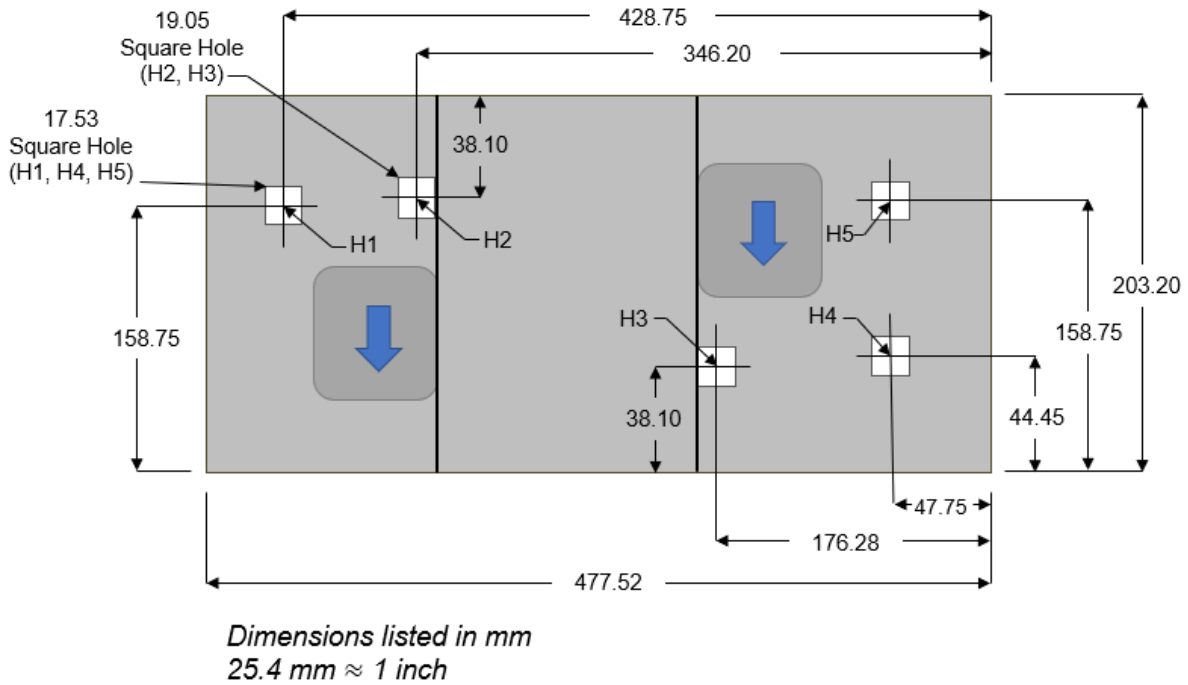


Figure 5.3: Example elastic fastening system plate with dimensions

The lack of engagement of some spikes would lead to a non-uniform force and stress distribution among the spikes. Non-uniform distributions have been reported by Bowman (2002) and Gao (2020) and the data from their instrumented spike studies indicate a single spike might receive between 50 – 70% of the applied force for a single rail seat.

Another factor that could affect the maximum stress in individual spikes is the quantity of spikes used in the fastening system. Standard practices for spiking patterns use only a subset of available plate holes. For instance, in demanding locations such as curves, special track work, or steep grades, four spikes are driven during construction and additional spikes are installed when required for additional strength. As the number of spikes installed per rail seat is increased, the stress in all spikes is expected to be reduced given that total bending strength is increased.

Therefore, to quantify the effect of disengaged spikes within a rail seat system, a parametric study was performed in which spikes were moved from one side of the plate hole to the other and the maximum spike stress was quantified. Further, to quantify the effect of increasing the quantity of spikes installed in a fastening system, a spike was installed in the fifth spike hole in the standard plate (Figure 5.3), a deviation from current practices.

5.3 Methodology and Model Details

Three unique FE models that leveraged knowledge gained from the model described in Chapter 3 were developed and used for the investigations presented in this chapter (Figure 5.4).

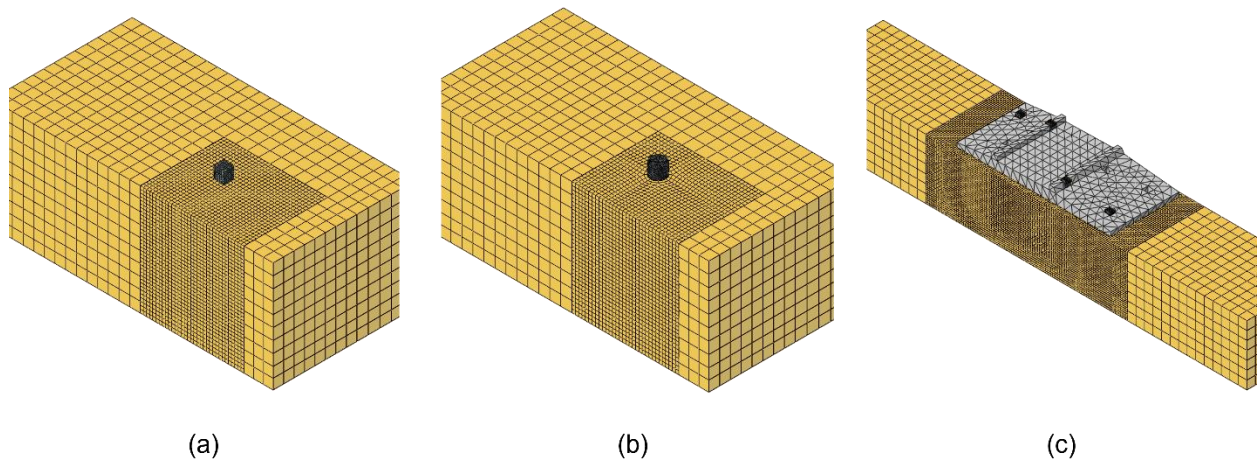


Figure 5.4: Visual representations of the assembled FEMs used in this investigation: (a) single cut spike, (b) single screw spike, (c) single rail seat with four spikes

The single cut-spike-timber-block model (Figure 5.4a) was used to quantify the effect of: spike cross-sectional area, spike loading location, and spike type. The spike was loaded over a 0.3125 in.^2 (100.3 mm^2) area (0.625 in. wide by 0.5 in. tall (7.9 by 12.7 mm) representing contact with a tie plate. The single screw-spike-timber-block model (Figure 5.4b) incorporated many of

the validated portions of the single cut-spike-timber-block model (e.g. timber and spike material properties, mesh densities, boundary conditions, etc.) and was used to quantify the effect of spike type and geometry. Loading was applied to the spike over a 0.368 in.² (237.5 mm²) area (0.737” wide by 0.5 in. tall (18.7 by 12.7 mm) representing the contact from a tie plate over 25% of the circumference of the screw spike. The single rail seat model (Figure 5.4c) expanded upon the validated single cut-spike model by increasing the number of spikes and adding the tie plate. It was used to quantify the effect of spike engagement with the plate, plate engagement with the crosstie, and number of spikes used in the system. Loading was applied to the plate at the location of the shoulders.

All components were modeled as 3D deformable solids using appropriate element types and enough elements to provide accurate responses (Table 5.2).

Table 5.2: Model element type and meshing details

Component	Element Type	Quantity of Elements			Hourglass Control	
		Standard	0.675	0.725		
Spikes	Cut	C3D8R	9,936	10,816	12,544	-
	Screw	C3D8R	47,104	-	-	-
Plate	Standard	C3D10	2,218	-	-	-
Timber Blocks	Single Cut Spike	C3D8R	30,924	46,295	47,535	Yes
	Single Screw Spike	C3D8R	28,304	-	-	Yes
	Rail Seat	C3D8R	186,399	-	-	Yes

The standard cut spikes and timber crosstie were modeled using the validated material properties, mesh densities, boundary conditions, etc. presented by Dersch et al. (2019). The standard cut spikes were 6 in. (152 mm) long by 0.625 in. (15.9 mm) square as described in Chapter 5 of the AREMA Manual on Railway Engineering (2017a). The standard AREMA

recommended Square Head Screw Spike was simplified in the model by removing the threads and head.

Dersch et al. (2019) reported the steel Young's Modulus of 30,850 ksi (212,700 MPa), a yield strength of 56,265 psi (390 MPa), and a tensile strength of 85,000 psi (585 MPa). I assumed that the spike had a Poisson's ratio of 0.3, and density of 0.029 lb./in.³ (8,050 kg/m³). The endurance limit was set at 33,800 psi (233 MPa) given that it was assumed to be approximately 40% of the ultimate strength, which is near the lower bound of the expected 35 – 60% range, thus leading to a conservative design.

The timber was modeled to account for the unique and independent mechanical properties in the directions of three mutually perpendicular axes: longitudinal (parallel to the direction of the timber fibers), tangential (perpendicular to the direction of the timber fibers and tangent to growth rings), and radial (perpendicular to the direction of the timber fibers and growth rings) (13). To account for this behavior, the validated timber user-defined material model (UMAT) developed by Sandhaas et al. (2011; 2012) and previously employed by Dersch et al. (2019) was used.

The single rail seat model consists of either four or five cut spikes, a timber block, and a single plate. The plate modeled represents the current design standard for at least one North American Class I HAL railroad. To save computational time, the geometry was simplified in areas that had less critical geometries and stresses. The part models (Figure 5.5) were sufficiently representative of their corresponding components.

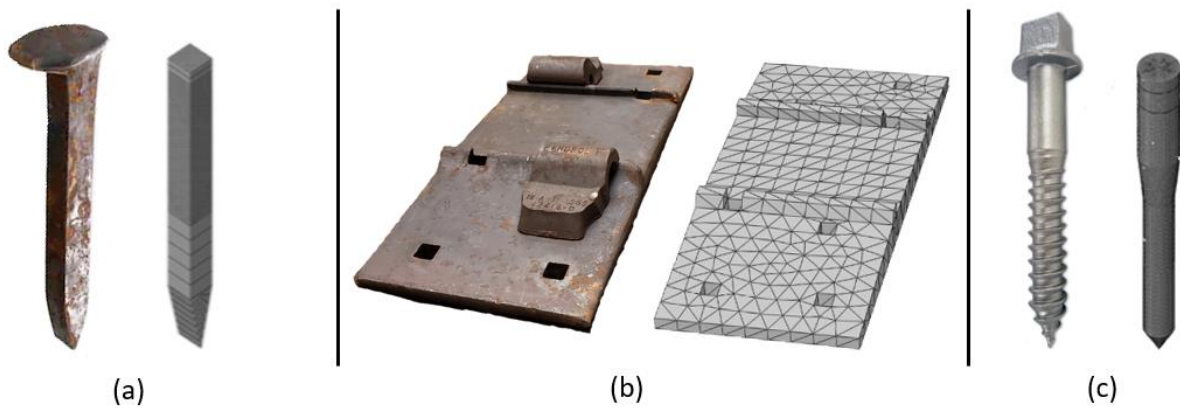


Figure 5.5: Actual fastening system components and simplified model representation: (a) cut spike, (b) fastening system plate, and (c) screw spike

The static coefficient of friction (CoF) between the cut spike and timber block as well as the plate and timber block was set at 0.7 (Forest Products Laboratory, 2010). The interactions between all components (e.g. spike and timber, plate and timber, etc.) were modeled as contact surfaces, and did not consider perfect bonding. Boundary conditions were applied to all nodes of the bottom of all cross-tie blocks restraining the displacement in the x, y, and z directions.

See Chapter 3 for additional details related to the validation comparing spike stress and displacement recorded in the laboratory with respect to load data to model outputs of the single cut spike-timber block model, please refer to Chapter 3. The subsequent models (e.g. substitution of the screw spike or addition of additional spikes and plate) are iterations of this validated model.

5.4 Results and Discussion

Each model was used to quantify the effect of specific variables on the maximum spike stress when the fastener is subjected to a longitudinal load. For single spike studies (i.e. spike cross-sectional area, spike type, and effect of plate to spike contact location), each spike was

subjected to a 2,500 lb. (11.12 kN) longitudinal load. For the single rail seat studies (i.e. effect of normal plate hold-down force and spike engagement with plate and quantity of spikes) each plate was subjected to a 2,500 lb. (11.12 kN) longitudinal load; half the load was applied at one shoulder and the other half applied to the other. This magnitude was considered reasonable and selected because AREMA recommends that a fastening system withstand at least a 2,400 lb. (10.7 kN) longitudinal load before rail slip for a single fastening system (or rail seat) (AREMA, 2017b) and the load is non-uniformly distributed within the spikes of fastening system (Gao and LoPresti, 2020).

5.4.1 Spike Cross-Sectional Area

Three spike cross-sectional areas were investigated: 0.625 in. (standard), 0.675 in., and 0.725 in. (15.88 mm, 17.15 mm, and 18.42 mm). Each was subjected to a 2,500 lb. (11.12 kN) longitudinal load and the maximum stress was recorded (Figure 5.6).

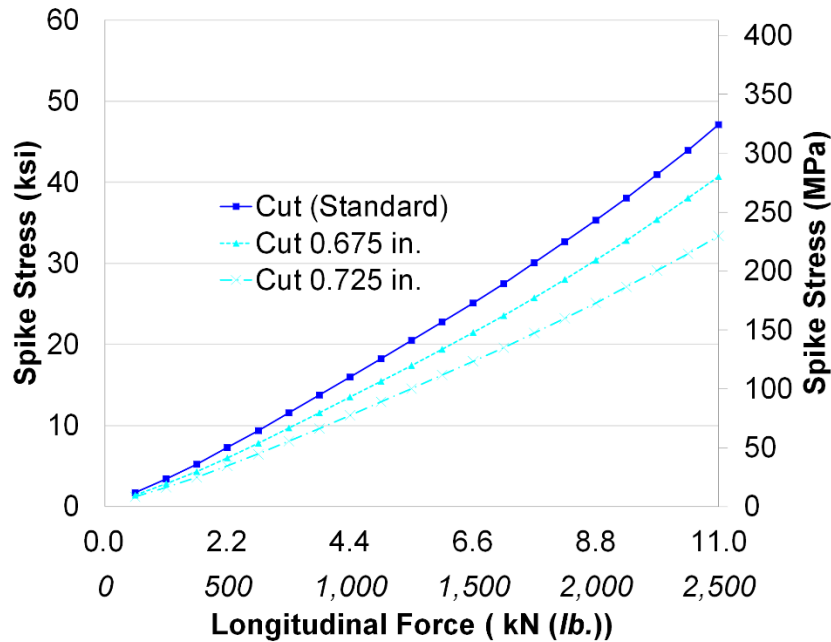


Figure 5.6: Maximum bending stress of spikes with changing cross-sectional areas at various load magnitudes

As expected, there was an inverse linear relationship between the increase in width (i.e. cross-section) and maximum spike stress. Increasing the spike width from 0.625” to 0.725” (15.88 mm to 18.42 mm) increases the cross-sectional area by 16%, increases the moment of inertia (I) by 81%, and resulted in a 29% reduction in spike stress. Given the change in stress for the spike sizes investigated are linear, for each 1% increase in width from the standard spike there is approximately a 2% reduction in stress. Additionally, as the cross-section increases, the longitudinal load magnitude required to exceed the endurance limit increases from 1,950 lb. (8.67 kN) to 2,500 lb. (11.12 kN), or 22%. This trend is linear; for each 1% increase in spike width, there is approximately a 1.6% increase in the load required to exceed the endurance limit, thus increasing resiliency and mitigating fatigue failures.

5.4.2 Spike Type (Cut vs. Screw)

Standard AREMA cut and screw spikes were subjected to a 2,500 lb. (11.12 kN) longitudinal load and the resulting maximum principal stress was visualized (Figure 5.7) and recorded (Figure 5.8).

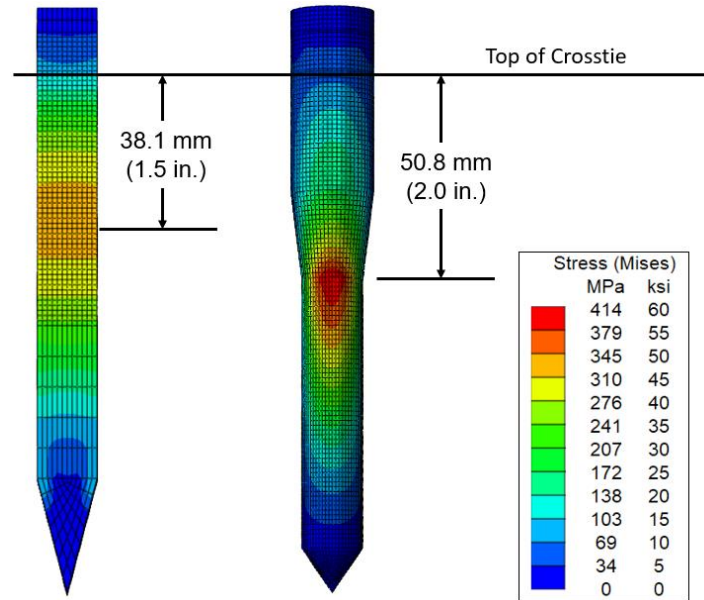


Figure 5.7: Qualitative principal stress comparison of cut and screw spike at 2,500 lb. (11.12 kN)

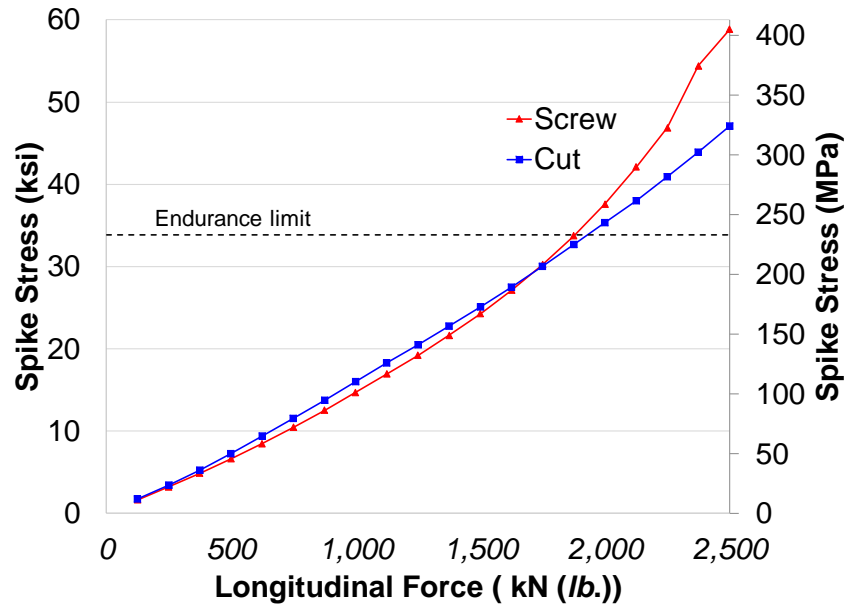


Figure 5.8: Maximum bending stress of cut and screw spike at various loading levels

The results indicated that the maximum stress in the cut spike occurred at 1.5 in. (38.1 mm) while the maximum stress in the screw spike occurred at approximately 2.00 in. (50.8 mm) below the top of the crosstie. The depth of maximum stress for the cut spike increases with load (Dersch et al., 2019); however, for the screw spike, maximum stress was consistently 2.00 in. (50.8 mm) below the crosstie surface, at the bottom of the transition from the upper shank to the threads. This is consistent with previous modeling results (Dick et al., 2007) and field investigations that found that screw spikes break at the first thread, approximately 2.00 in. (50.8 mm) below the top of the crosstie.

The data also indicate that at longitudinal loads below 2,000 lb. (8.90 kN) the two spike types are similar with less than 10% difference in their maximum stress; however, above 2,000 lb. (8.90 kN) the increase in stress accelerates in the screw spike (Figure 5.8). This is likely due to the abrupt change in geometry and the consequent stress concentration at the spike threads, leading to localized plastic deformation. Given the similar response below 2,000 lb. (8.90 kN)

both spikes require the same magnitude of force to exceed the endurance limit. Therefore, for most loading scenarios (Khachaturian et al., in review), there is minimal difference in stress state or required load to exceed the endurance limit when comparing AREMA cut and screw spikes. However, when loads exceed 2,000 lb. (8.90 kN) the stress in the cut spike can be as much as 25% lower than the screw spike leading to its relatively shorter fatigue life.

5.4.3 Effect of Plate to Spike Contact Location

The AREMA cut spike was subjected to longitudinal loads up to a maximum of 2,500 lb. (11.12 kN). For the standard load case, the centroid of loading was 0.25" (6.35 mm) above the top of crosstie (the standard case assuming a uniformly distributed load over a 0.5 in. (12.7 mm) deep plate hole). However, to account for changes in load location this centroid location was changed to 0.475 in. (12.1 mm) above the top of the crosstie (i.e. High Contact) and 0.025 in. (0.635 mm) above the top of the crosstie (i.e. Low Contact). The maximum stress for each case was recorded at 125 lb. (555 N) increments up to the maximum applied load (Figure 5.9).

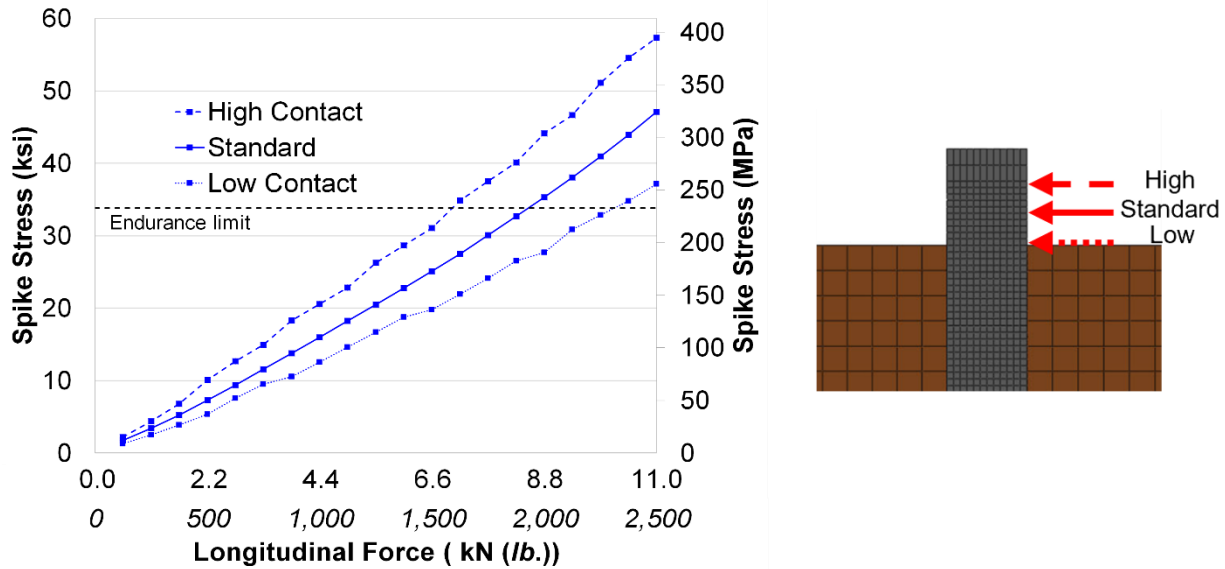


Figure 5.9: Maximum bending stress of spikes at various loading levels and load locations

The data indicate that there is a direct linear relationship between the change in load location and maximum stress. Regardless of applied load magnitude, there is approximately a +/- 20% change from the control case when the load location moves up or down, respectively. Additionally, when comparing the load required to exceed the endurance limit, there is also an approximately 20% increase or decrease when changing from the standard contact position to the high or low contact positions, respectively.

5.4.4 Effect of Normal Plate Hold-down Force

A longitudinal load of 2,500 lb. (11.12 kN) was applied to the single fastening system model while a normal plate hold-down force of 0 (control), 1,000, and 3,400 lb./spike (0, 4.45, and 15 kN/spike) was introduced. These hold-down force values represented conditions where

there would be no spring washer installed and 0.039 in. (1 mm) and 0.079 in. (2 mm) settlement or wear of the tie plate into the crosstie or uniform loosening of the spikes, respectively.

Dick et al. (2007) and Dersch et al. (2019) found that the stress in a spike can vary due to a variety of factors (e.g. loading location, spike orientation, load magnitude, etc.), so a normalized stress value is reported for each case. A stress of “1.0” is the average stress distributed over four engaged spikes with the control spiking pattern and no normal plate hold-down force applied. The spike stress data were recorded when the maximum longitudinal load was applied for each normal plate hold-down force considered (Figure 5.10).

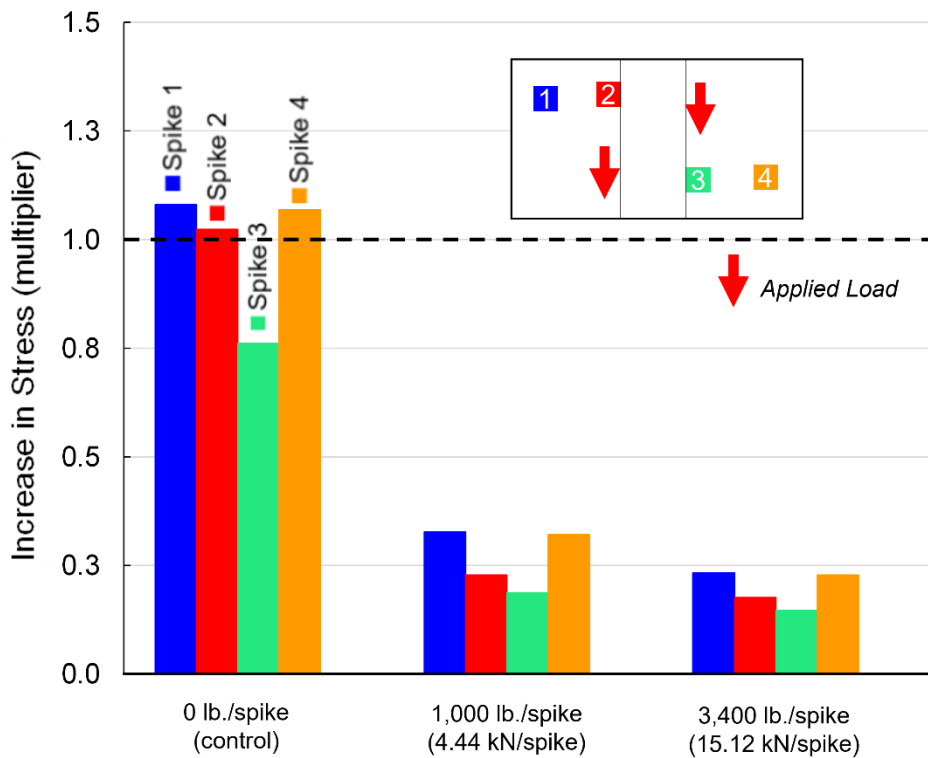


Figure 5.10: Effect of normal hold-down force on maximum spike stress at 2,500 lb. (11.12 kN) longitudinal load

When the hold-down force per spike was 3,400 lb. (15 kN) the average spike stress was reduced 80%. Even when there is additional settlement of the tie plate or loosening of the spikes, and the hold-down force per spike declined to 1,000 lb. (4.45 kN),) the average spike stress was reduced 70%, compared to the control. This 70 – 80% reduction indicates that most longitudinal force would be transferred by friction when applying a vertical force to the tie plate. Developing friction at this interface aligns with design fundamentals for bolted shear joints (Bickford, 2007) and direct fixation fastening systems (Grondin et al., 2008) that are expected to transfer load through a combination of friction and bearing.

5.4.5 Spike Engagement with Plate and Quantity of Spikes

The single fastening system model was subjected to a maximum longitudinal load of 2,500 lb. (11.12 kN). A normalized stress value is reported for each case where a stress of “1” is the average stress distributed over four engaged spikes installed with the standard spiking pattern. The maximum spike stress in each condition was then compared to this average baseline stress. The maximum spike stress data for each case considered was recorded at the maximum applied longitudinal load (Figure 5.11)

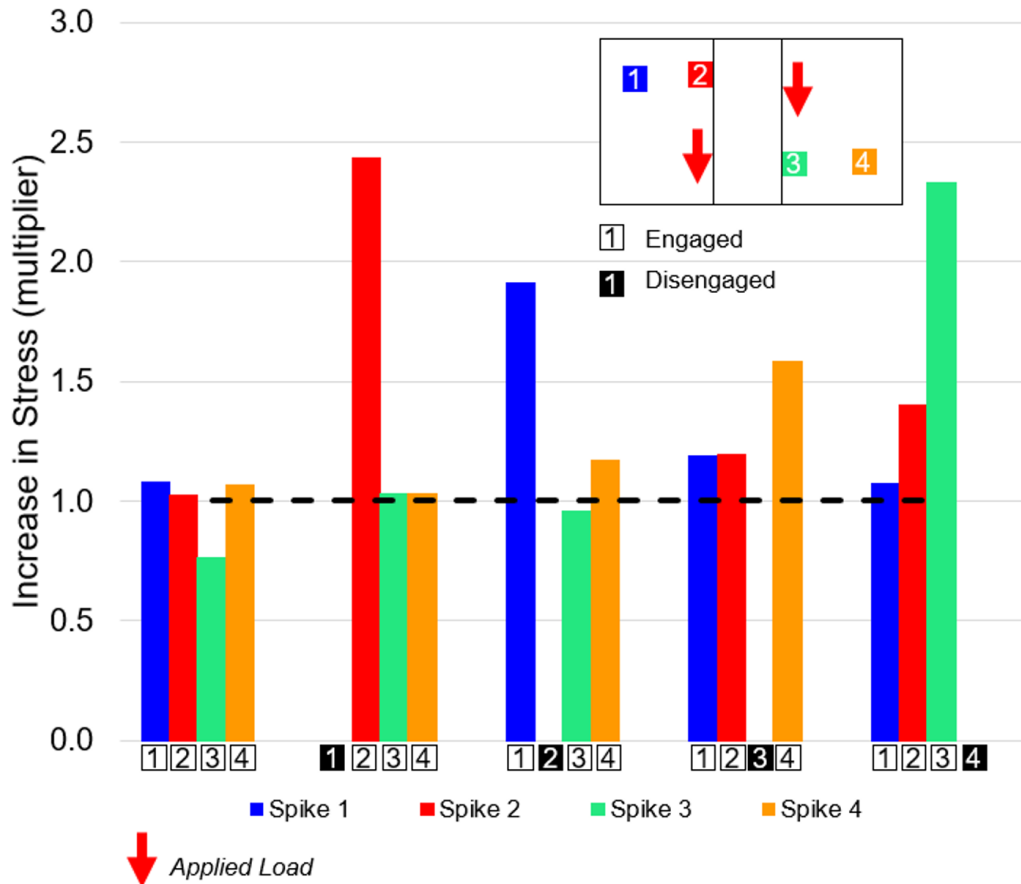


Figure 5.11: The effect of spike engagement on maximum spike stress at 2,500 lb. (11.12 kN) longitudinal load application with disengagement of one spike at a time

In all cases, there is non-uniform force distribution in the fastening system. This can probably be attributed to the asymmetric placement of spikes relative to the point of loading. Further, though the fourth spike is present in each case, it carries no load and behaves as if it has been removed. This behavior occurs because the tolerances of the holes in the plate (e.g. 0.69 in. or 0.75 in. (17.53 mm or 19.05 mm)) are greater than the expected deflection of any spike (0.04” at 2,000 lb. (1.02 mm at 8.90 kN)). The data also indicate that the force previously carried by the “removed” spike is not evenly distributed among the remaining spikes. Instead, the load is carried primarily by the adjacent spike. Regarding magnitude, when a single spike is removed from the load path, the adjacent spike’s stress can increase as much as 140% (or 2.4 times).

This more than doubling is likely driven by the plate rotation, which changes the contact point between the spike and plate thereby introducing additional stresses into the spike.

The effect of the number of engaged spikes (i.e. 3, 4, and 5) was investigated by quantifying the maximum spike stress at the maximum applied longitudinal load (Figure 5.12).

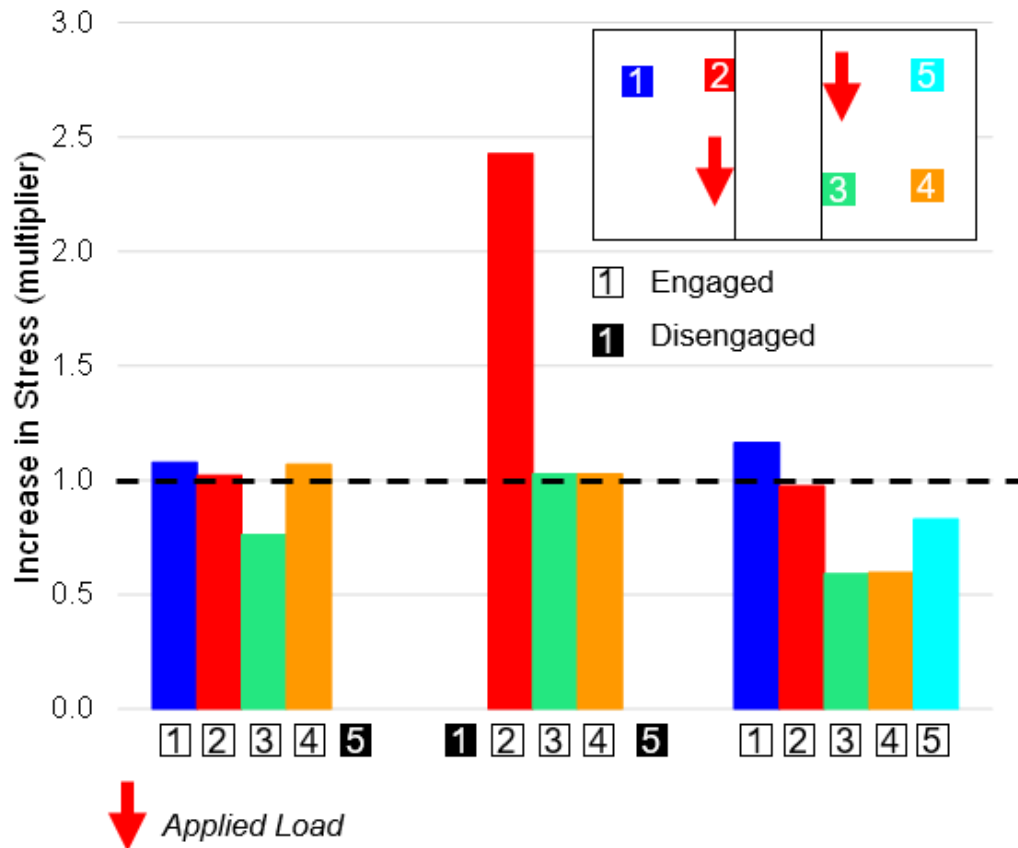


Figure 5.12: The effect of quantity of spikes engaged on maximum spike stress under a longitudinal load application of 11.12 kN (2,500 lb.)

The addition of the fifth spike reduced the stress in spikes 3 and 4 but not spikes 1 or 2. Therefore, even in the unlikely scenario of all spikes being engaged, increasing the number of spikes will not ensure a uniform reduction in maximum stress. Therefore, if spike engagement cannot be ensured, other methods to transfer the forces should be developed as discussed previously in this chapter (e.g. friction between the plate and crosstie).

5.5 Conclusions

In this chapter I present the results of five FEM studies representing varying fastening system conditions that affect spike-stress magnitude. The results indicate that the most effective methods for reducing spike stress, and thus reducing or preventing spike failures, is to develop additional frictional forces between the tie plate and crosstie. A proposed method for generating this additional plate hold-down force is use of spring washers.

The results also indicate that changes in spike type, cross-sectional area, quantity of spikes, and loading location have an effect, though not as significant as the development of plate to crosstie friction. Following is a summary of the novel findings stemming from this investigation:

- There is an inverse relationship between plate hold-down force and spikes stress.
 - For example, a hold-down force of 4.5 kN (1,000 lbs.) at each spike can lead to a 70% reduction in spike stress.
- The disengagement of a single spike (reduction from 4 to 3) can lead to a 140% (2.4 times) increase in the stress experienced by a remaining spike.
- There is little difference in cut and screw spike expected performance (load required to exceed fatigue limit) or strength (capacity) at longitudinal loads below 8.90 kN (2,000 lb.).
- There is an inverse linear relationship between spike cross-section and resulting stress as well as load required to exceed the endurance limit.
 - For each 1% increase in spike width from the standard spike condition there is approximately a 2% reduction in stress.

- For each 1% increase in spike width, from the standard spike condition there is approximately a 1.6% increase in the load required to exceed the endurance limit.
- There is an inverse linear relationship between spike contact location and resulting stress as well as load to exceed the endurance limit.
 - A +/- 6.22 mm (0.245") change in load location can lead to approximately a -/+ 20% change in maximum stress and load required to exceed the endurance limit.

These findings align with recommendations originally proposed by AREA and further developed by Kerr (2003a), fastening systems installed in demanding locations should employ fasteners whose only function is holding down the tie-plate to the tie and not transferring additional loads from the rail. Future fastening system designs can consider these results to mitigate spike fastener failures. That is, fasteners should be designed to transfer forces via friction when possible, encourage uniform engagement of the spikes, as well as encouraging forces to be transferred as close to the crosstie top surface as feasible. If additional capacity is still required, increasing the spike size could be considered.

6 ANALYTICAL NON-LINEAR MODELING OF RAIL AND FASTENER LONGITUDINAL RESPONSE

In this chapter I present the development, validation, and application of a non-linear 3D finite element model (FEM) to quantify the longitudinal load demand on fastening systems. The model accounts for the non-linear behavior of the fastener and ballast and provides a tool to quantify the effect of fastener and ballast condition on rail seat load magnitude. A paper related to this chapter is in review in *Transportation Research Record (TRR)*⁵.

6.1 Introduction

A sizeable body of research has been undertaken to quantify the structural response of concrete cross-ties or establish their failure criteria (Zeman et al., 2012; Kernes et al., 2014; Edwards et al., 2017b; Edwards et al., 2017c; Bastos et al., 2018; Edwards et al., 2020). There has also been substantial research quantifying the vertical and lateral wheel loading environment in North America (Kerchof and Wu, 2014; Van Dyk et al., 2014; Van Dyk et al., 2016; Holder et al., 2017b). Recently, there has been a focus on development of tools to quantify the structural response of fastening system components (Gao et al., 2018; Yu and Liu, 2019; Dersch et al., 2019; Marquis et al., 2020; Dersch et al., 2020b; Dersch et al., 2020a). However, there has been comparatively little attention given to the quantification of fastening system demands and the manner by which loads are transferred between fastener components.

As discussed in Chapter 1, fastening system designs have evolved iteratively, through a trial-and-error design approach aimed at addressing conditions symptomatic of track strength and force transfer deficiencies (e.g. plate cutting, rail seat deterioration (RSD), rail rollover, rail pad

⁵ Dersch, M.S., M. Trizotto Silva, J.R. Edwards, and A. de O Lima. Accepted. Analytical non-linear modeling of rail and fastener longitudinal response. *Research Record: Journal of the Transportation Research Board*

movement) (Kerr, 2003c). These deficiencies have led to a variety of track component failures (e.g. broken spikes, shoulders, threaded rods, etc.) that have caused derailments (Choros et al., 2007; Wolf, 2014; Wu and Kerchof, 2014; McHenry and LoPresti, 2015; Roadcap et al., in review). Many of these failures were a result of a combination of vertical, lateral, and longitudinal loads.

I quantified vertical, lateral, and longitudinal rail and fastener loads in Chapter 2 and Khachaturian et al. (In Review) quantified the effect of fastening system stiffness on longitudinal fastener load magnitude. Both efforts leveraged a one-dimensional (1D) analytical model that was validated by Trizotto et al.'s (2021) limited linear elastic model. The development, validation, and application of a novel non-linear parametric track model will provide data that are widely applicable to fastening system design for heavy axle load (HAL) freight, intercity and high-speed passenger rail, and rail transit. Additionally, the model will aid researchers in quantifying broken spike failure modes that have led to at least 12 derailments on HAL freight railroads over the past 20 years, as discussed in greater detail in Chapter 2.

6.2 Previous Models

Multiple analytical methods for modeling the longitudinal track behavior have been developed to understand the influence of axial loading (thermal or mechanical) on track buckling and rail pull-aparts. Longitudinal rail loading may occur for a variety of reasons (Kerr, 2003c):

- internal residual stresses developed in the manufacturing processes,
- longitudinal forces due to temperature deviation from the RNT,
- bending moments due to vertical and lateral forces caused by wheels,
- longitudinal forces due to steering action of axles, or

- longitudinal forces due to tractive and braking efforts of axles.

Although each of these loads affect rail stresses and thus the likelihood of a track buckle or pull-apart, not all of them affect fastener forces. For example, internal residual stresses would not be expected to increase fastening system forces. To achieve the objectives set forth for this chapter, I must determine how longitudinal forces are transferred to the fasteners.

I reviewed the literature for existing longitudinal track models that could be used to quantify the rail seat load given an applied tractive or braking force. The following section highlights five methods that have been used to improve current design recommendations. None of these were developed exclusively for the quantification of fastener loads.

6.2.1 Analytical Approach Leveraging Mechanics

Kerr (2003d) presents two methods using 1D analytical approaches rooted in mechanics to calculate the distribution of rail longitudinal (axial) force in response to an applied wheel load (Figure 6.1a). Though Kerr acknowledges that a bi-linear approximation of longitudinal track resistance and displacement (Figure 6.1b) produces the most accurate results, the derivation of a simplified approach is the primary focus of his analysis (Kerr, 2003b). In his simplified method, only the linear region of axial rail displacement is considered, and the rail is not represented by a bilinear approximation.

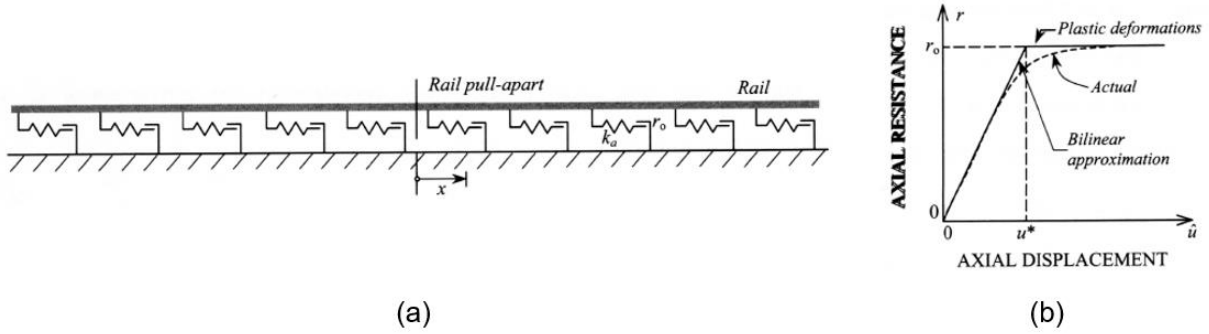


Figure 6.1: Visual representation of simplified track model (a) and bilinear relationship between track resistance and displacement (b) (Kerr, 2003d)

Kerr's (2003b) analysis is based on the governing differential equation for a bar subjected to longitudinal (axial) loading (Equation 6.1).

$$(EAu')' = f(x) \quad \text{Eq. 6.1}$$

The longitudinal load in the bar will be EAu' , where u' is the strain of the bar and $f(x)$ is the force at a given location, x . Therefore, the change in internal longitudinal load is related to the external distributed force. This external distributed force is caused by the track's resistance to longitudinal movement of the rail. The applied external force is related to the reaction of the track in terms of rail movement at that location (Equation 6.2).

$$(EAu')' = (k_a/2)u \quad \text{Eq. 6.2}$$

Further developing Equation 6.2, the governing equations and boundary conditions are obtained (Equation 6.3).

$$\underbrace{\left. \begin{aligned} u_r''(x) - \kappa^2 u_r(x) &= 0 & 0 \leq x < \infty \\ u_l''(x) - \kappa^2 u_l(x) &= 0 & -\infty < x \leq 0 \end{aligned} \right\}}_{\text{Governing differential equations}} \text{ where } \kappa^2 = \frac{\frac{k_a}{2}}{\underbrace{EA}_{\text{rail}}} \quad \text{Eq. 6.3}$$

$$\begin{aligned} u_l(0) &= u_r(0) \\ \underbrace{u_l'(0) - u_r'(0)}_{\text{Boundary conditions}} &= \frac{R}{EA} \end{aligned}$$

Kerr then solves for displacement and longitudinal force (Equations 6.4 and 6.5).

$$\left. \begin{aligned} u_r(x) &= \frac{R}{2\kappa EA} e^{-\kappa x} \\ u_l(x) &= \frac{R}{2\kappa EA} e^{+\kappa x} \end{aligned} \right\} \text{Rail Displacement} \quad \text{Eq. 6.4}$$

$$\left. \begin{aligned} N_r(x) &= EAu_r'(x) = -\frac{R}{2} e^{-\kappa x} \\ N_l(x) &= EAu_l'(x) = +\frac{R}{2} e^{+\kappa x} \end{aligned} \right\} \text{Rail Axial Force} \quad \text{Eq. 6.5}$$

I expanded this method to develop equations estimating distributed fastener forces. These forces are obtained by multiplying the stiffness of the spring by the calculated displacement of the rail (Trizotto et al., 2021) (Equation 6.6).

$$\left. \begin{aligned} F_r(x) &= \frac{k_a}{2} u_r(x) = \frac{\kappa R}{2} e^{-\kappa x} \\ F_l(x) &= \frac{k_a}{2} u_l(x) = \frac{\kappa R}{2} e^{+\kappa x} \end{aligned} \right\} \text{Distributed Fastener Force} \quad \text{Eq. 6.6}$$

While this expanded approach provides a reasonable estimate of the fastener forces, there are some limitations. First, to eliminate complexities of thermal-induced fastener loading, this method only considers open track (i.e. outside of areas with fixed track elements or rail joints). Second, to eliminate any temperature-induced fastener forces, this method assumes a uniform temperature throughout the zone of influence (i.e. no temperature gradient in the section studied). Furthermore, to satisfy the boundary conditions, the rail must be fixed at both ends and sufficiently far from the locations of assessment under the model. Additionally, the track resistance simplifies the rail and ballast as a single, combined spring. Finally, nonlinear analysis results have shown that track buckling is a three-dimensional problem and the 1D beam model overestimates track stability. Although Kerr (2003d) provides a derivation that includes a bilinear approximation, it oversimplifies the problem and is subject to the assumptions and limitations listed above.

6.2.2 Advanced Analytical Approaches Leveraging Discrete Element Modeling, Systems of Differential Equations, and Finite Element Modelling

Four advanced analytical approaches have been developed that build upon Kerr's theory presented in Section 6.2.1 and are relevant to the research presented in this chapter (Table 6.1).

Table 6.1: Overview of advanced analytical approaches and select details

Model	Year Developed	Developer	Analytical Approach	Primary Focus	Primary Output	Dimensions
PROLIS	1988	Delft University of Technology	Discrete element	Rail, bridge, and foundation interaction	Rail and bridge force and displacement	2D
NUCARS	1989	Transportation Technology Center, Inc.	Multibody dynamics	Train dynamics	Vehicle response	3D
LONGIN	1994	Technical University of Cracow	System of differential equations	Longitudinal track creep	Rail and ballast displacement	2D
CWERRI	1997	Technical University of Delft	Finite element	General stability analysis of CWR track	Rail and bridge force and displacement	3D

PROLIS was developed in 1988 to quantify the force and displacement at fixed structures (e.g. bridges) (Van, 1997). This 2D method uses discrete element modelling (DEM). NUCARS was originally released in 1989 by the Transportation Technology Center, Inc. (TTCI) (Rakoczy et al., 2016). NUCARS is a multibody dynamics (MBD) analysis and is primarily used to quantify rail vehicle response to track geometry. NUCARS has recently been adapted to quantify forces on track infrastructure (rail, bridges, and crossties) (McHenry and Klopp, 2017; Gao et al., 2018) by representing the fasteners and ballast using springs and dashpots (Figure 6.2). A recent study used this method to quantify the vertical and lateral loads placed on crossties (Gao et al., 2018). NUCARS has not been adapted to quantify longitudinal rail seat loads and the spring and damper characteristics are not defined.

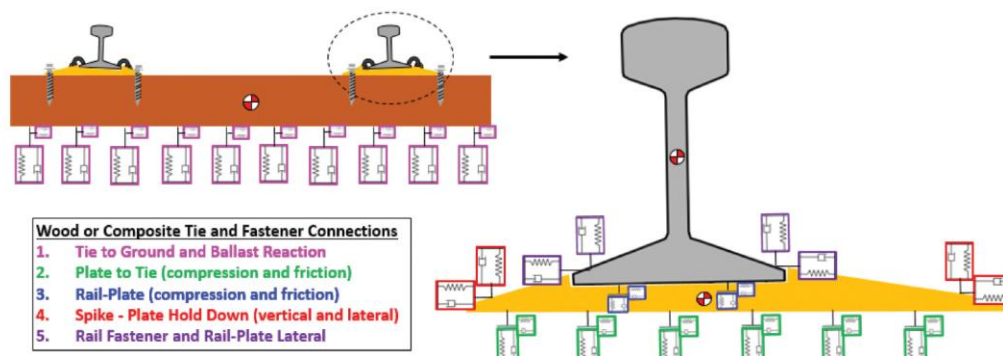


Figure 6.2: Visual representation of NUCARS fastener model (McHenry and Klopp, 2017)

LONGIN was developed in 1994 to quantify longitudinal creep of the rail and ballast when track was subjected to train loading (Figure 6.3) (Czyczula and Solkowski, 1994). The 2D method uses a system of differential equations. LONGIN has been used to investigate the effect of fastening system components on track creep (Rhodes et al., 2005). CWERRI was developed in 1997 to provide a general tool for analyzing CWR track stability and quantifies the rail and bridge forces (Van, 1997). CWERRI uses numerical methods to consider lateral ballast softening behavior and the effect of vertical forces on the fastener and ballast slip-limits. CWERRI continues to be used by researchers to analyze lateral track stability (Bae et al., 2016).

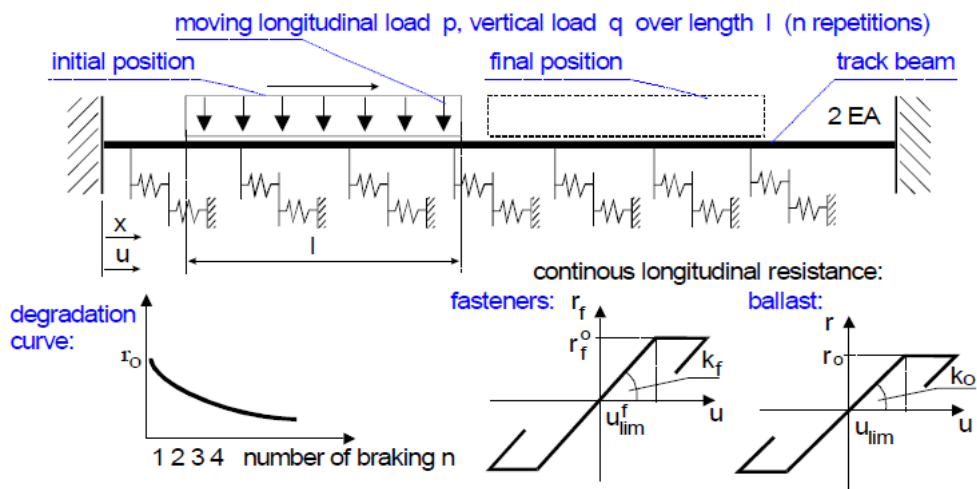


Figure 6.3: Visual representation of LONGIN model (Van, 1997)

To date, no 3D approach has been developed to quantify the longitudinal fastener loads using non-linear approximations of both the fasteners and ballast while accounting for the interaction of vertical, lateral, and longitudinal loads. Therefore, in this chapter, I present the development, validation, and application of a 3D non-linear parametric track model (hereafter referred to as “Ill3D”) using finite element analysis (FEA) I specifically developed for this

dissertation. Illi3D leverages multiple, bi-linear springs at the ballast–crosstie and crosstie–fastener interfaces and is used to quantify the effect of variables (e.g. ballast and fastener condition) on load distribution within the track structure.

6.3 Model Overview and Validation

This section documents the development and validation of Illi3D (Figure 6.4) for the quantification of fastener loads for various track types and operating conditions. Illi3D uses finite element formulation and a combination of linear beams and non-linear springs in three dimensions to simulate the bi-linear behavior found in previous models. The rail-to-crosstie interface (i.e. fastener) and crosstie-to-ballast interface are both represented by friction-based elements placed in series with the elastic elements.

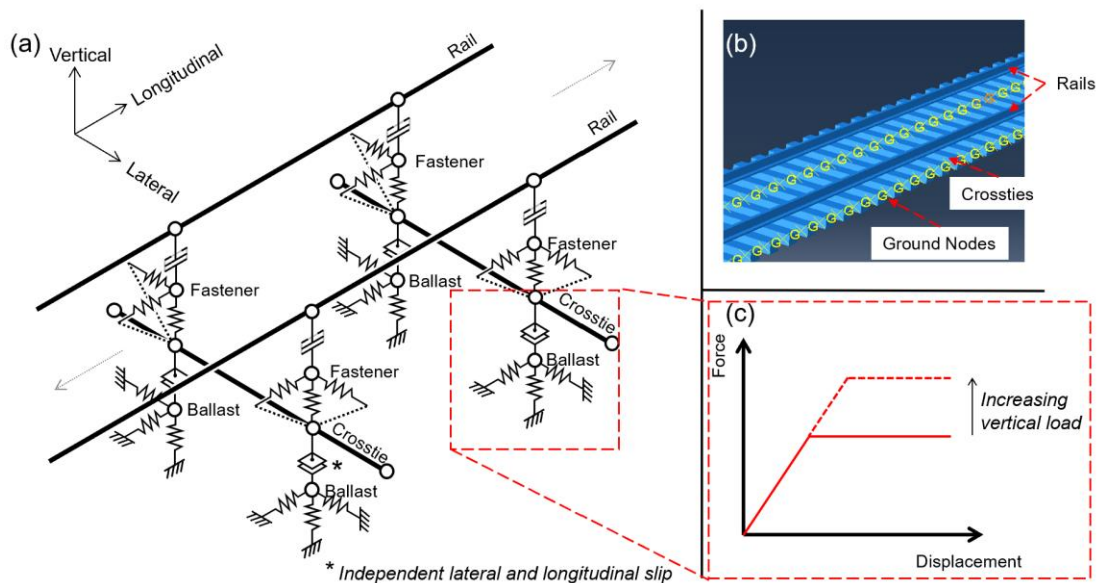


Figure 6.4: Visual representation of Illi3D which (a) details the fastening system and ballast non-linear springs, (b) provides a simplified 3D view from Abaqus, and (c) describes generic interaction between slip-force and vertical load

Illi3D represents track components (i.e. the fasteners and ballast under a crosstie) as discrete elements. The elastic and friction connector-elements were used to describe the complex kinematic and kinetic relationships between nodes using the FEA program, Abaqus. Each of the track components represented in the model were split into two elements in-series to consider the friction and elastic properties desired, since Abaqus interprets all connector properties in parallel.

The first element in series contains the elastic properties of the track component represented for each nodal degree of freedom. This is used to introduce the vertical, lateral, and longitudinal stiffness of fasteners and ballast assuming independence from vertical loads (ERRI, 1997).

The second element contains descriptions of the normal forces and coefficients of friction of the represented track component for each nodal degree of freedom. This element is rigid in the remaining degrees of freedom, so as to transfer loads but not introduce additional displacements. This allows the slip behavior at the crosstie-ballast and rail-fastener interfaces and for the resistances to be affected by vertical forces. The crosstie-ballast interface is modeled to slip in the lateral and longitudinal directions independently from each other as suggested by Van (1997) and satisfy the constraint in Equation 6.7.

$$F_T - \mu | F_i + F_V | \leq 0 \quad \text{Eq. 6.7}$$

where,

μ is the coefficient of friction.

F_T is the tangential load (lateral or longitudinal).

F_v is the vertical load.

F_i is the internal load, such that the initial slip force is $\mu \cdot F_i$.

Further, to facilitate track creation and parametrization, the procedure was scripted using Python and the Abaqus Scripting Interface, an Application Programming Interface (API) for Abaqus (Dassault Systèmes, 2014). End boundary elements were implemented (Van, 1997) to simulate the elastic behavior of the continuation of a tangent track with uniform properties to infinity, which significantly reduced the number of elements and track components modeled. The stiffness of the elastic boundary (k_{end}) can be calculated by the ratio of elastic longitudinal force to longitudinal displacement at a track section (Equation 6.8).

$$k_{end} = \frac{N(x)}{u(x)} = \frac{N_0 e^{-\kappa x_i}}{\frac{N_0}{\sqrt{k_a EA}} e^{-\kappa x_i}} = \sqrt{k_a EA} \quad \text{Eq. 6.8}$$

where,

$N(x)$ is the longitudinal rail load at location x .

$u(x)$ is the longitudinal rail displacement at location x .

N_0 is the longitudinal rail load at the origin.

k_a is the longitudinal track stiffness.

E is the Young's modulus of rail.

A is the rail cross sectional area.

Illi3D was validated by comparing the rail load, fastener rail displacement, and/or fastener load to two field-validated models found in the literature; an analytical linear model developed

by Trizotto et al. (2021) and an approach that accounts for the non-linear behavior of track developed by Samavedam et al. (1997). The Trizotto et al. (2021) model was selected to validate the linear behavior of Illi3D, as it had been validated using revenue-service field data and outputs rail load, fastener load, and rail displacement. The Samavedam et al. (1997) model was selected to validate the non-linear response of Illi3D, as it had been validated using field data from the Transportation Technology Center (TTC).

Track loading and design parameters representing HAL operations on timber crosstie track with every tie anchored (ETA) were selected from the literature for validation (Table 6.2). Additional model parameters were calculated using the general values and by selecting parameters (e.g. number of locomotives and load) that aligned with the given model.

Table 6.2: Model parameters selected for validation from literature (Kerokoski, 2010; Kish, 2013; AREMA, 2017b; Marquis et al., 2020; Khachaturian et al., In Review)

Track parameter	Symbol	Trizotto et al.	Samavedam et al.
Load (per wheel)	-	1 kip (4.45 kN)	-
Number of locomotives	-	2	-
Number of sleepers	-	361	601
Fastener longitudinal resistance	$f_{0,fastener}$	-	300 lb./in. (52.5 kN/m)
Fastener slip force	-	-	6 kips (27.0 kN)
Ballast longitudinal resistance	$f_{0,ballast}$	-	34 lb./in. (6.0 kN/m)
Ballast slip force	-	-	46.7 kips/in. (8,200 kN/m)
End of track stiffness	-	-	520 kips/in. (91,100 kN/m)
Temperature differential	ΔT	-	60 F
Coefficient of linear thermal expansion of steel	α	-	6.5×10^{-6} 1/F
Force at rail break	$N_{\Delta T}$	-	150.6 kip (700.0 kN)
Crosstie spacing	a	20 in. (510 mm)	
Track longitudinal modulus	k_a	700 lb./in./in. (4,830 kN/m/m)	
Track vertical modulus		3,000 lb./in./in. (20,700 kN/m/m)	
Fastener longitudinal modulus	k_f	1,000 lb./in./in. (6,900 kN/m/m)	
Fastener longitudinal stiffness	$s_f = k_f \cdot a$	20 kips/in. (3,500 kN/m)	
Ballast longitudinal modulus	k_b	2,333 lb./in./in. (16,100 kN/m/m)	
Ballast longitudinal stiffness	$s_b = k_b \cdot a$	46.7 kips/in. (8,200 kN/m)	
Rail	-	RE 136	

With the parameters above selected, data obtained from Illi3D were compared to output from the previously-validated elastic and slip models (Figures 6.5 and 6.6, respectively).

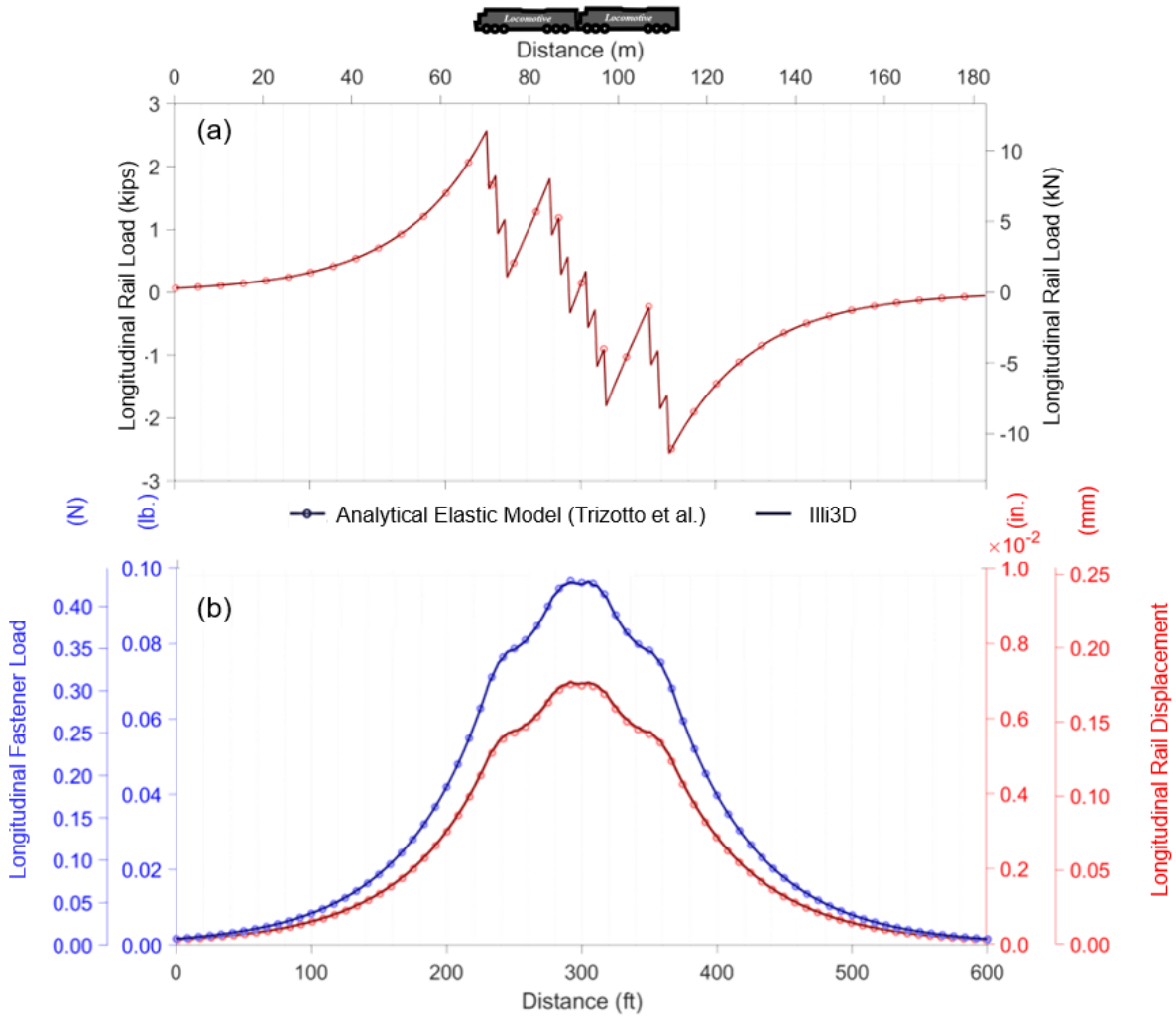


Figure 6.5: Linear validation of Illi3D with previously validated linear elastic model comparing (a) rail load over distance, (b) rail displacement over distance, and fastener force over distance given two locomotives with loads that would not induce slip

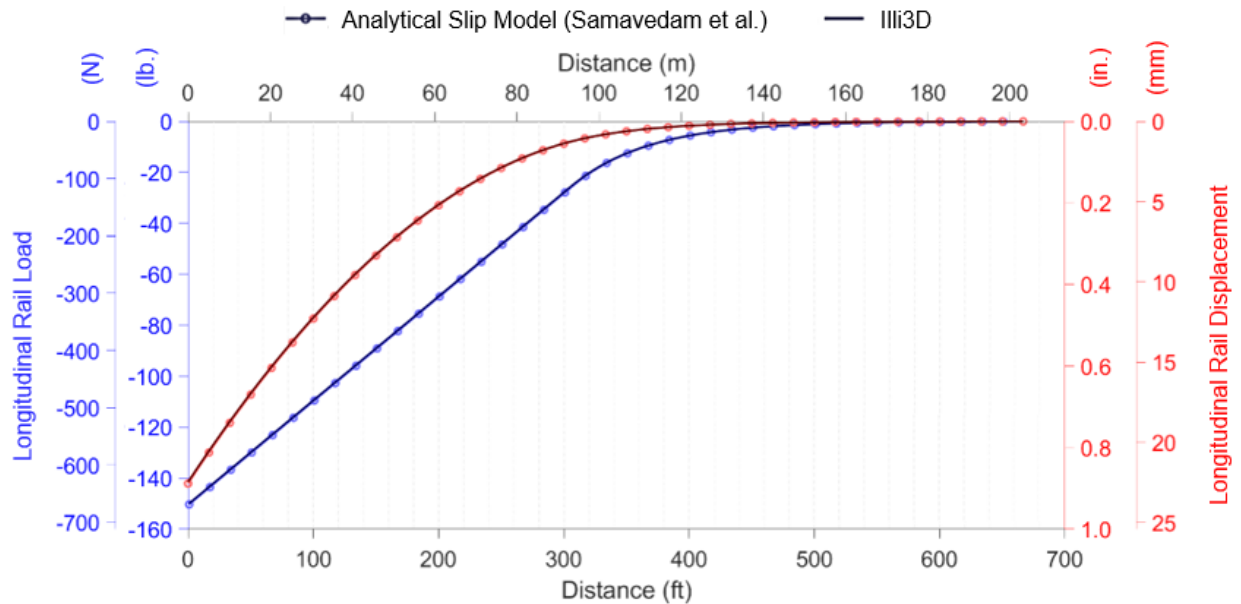


Figure 6.6: Non-linear comparison of Illi3D with previously validated non-linear approach comparing rail load over distance and rail displacement over distance given a 150-kip (667 kN) thermal force causing a rail break

Illi3D accurately represented the force and displacement response of the track to both the forces applied by passing trains and thermal-induced axial stresses. There was a maximum 3.4% and -0.2% difference between Illi3D and the validated linear model and non-linear approach, respectively. Therefore, Illi3D was considered validated for a typical range of use cases.

6.4 Model Application, Results, and Discussion

To demonstrate the importance of incorporating non-linear rail behavior and slip in Illi3D, outputs from Trizotto et al.'s (2021) linear model and Illi3D were further compared. Two locomotives with longitudinal and vertical wheel loads of 10 kips (44.5 kN) and 39 kips (173 kN) per wheel, respectively, were investigated. This vertical load is different than the 1 kip (4.45 kN) per wheel (Figure 6.5). The non-linear parametric track model was first run without accounting for the interaction between vertical load and longitudinal slip (Figure 6.7)

and then again when accounting for this interaction (Figure 6.8). Given the literature indicates that as vertical load increases, the load at which slip occurs also increases (Van, 1997; ERRI, 1997; Kerokoski, 2010), I also investigated these conditions.

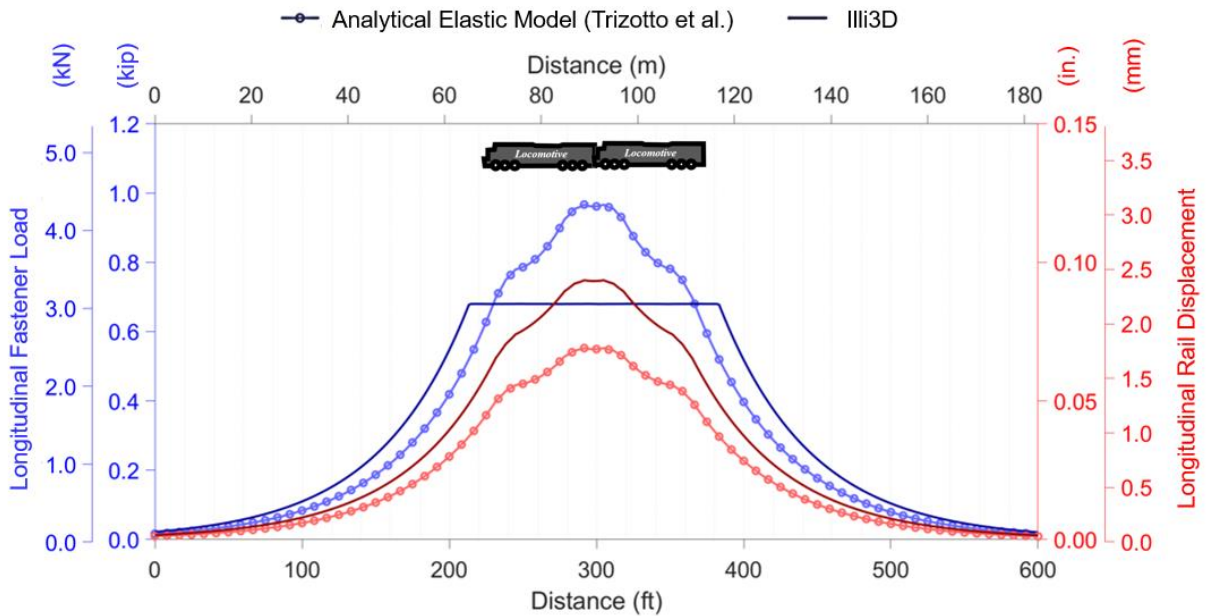


Figure 6.7: Comparison of Trizotto et al. (2021) analytical elastic model and Illi3D longitudinal fastener load (blue) and rail displacement (red) over distance, not accounting for applied vertical load

When the influence of vertical load on longitudinal slip is not accounted for (Figure 6.7), the tractive effort applied to the rail by the train leads to fastener forces that exceed the slip threshold (0.68 kips (3.025 kN)) at the crosstie-ballast interface. Since there are no vertical loads, the maximum tangential force becomes constant, and a longitudinal load plateau is identified in the most demanding loading region. The Trizotto et al. linear elastic model does not consider the limitations of the track to resist longitudinal load and overestimates the maximum fastener force by 42% (0.96 kips (4.27 kN) vs 0.68 kips (3.03 kN)) and underestimates the rail displacement by 35% (0.093 in. (2.36 mm) vs 0.069 in. (1.75 mm)). Additionally, slip leads to a

larger zone of influence than the elastic model. Therefore, modelling the slip behavior provides more accurate quantification of demands placed on track infrastructure components.

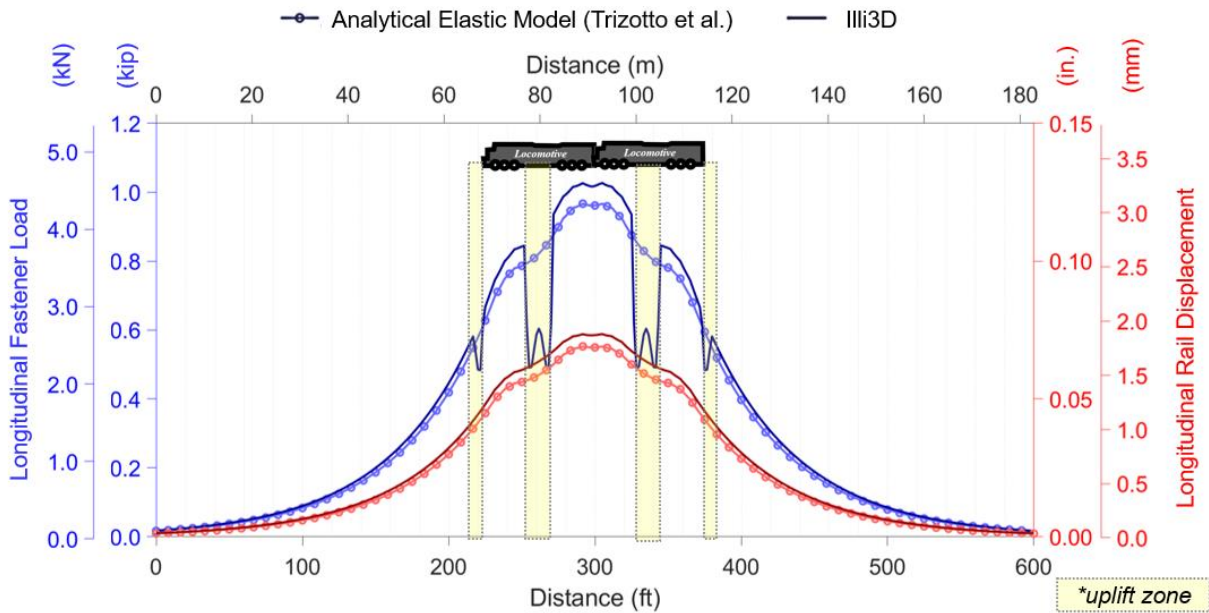


Figure 6.8: Comparison of Trizotto et al. analytical elastic model and Illi3D longitudinal fastener load (blue) and rail displacement (red) over distance, accounting for applied vertical load

When Illi3D accounts for the interaction between vertical load and longitudinal slip, slip does not occur in the same way for the loading considered. This is because the components are subjected to the downward vertical loads, which increase the frictional force between at the rail-crosstie and crosstie-ballast interfaces. However, localized slip is occurring at locations where upward vertical loads create uplift zones, reducing the capacity of the crosstie-ballast interface to resist longitudinal load. In this case, the maximum fastener force increased to 1.03 kips (4.57 kN) which is 51% higher than the case that does not account for vertical load and is 7% higher than results obtained from the Trizotto et al. elastic model. This increase may be caused by the transfer of forces from adjacent locations along the rail that are experiencing uplift due to the

wave action of the rail. The maximum displacements are also 7% greater than what is predicted by the Trizotto et al. elastic model. Under typical conditions, slip would not be expected outside uplift zones because of the presence of vertical load. However, slip could occur at locations with inadequate crosstie support leading to poor vertical load transfer. Even when slip occurs, the additional force placed on the fastening system would not be concerning given that it would be distributed over many (e.g. dozens) crossties. Slip would be more of a concern when considering the complexity of maintaining the desired RNT of track and its relationship to track integrity and stability.

To investigate how track component stiffness and slip strength can impact longitudinal fastener force, I conducted a parametric study. Ballast and fasteners with resistance (f_0) and slip forces as presented previously (Table 6.2) were used for the control case. Additional cases included soft and stiff ballast (e.g. wet or fouled vs. frozen or dry-mud-fouled) as well as weak and strong fasteners (Table 6.3) with the same two-locomotive load conditions stated previously. The maximum fastener force was quantified for each case investigated (Figure 6.9).

Table 6.3: Parametric study’s ballast, fastener properties, and resulting track stiffness

Model Case	Description		Ballast		Fastener		Track
	Ballast	Fasteners	Slip (kip (kN))	Stiffness (kip/in. (kN/m))	Slip (kip (kN))	Stiffness (kip/in. (kN/m))	Stiffness (kip/in. (kN/m))
1	Control	Control	0.68	47	6.0	20	14
			3.025	8,230	26.7	3,500	2,450
2	Control	High-stiffness	0.68	47	6.0	160	36
			3.025	8,230	26.7	2,800	6,300
3	High-stiffness	Control	0.68	160	6.0	20	18
			3.025	28,000	26.7	3,500	3,150
4	High-stiffness	High-stiffness	0.68	160	6.0	160	80
			3.025	28,000	26.7	28,000	14,000
5	Unconsolidated	Low-toe load	0.50	47	0.5	20	14
			2.22	8,230	2.2	3,500	2,450
6	Unconsolidated	High-toe load	0.50	47	10.0	20	14
			2.22	8,230	44.5	3,500	2,450
7	Frozen/dry mud	Low-toe load	10.0	47	0.5	20	14
			44.5	8,230	2.2	3,500	2,450
8	Frozen/dry mud	High-toe load	10.0	47	10.0	20	14
			44.5	8,230	44.5	3,500	2,450

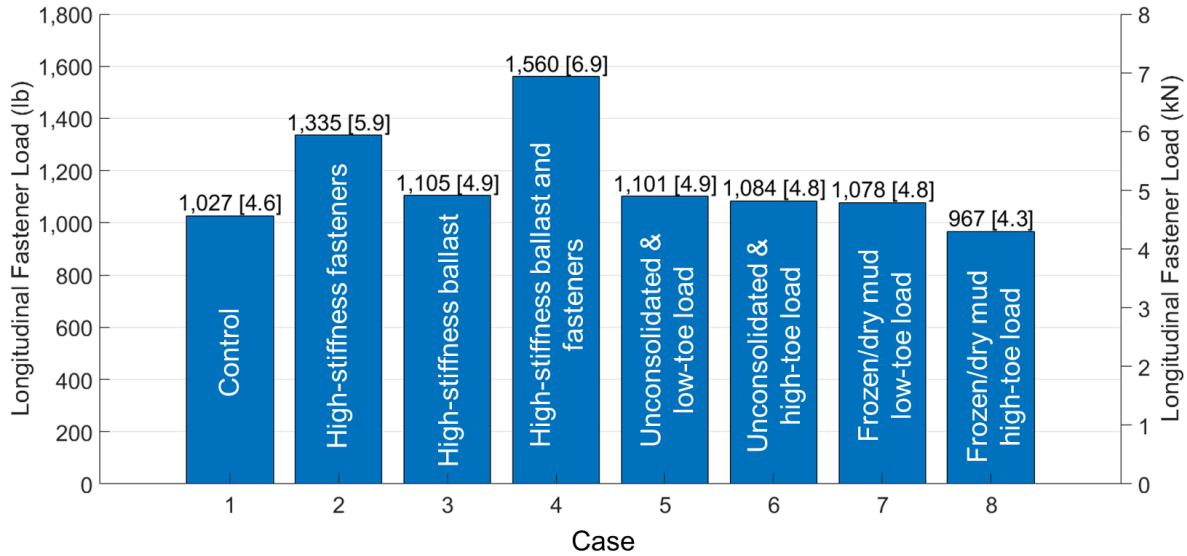


Figure 6.9: Maximum fastener force quantified by Illi3D for each case considered

For the loads considered, component stiffness affects the fastener loads more than the force at which slip occurs. With an approximately six-fold increase in track stiffness, there was a 50%

increase in fastener demand. When examining the data from Cases 1 – 4 more closely, the increase in fastener demand was found to follow a logarithmic relationship (Figure 6.10).

Therefore, if the components experienced further stiffening, the fastener load would increase at a decreasing rate.

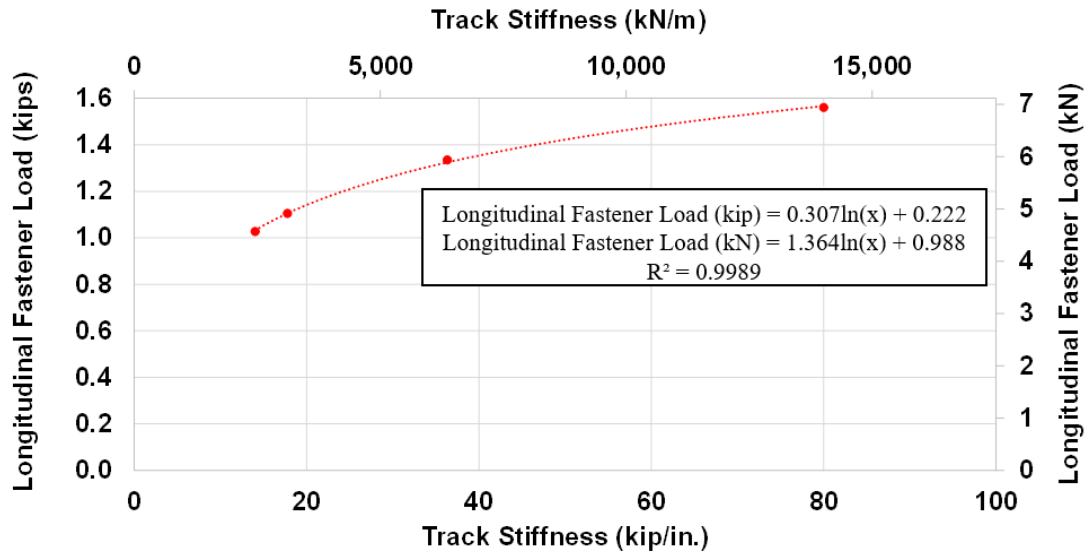


Figure 6.10: Track stiffness and longitudinal fastener load as quantified by Illi3D

One example use-case for Illi3D is the quantification of the effect of fastener type on timber crosstie track to assess the mechanics of fatigue failed spikes (Dersch et al., 2019). Historically, anchors have been used to restrain the longitudinal rail displacement in North American timber crosstie track. However, in recent decades, elastic fasteners have been used (in-lieu of the anchors) in demanding curves to provide improved rail rollover resistance. One way these fasteners are different is their longitudinal stiffness; anchors are four times less stiff than the elastic fastening system that replaced them (i.e. 16.6 kips/in. (2,907 kN/m) and 65.3 kips/in. (11,436 kN/m), respectively) (Khachaturian et al., In Review)). Keeping all other Illi3D

model input values constant, the longitudinal rail seat load increased by 24% (1.28 kips (5.69 kN) compared to 0.99 kips (4.404 kN)) when anchors were replaced with elastic fasteners. Therefore, changing a fastening system can alter the distribution of forces and increase the demand on components by a meaningful amount.

Cases 5 – 8 indicate that with the range of vertical loads considered, there is at most a 6% decrease or 7% increase in the fastener demand as the slip levels are changed within the ballast or fastening system. The reason for this minimal change is because the presence of the vertical load increases the actual load required to achieve slip. Therefore, while the track and component resistance values are critical in maintaining uniform rail stresses, the vertical load applied by a passing train will govern the component slip values in most track scenarios. Thus, to reduce the load applied to the fastening system, it would be more effective to reduce the component stiffnesses than allow for slip to occur at lower thresholds.

6.5 Conclusions

In this chapter I advance the mechanistic-empirical (M-E) track analysis and design approach presented by Edwards et al. (2021) through the development, validation, and application of a 3D non-linear parametric track model that quantifies longitudinal fastener demands. Longitudinal fastener demands are a required input for the M-E process and have largely been unknown. Additionally, longitudinal forces play a prominent role in many fastener failures and thus highlight the importance of this work given that they have not been previously quantified. Specific findings from this research are:

- Bi-linear approximations, in combination with considering the interaction between vertical loads and slip, are necessary for accurately quantifying fastener forces.

- When not accounting for vertical load, fastening system loads were 51% lower.
- There was a 7% increase in fastening system loads using the parametric model compared to the linear analysis.
- Ballast and fastener stiffness have a direct logarithmic relationship with longitudinal rail seat load.
 - Timber crosstie elastic fasteners produced a 24% increase in longitudinal rail seat load compared to anchored track.
- Changes in component resistance (slip forces) produced minimal changes in fastener demands given that vertical applied load increased the required load to produce slip.
 - With an increase in force required to slip by a factor of 20 (0.5 kips (2.22 kN) to 10 kips (44.5 kN)), there was only a minor (6% decrease to 7%) increase in the fastener demand.

7 CONCLUSIONS

The research described in this dissertation advances the concept of railway track mechanistic-empirical (M-E) analysis and design by quantifying the demands on track fastening systems and measuring their response to these demands. I conducted field experiments and developed, validated, and used analytical models (Table 7.1) that leveraged laboratory experimental data.

Table 7.1: Analytical tools developed, validated, and used throughout dissertation

Chapter	Dimensions	Methodology	Analytical Tool Description	Validation Data	Overview of Questions Investigated
3	3	FEA	Single cut-spike-in-crosstie	Laboratory instrumented spike in crosstie block	Effect of load magnitude and direction and timber grain direction on spike stress
4	2	Differential equations	Analytical method based on BOEF	Laboratory instrumented spike in crosstie block	Effect of spike cross-sectional area, applied load, and crosstie modulus on spike stress
5	3	FEA	Full rail seat with fastening system	Four laboratory instrumented spikes in a full fastening system	Effect of spike cross-sectional area, loading location, engagement with plate, and quantity, as well as plate hold-down force on spike stress
5	3	FEA	Single screw-spike-in-crosstie	Not validated	Effect of spike type on spike stress
6	3	FEA	Nonlinear parametric track model (Illi3D)	Formerly field-validated models	Effect of component and track longitudinal stiffness and strength on rail seat load magnitude

These data and methods were then used to improve the mechanistic component of M-E analysis and design of fastening systems. I also identified the root cause of spike fatigue failures that have led to at least 12 derailments. I subsequently investigated methods to reduce the occurrence of spike fatigue failures to improve safety and the state of good repair of rail infrastructure. Based on this research I am able to make a number of conclusions that I summarize in the following sections.

7.1 Conclusions

7.1.1 Chapter 2: *Quantification of Vertical, Lateral, and Longitudinal Fastener Demand in Broken-Spike Track: Inputs to Mechanistic-Empirical (ME) Design*

In this chapter I quantified vertical, lateral, and longitudinal fastening system demands in locations with failed elastic fastening system components and illustrated the impact of friction in fastening system load transfer. These data and insights into the importance of friction can be used to inform future fastening system design for demanding track locations. Additionally, this research identified the relationship between track superelevation, train operation, and failures and how these parameters affect the stress state of track components.

Revenue service field data were collected on a freight railroad mainline curve that has historically experienced broken spikes. While the magnitude of the applied vertical load was the lowest on the high rail of Track 3 (the location of the majority of failures), the failure threshold is also the lowest. This is because the high-rail was subject to lower-magnitude rail seat loads that, in-turn, reduced the frictional capacity to a level that was exceeded more often than on Track 1. The high rail of Track 3 was subjected to the highest lateral/vertical (L/V) load ratios and was an outlier in the typical lateral load reversals applied that would likely lead to a reversal in stress in the spike and thus shorter fatigue life. A summary of additional findings from this investigation include:

- The maximum vertical, lateral, and longitudinal load percentage of wheel load transferred to the fastening system was approximately 26%, 35%, and <10%, respectively.

- Underbalance operations led to a median rail seat vertical load of 2.8 kips (12.5 kN) on the high rail of Track 3 and thus the lowest lateral and longitudinal capacity of all rail seats.
 - The higher magnitude vertical loads on both rails of Track 1 and the low rail of Track 3 provide greater frictional resistance as compared to the high rail on Track 3, likely reducing the amount of load transferred into the spikes.
- Longitudinal fastener loads ranged from 1.29 to 2.40 kips (5.8 to 10.7 kN) for Track 3 and 0.84 and 1.64 kips (3.7 to 7.3 kN) for Track 1 for the nominal and 95% loads, respectively.
- Lateral fastener loads ranged from 0.11 to 2.88 kips (0.5 to 12.8 kN) for Track 3 and 1.61 and 5.97 kips (7.1 to 26.6 kN) for Track 1 for the nominal and 95% loads, respectively.
- The 95th percentile rail seat L/V ratio of 0.78 on the high rail of Track 3 is 50% higher than the 0.52 values fastening systems are subjected to during severe service testing as recommended by AREMA.
- Spike fatigue failures are caused by a combination of lateral and longitudinal loading.
 - The longitudinal load magnitudes, which are present even when vertical and lateral loads are not applied, are insufficient to independently cause fatigue failures.

To mitigate spike failures at this location, as well as similar failures in other track types (e.g. rail seat deterioration, etc.) railroads should encourage train operating speeds close to balanced speed. This increases the vertical force on the high rail of Track 3 while reducing the L/V ratios

and lateral load reversal. Finally, encouraging friction between the tie plate and crosstie is critical in reducing the forces transferred to the spike.

7.1.2 Chapter 3: 3D Finite Element Modeling of the Effect of Load Magnitude/Direction and Timber Species on Spike Stress

In this chapter I developed and validated a 3D finite element model (FEM) consisting of a single cut spike fastener and timber crosstie block. The model was validated using laboratory data and the outputs were representative of field performance, with the depth to maximum stress location consistent with broken spikes observed in the field.

Timber species affects the maximum stress magnitude and location. Consequently, use of premium fastening systems should include consideration of the effect of timber species on possible spike fatigue failure. Additionally, hardwood species differ in key characteristics, therefore, simply specifying hardwoods is insufficient for ensuring acceptable behavior. The data indicate that as the value of critical mechanical properties of the timber are increased, spike stress will decrease and the depth to maximum stress will be reduced. The use of premium fastening systems and hardwood timber collectively increase the compressive, tensile, and shear strength properties. This will delay premature failure of the timber which leads to excessive deflections and spike stresses. Additional research is needed to quantify recommended strength values, and all recommendations must be considered in light of timber sourcing and other economic considerations. Additional findings from this study include:

- When longitudinal and lateral loads are applied at equal magnitudes, the fatigue strength of the spike can be exceeded with a load of only 1,500 lb. (6.7 kN) in each direction.

- Longitudinal load had a more detrimental effect on spike stress state than lateral load.
 - To exceed the fatigue strength of the cut spike, a longitudinal load 30% lower than a lateral load (2,000 lb. (8.9 kN) vs. 2,750 lb. (12.2 kN)) is required.
- Loading direction had a significant effect on maximum stress depth.
 - When only longitudinal load was applied, the depth of maximum stress could be up to two times deeper than when lateral load only was applied.
- Timber species significantly affected the magnitude and depth of maximum stress.
 - I hypothesize that the timber mechanical properties driving this are compressive, tensile, shear, and rolling shear strengths.

7.1.3 Chapter 4: Analytical Method to Estimate Railroad Spike Fastener Stress

In this chapter I presented the development and validation of an analytical model leveraging beam on elastic foundation (BOEF) principles. The analytical model was used to accurately and economically analyze the effect of design variables (e.g. timber type and spike size) on component stresses thereby providing a useful tool to guide future M-E design of fastening systems.

This analytical method was applied to multiple case studies quantifying the effect of key variables on spike stress. Results demonstrate that the model can be used to improve fastener resiliency and railway safety through revised design recommendations. While this study only investigated unidirectional loading, the findings can be generalized to account for bi-directional loading. I found that regardless of loading direction, a decrease in modulus, decrease in spike size, or increase in load, will lead to increased spike stress. Key findings from this research and the model generated are as follows:

- As timber modulus increased from 100 to 500 ksi, the:
 - induced bending moments decreased (1.98 to 1.24 kip-in. (0.223 to 0.140 kN-m)),
 - depth to maximum stress decreased (1.2 to 0.8 in. (30.5 to 20.2 mm)), and
 - fatigue limit was not exceeded when modulus exceeded 500 ksi.

- As spike width is increased (0.500 to 0.700 in. (12.7 to 17.8 mm)), the:
 - factor of safety increases (0.8 to 1.9) at a greater rate than the induced bending moment (1.50 to 1.72 kip-in. (0.169 to 0.194 kN-m)) leading to increased resiliency,
 - fatigue limit is not exceeded when spike width exceeds 0.700 in. (17.8 mm) for this load case, and
 - depth to maximum stress does not significantly increase (1.0 to 1.2" (25.4 to 30.5 mm)).

- As loads applied perpendicular to the timber grain increase (500 to 2,500 lbs), the:
 - induced bending moments increase (0.83 to 2.48 kip-in. (0.093 to 0.280 kN-m)) and
 - depth to maximum stress increase (0.8 to 1.2" (20.2 to 30.5 mm)).

Therefore, to reduce spike stress and spike fatigue failures, railroads could ensure timber cross-ties installed with premium elastic fasteners in demanding locations have high modulus, could increase the size of spikes installed, and/or, reduce the longitudinal and lateral loads through proven methods (e.g. distributed power and gage-face lubrication). Future work could include further model refinement and validation to provide greater applicability to a wider range

of problems. Additionally, this method can be used to conduct additional case studies to further improve recommendations for spike resiliency.

7.1.4 Chapter 5: Methods to Mitigate Railway Premium Fastening System Spike Fatigue Failures Using Finite Element Analysis

In this chapter I presented the results from five FEM studies representing varying fastening system conditions that are expected to affect spike-stress magnitude. The most effective method for reducing spike stress, thereby reducing or preventing spike failures, is to develop additional frictional forces between the tie plate and crosstie. I proposed that railroads could use spring washers to develop this plate hold-down force.

Changes in spike type, cross-sectional area, quantity of spikes, and loading location have an effect on spike stress magnitude, though not as significant as the development of plate to crosstie friction. Following is a summary of the novel findings stemming from this investigation:

- There is an inverse relationship between plate-crosstie normal hold-down force and spikes stress.
 - For example, a hold-down force of 4.5 kN (1,000 lbs.) at each spike can lead to a 70% reduction in spike stress.
- The disengagement of a single spike (reduction from four to three) can lead to a 140% (2.4 times) increase in the stress experienced by a remaining spike
- There is little difference in cut and screw spike expected performance (load required to exceed fatigue limit) or strength (capacity) at longitudinal loads below 8.90 kN (2,000 lb.).

- There is an inverse linear relationship between spike cross-section and resulting stress as well as load required to exceed the endurance limit.
 - For each 1% increase in spike width there is a 2% reduction in stress.
 - For each 1% increase in spike width there is a 1.6% increase in the load required to exceed the endurance limit.

- There is an inverse linear relationship between spike contact location and resulting stress as well as load to exceed the endurance limit.
 - A +/- 6.22 mm (0.245") change in load location can lead to approximately a -/+ 20% change in maximum stress and load required to exceed the endurance limit.

These findings are consistent with recommendations originally proposed by the American Railway Engineering Association (AREA) and further developed by Kerr (2003a); fastening systems installed in demanding locations should employ fasteners whose only function is holding down the tie-plate to the crosstie and not transferring additional loads from the rail. Future fastening system designs can consider these results to mitigate spike fastener failures. Fasteners should be designed to transfer forces via friction, when possible, encourage uniform engagement of the spikes, and encourage forces to be transferred as close to the top of the crosstie as feasible. If additional capacity is required beyond what can be generated by the above mitigation methods, increasing the spike size could also be considered.

7.1.5 Chapter 6: Longitudinal Rail Seat Load Distribution: Critical Considerations

In this chapter I advanced the M-E track analysis and design approach presented by Edwards et al. (2021) through the development, validation, and application of a 3D non-linear parametric track model that quantifies the longitudinal fastener demands. Such demands are a required input for the M-E analysis and design process. Longitudinal forces play a role in many fastener failures and thus highlight the importance of this work given they had not been quantified previously. Specific findings from this research are:

- Bi-linear approximations, in combination with the interaction between vertical loads and slip, are necessary for accurately quantifying fastener forces.
 - When not accounting for vertical load, fastening system loads were 51% lower.
 - There was a 7% increase in fastening system loads using the parametric model compared to the linear analysis.
- Ballast and fastener stiffness have a direct logarithmic effect on fastener load.
 - Timber crosstie elastic fasteners produced a 24% increase in fastener load compared to anchored track.
- Changes in component resistance (slip forces) produced minimal changes in fastener demands given the vertical applied load increased the required load to produce slip.
 - There was a 6% -7% decrease in the fastener demand when the force required to have fastener slip increased by a factor of 20 (0.5 kips (2.22 kN) to 10 kips (44.5 kN)).

7.2 Future Research

The results presented in this dissertation will facilitate improved fastening system designs based on field demands and validated models and can guide future M-E analysis and design of track fasteners. However, additional questions remain, and this research could be advanced through the further development of the non-linear parametric track model that can be used to improve rail safety by reducing track-caused derailments. Analysis of FRA derailment data for Class I railroad mainline and sidings between 2006 and 2015 (Figure 7.1) showed that “Broken rails or welds” and “buckled track” derailments occur at an above average frequency and result in an above average number of cars derailed per accident (Wang et al., 2020).

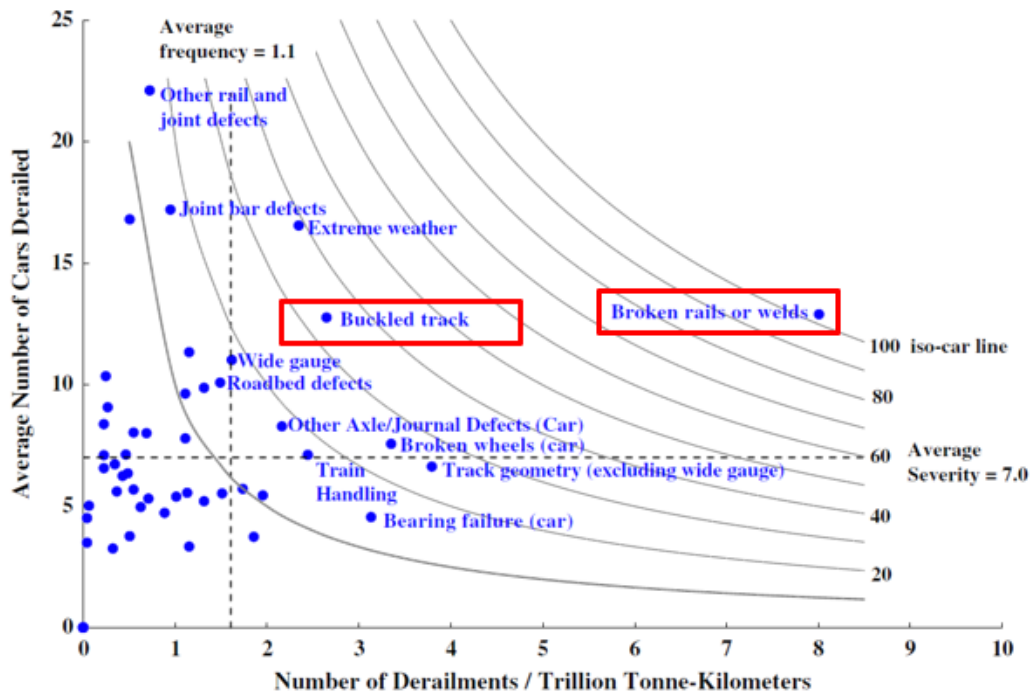


Figure 7.1: Frequency severity for mainline derailment causes on U.S. Class 1 railroads from 2006 to 2015 (Wang et al., 2020)

While there are multiple failure mechanisms causing broken rails and buckled track, improved management of longitudinal rail stress could lead to fewer track-caused derailments (Kish, 2013). Effective management of longitudinal rail stress requires knowledge of rail neutral temperature (RNT), which is defined as the temperature at which the net longitudinal force in the rail is zero (Read et al., 2005). However, RNT is difficult to quantify (Kish, 2013) and can change over time due to rail traffic and maintenance (e.g. tamping, etc.) (Harrison, 2005; Read et al., 2005; Kish, 2013). Furthermore, broken rails lead to local changes in the RNT.

If RNT is set too low or too high then the rail may buckle or pull apart, respectively, creating unsafe operating conditions. To prevent this, researchers have used data from field, laboratory, and analytical models to develop guidelines for managing RNT maintenance activities. Nonetheless, there were 24 derailments caused by buckled track between 2009 and 2018. Consequently, longitudinal stress management maintenance guidelines can be improved using this non-linear parametric track model.

Current guidelines estimate RNT before a rail break or cut based on the resulting rail gap size, and high-level factors related to the track's method of longitudinal anchorage (Kish, 2013). The model discussed in Chapter 6 can be used to predict broken rail gap-size and estimate the pre-break RNT given various ballast and fastening system conditions. This approach has been pursued by others (Kerr, 2003c; Kish, 2013), but there are opportunities for further advancement.

REFERENCES

- Ahmad, S.S.N., N.K. Mandal, G. Chattopadhyay, J. Powell and P. Micenko. 2011. Improvement of rail creep data to measure the stress state of a tangent continuously welded rail (CWR) track. In: *Proceedings of the 2011 International Heavy Haul Association Conference*, Calgary, Canada, pp. 8 pages.
- Akhtar, M.N., D.D. Davis and J.A. LoPresti. 2012. *Improving Performance of Crossties and Fasteners*. Association of American Railroads, Transportation Technology Center, Inc., TD-12-013. Pueblo, CO, USA.
- American Association of State Highway and Transportation Officials (AASHTO). 2008. *Mechanistic-Empirical Pavement Design Guide*. American Association of State Highway and Transportation Officials (AASHTO). Washington, DC, USA.
- American Railway Engineering and Maintenance-of-Way Association (AREMA). 2017a. Chapter 5, Track, In: *Manual for Railway Engineering*. The American Railway Engineering and Maintenance-of-Way Association, Landover, MD, USA.
- American Railway Engineering and Maintenance-of-Way Association (AREMA). 2017b. Chapter 30, Ties, In: *Manual for Railway Engineering*. The American Railway Engineering and Maintenance-of-Way Association, Landover, MD, USA.
- American Wood Council. 2017. *National Design Specification for Wood Construction*, 2018th ed. American Wood Council, Leesburg, VA, USA.
- Bae, H.U., J.Y. Choi, J. Moon and N.-H. Lim. 2016. Development of a probabilistic buckling analysis scheme for continuous welded rail track. *Proceedings of the Institution of Mechanical Engineers, Part F: Journal of Rail and Rapid Transit*, 230(3): 747–758 doi:10.1177/0954409714564001.
- Bastos, J.C., A. Álvarez-Reyes, M.S. Dersch, J.R. Edwards and C.P.L. Barkan. 2018. Laboratory characterization of structural capacity of North American heavy haul concrete crossties. In: *Proceedings of the 97th Annual Meeting of the Transportation Research Board of the National Academies*, Washington, DC, USA.
- Bickford, J.H. 2007. *Introduction to The Design and Behavior of Bolted Joints: Non-Gasketed Joints*, Fourth ed. CRC Press, Boca Raton, FL, USA.
- Bose, T., E. Levenberg and V. Zania. 2018. Analyzing track responses to train braking. *Proceedings of the Institution of Mechanical Engineers, Part F: Journal of Rail and Rapid Transit*, 232(7): 1984–1993 doi:10.1177/0954409718761242.
- Bowman, R. 2002. *Internal NS Report, Reduce Spike Breakage*. Roanoke, VA, USA.
- Campbell, F.C. 2008. Chapter 14. Fatigue, In: *Elements of Metallurgy and Engineering Alloys*. ASM International, Materials Park, OH, USA.

- Chen, Z. and B. Andrawes. 2017. A mechanistic model of lateral rail head deflection based on fastening system parameters. *Proceedings of the Institution of Mechanical Engineers, Part F: Journal of Rail and Rapid Transit*, 231(9): 999–1014 doi:10.1177/0954409716642485.
- Chen, Z., B. Andrawes and J.R. Edwards. 2016. Finite element modelling and field validation of prestressed concrete sleepers and fastening systems. *Structure and Infrastructure Engineering*, 12(5): 631–646 doi:10.1080/15732479.2015.1034140.
- Chen, Z., M. Shin, B. Andrawes and J.R. Edwards. 2014a. Parametric study on damage and load demand of prestressed concrete crosstie and fastening systems. *Engineering Failure Analysis*, 46: 49–61 doi:10.1016/j.engfailanal.2014.08.002.
- Chen, Z., M. Shin, S. Wei, B. Andrawes and D.A. Kuchma. 2014b. Finite element modeling and validation of the fastening systems and concrete sleepers used in North America. *Proceedings of the Institution of Mechanical Engineers, Part F: Journal of Rail and Rapid Transit*, 228(6): 590–602 doi:10.1177/0954409714529558.
- Cho, S., K.-C. Lee, S.Y. Jang, I. Lee and W. Chung. 2020. Sequential track–bridge interaction analysis of quick-hardening track on bridge considering interlayer friction. *Applied Sciences*, 10(15): 5066 doi:10.3390/app10155066.
- Choros, J., M.N. Coltman and B. Marquis. 2007. Prevention of derailments due to concrete tie rail seat deterioration. In: *Proceedings of the 2007 Joint Rail Conference and Internal Combustion Engine Division Spring Technical Conference*, American Society of Mechanical Engineers (ASME), Pueblo, CO, USA, pp. 173–181.
- Csenge, M.V., X. Lin, H. Wolf, M.S. Dersch and J.R. Edwards. 2015. Mechanistic design of concrete monoblock crossties for rail transit loading conditions. In: *Proceedings of the 2015 APTA Rail Conference*, American Public Transportation Association (APTA), Salt Lake City, UT, USA.
- Czyczula, W. and J. Solkowski. 1994. *Development of A Computer Program for CWR Track Behavior Analysis*. Technical University of Cracow. Cracow.
- Dassault Systèmes. 2014. *Abaqus Scripting User's Guide*. Dassault Systèmes. Waltham, MA, USA
- Dean, F.E. 1982. *Investigation of Rail Fastener Performance Requirements*. Federal Railroad Administration, Office of Research and Development, FRA/OR&D-82/10. Washington, DC, USA.
- Dersch, M., T. Roadcap, J.R. Edwards, Y. Qian, J.-Y. Kim and M. Trizotto. 2019. Investigation into the effect of lateral and longitudinal loads on railroad spike stress magnitude and location using finite element analysis. *Engineering Failure Analysis*, 104: 388–398 doi:10.1016/j.engfailanal.2019.06.009.

- Dersch, M.S., C. Khachaturian and J.R. Edwards. 2020a. Methods to mitigate railway premium fastening system spike fatigue failures using finite element analysis. *Engineering Failure Analysis*. DOI: 10.1016/j.engfailanal.2020.105160
- Dersch, M.S., M.T. Silva, J.R. Edwards and A. de Oliveira Lima. 2022. Analytical Nonlinear Modeling of Rail and Fastener Longitudinal Response. *Transportation Research Record: Journal of the Transportation Research Board*. DOI: 10.1177/03611981211069350
- Dersch, M.S., M. Trizotto, J.R. Edwards and A. de O. Lima. 2021. Quantification of vertical, lateral, and longitudinal fastener demand in broken spike track: Inputs to mechanistic-empirical design. *Proceedings of the Institution of Mechanical Engineers, Part F: Journal of Rail and Rapid Transit*. DOI: 10.1177/09544097211030736.
- Dersch, M.S., M. Trizotto Silva, J.R. Edwards, A. de O Lima and T. Roadcap. 2020b. Analytical method to estimate railroad spike fastener stress. *Research Record: Journal of the Transportation Research Board*, 2674(11): 11 pages. DOI: <https://doi.org/10.1177/0361198120949259>
- Deshimaru, T., S. Tamagawa and H. Kataoka. 2017. Permissible lateral force and fatigue life for rail fastening system. *Quarterly Report of RTRI*, 58(3): 236–241 doi:10.2219/rtriqr.58.3_236.
- Dick, M.G., D.S. McConnell and H.C. Iwand. 2007. Experimental measurement and finite element analysis of screw spike fatigue loads. In: *Proceedings of the 2007 Joint Rail Conference and Internal Combustion Engine Division Spring Technical Conference*, American Society of Mechanical Engineers (ASME), Pueblo, CO, USA, pp. 161–166.
- Dick, T. and C. Ruppert Jr. 2019. *Mixed Freight and Higher-Speed Passenger Trains: Framework for Superelevation Design*. Federal Railroad Administration (FRA), DOT/FRA/ORD-19/42. Washington, D.C., USA.
- Edwards, J.R. 2019. *Quantification of Prestressed Concrete Railway Crosstie Flexural Response: Implications for Mechanistic Design*. Doctoral Thesis, University of Illinois at Urbana-Champaign, Department of Civil and Environmental Engineering, Urbana, IL, USA.
- Edwards, J.R., A.E. Canga Ruiz, J.C. Bastos, Y. Liang and M.S. Dersch. 2020. Use of Field Flexural Demand Data for Reliability-Based Analysis and Design of Concrete Railroad Sleepers. *Frontiers in Built Environment*. DOI: 10.3389/fbuil.2020.582948.
- Edwards, J.R., L. Chavez, Y. Qian and A. de Oliveira Lima. 2018a. *Field Study and Analytical Modeling of The Performance of Existing WMATA Anchor Bolt System*. Washington Metropolitan Area Transit Authority, CQ17066. Washington, DC, USA.
- Edwards, J.R., A. Cook, M.S. Dersch and Y. Qian. 2018b. Quantification of rail transit wheel loads and development of improved dynamic and impact loading factors for design. *Proceedings of the Institution of Mechanical Engineers, Part F: Journal of Rail and Rapid Transit*, 232(10): 2406–2417 doi:10.1177/0954409718770924.

- Edwards, J.R., M.S. Dersch and R.G. Kernes. 2017a. *Improved Concrete Crosstie and Fastening Systems for US High Speed Passenger Rail and Joint Corridors – Project Summary Report (Volume 1)*. US Department of Transportation, Federal Railroad Administration, DOT/FRA/ORD-17/23. Washington, DC, USA.
- Edwards, J.R., M.S. Dersch and R.G. Kernes. 2017b. *Improved Concrete Crosstie and Fastening Systems for US High Speed Passenger Rail and Joint Corridors – Technical Report (Volume 2)*. US Department of Transportation, Federal Railroad Administration, DOT/FRA/ORD-17/23. Washington, DC, USA.
- Edwards, J.R., Z. Gao, H.E. Wolf, M.S. Dersch and Y. Qian. 2017c. Quantification of concrete railway sleeper bending moments using surface strain gauges. *Measurement - Journal of the International Measurement Confederation*, 111: 197–207.
- Edwards, J.R., R.J. Quirós-Orozco, J.C. Bastos, M.S. Dersch and E. Tutumluer. 2021. A vision for mechanistic-empirical railway track system and component analysis and design. *Transportation Research Record: Journal of the Transportation Research Board*: 20.
- Eisenmann, J. 1970. Stress distribution in the permanent way due to heavy axle loads and high speeds. In: *Proceedings of the 69th Annual Convention of The American Railway Engineering Association (AREA)*, AREA, Chicago, IL, USA, pp. 24–59.
- El-Sibaie, M. and G. Anderson. 1994. *Measurement of Rail Forces and Displacements Under AC-Traction And DC-Traction Locomotives*. Association of American Railroads, Chicago Technical Center, R-869. Chicago, IL, USA.
- ERRI, D.C. 1997. *Improved Knowledge Of Forces In CWR Track (Including Switches)*. European Rail Research Institute (ERRI), D202.
- European Committee for Standardization. 2002. Railway applications - Track - Performance requirements for fastening systems - Part 2: Fastening systems for concrete sleepers, In: *Norme Européenne*. European Committee for Standardization (CEN), Brussels, Belgium.
- Federal Highway Administration. 2006. Chapter 8, Analyses of the Lateral Load Tests at the Route 351 Bridge, In: *A Laboratory and Field Study of Composite Piles for Bridge Substructures*. US Department of Transportation, Federal Highway Administration, Charlottesville, VA.
- Federal Railroad Administration. 2016. *Derailment of Union Pacific's Unit Crude Oil Train ONETU 02 Transporting Bakken Crude Oil for U.S. Oil Mosier, Oregon*. US Department of Transportation, Federal Railroad Administration. Washington, DC, USA.
- Federal Railroad Administration (FRA). 2011. Part 213 - Track Safety Standards, In: *Title 49 of the Code of Federal Regulations*. US Department of Transportation, Federal Railroad Administration, Washington, DC, USA.

- Forest Products Laboratory. 2010. *Wood Handbook, Wood as An Engineering Material*, Centennial Edition ed. United States Department of Agriculture, Forest Service, Madison, WI.
- Gao, Y. and J. LoPresti. 2020. *Interim Report Broken Spike Remediation*. Transportation Technology Center, Inc., TD-20-004. Pueblo, CO, USA.
- Gao, Y., M. McHenry and B. Kerchof. 2018. Investigation of broken cut spikes on elastic fastener tie plates using an integrated simulation method. In: *Proceedings of the 2018 Joint Rail Conference*, Pittsburgh, PA, USA.
- Green, D.W., J.E. Winandy and D.E. Kretschmann. 1999. *Mechanical Properties of Wood*. USDA Forest Service, Forest Products Laboratory, Wood handbook: Wood as an Engineering Material, GTR-113. Madison, WI.
- Greve, M.J., M.S. Dersch, J.R. Edwards, C.P. Barkan, J. Mediavilla and B. Wilson. 2016. Effect of particle intrusion on rail seat load distributions on heavy haul freight railroads. *International Journal of Rail Transportation*, 4(2): 98–112
doi:10.1080/23248378.2016.1157048.
- Grondin, G., P. Eng and M. Jin. 2008. *Slip Critical Bolted Connections - A Reliability Analysis for Design at The Ultimate Limit State*. University of Alberta, The American Institute of Steel Construction. Edmonton, Canada.
- Gurfinkel, G. 1981. *Wood Engineering*, Second ed. Kendall/Hunt Publishing Company, Dubuque, IA, USA.
- Harrison, H. 2005. Managing the Longitudinal Forces in Heavy Haul Track. In: *International Heavy Haul Association*, Brazil, 6 pages.
- Harrison, H., A. Sluz and D. Clark. 1999. Monitoring CWR longitudinal force behavior using remote sensing technology. In: *International Conference on Innovations in The Design & Assessment of Railway Track*, Delft, Netherlands.
- Hasan, N. 2015. Railroad tie spacing related to wheel-load distribution and ballast pressure. *Practice Periodical on Structural Design and Construction*, 20(4): 04014047
doi:10.1061/(ASCE)SC.1943-5576.0000243.
- Hay, W.W. 1982. *Railroad Engineering*, Second ed. John Wiley & Sons, New York, NY, USA.
- Hetenyi, M. 1946. *Beams on Elastic Foundation; Theory with Applications in The Fields of Civil and Mechanical Engineering*. The University of Michigan Press, Ann Arbor, MI, USA.
- Holder, B.G., Y. Qian, M.S. Dersch and J.R. Edwards. 2017a. Lateral load performance of concrete sleeper fastening systems under non-ideal conditions. In: *Proceedings of the 11th International Heavy Haul Association Conference*, Cape Town, South Africa.

- Holder, D.E., M.V. Csenge, Y. Qian, M.S. Dersch, J.R. Edwards and B.J. Van Dyk. 2017b. Laboratory investigation of the SKL-style fastening system's lateral load performance under heavy haul freight railroad loads. *Engineering Structures*, 139(2017): 71–80 doi:10.1016/j.engstruct.2017.02.039.
- Icke, P. and G. Paice. 2014. Track-structure interaction analysis using FE modelling techniques. In: *Proceedings of The International Conference on Road and Rail Infrastructure CETRA*, University of Zagreb, Spilt Dalmatia, Croatia, 8 pages.
- Kaewunruen, S., E. Kahawatta Gamage and A.M. Remennikov. 2016. Modelling railway prestressed concrete sleepers (cross ties) with holes and web openings. *Procedia Engineering*, (161): 1240–1246 doi:10.1016/j.proeng.2016.08.556.
- Kerchof, B. 2017. A derailment investigation and broken spikes. In: *Proceedings Of 2017 Wheel Rail Interaction Heavy Haul Seminar*, Chicago, IL, USA.
- Kerchof, B. and H. Wu. 2014. Controlling Rail Cant and Lateral Forces by Managing the Wheel/Rail Interface. In: *Proceedings of 2014 Wheel Rail Interaction Heavy Haul Seminar*, Chicago, IL, USA.
- Kernes, R.G. 2013. *The Mechanics of Abrasion on Concrete Crosstie Rail Seats*. Master's Thesis, University of Illinois at Urbana-Champaign, Department of Civil and Environmental Engineering, Urbana, IL, USA.
- Kernes, R.G., A.A. Shurpali, J.R. Edwards, M.S. Dersch, D.A. Lange and C.P.L. Barkan. 2014. Investigation of the mechanics of rail seat deterioration and methods to improve the abrasion resistance of concrete sleeper rail seats. *Proceedings of the Institution of Mechanical Engineers, Part F: Journal of Rail and Rapid Transit*, 228(6): 581–589.
- Kerokoski, O. 2010. Determination of longitudinal and transverse railway track resistance. In: *2010 Joint Rail Conference, Volume 1*, ASMEDC, Urbana, Illinois, USA, pp. 157–165.
- Kerr, A.D. 2003a. III. The Evolution of Track Components, In: *Fundamentals of Railway Track Engineering*. Simmons Boardman, Omaha, NE, USA. pp.25–84.
- Kerr, A.D. 2003b. IV. Response of Track to Wheel Loads, In: *Fundamentals of Railway Track Engineering*. Simmons Boardman, Omaha, NE, USA. pp.84–134.
- Kerr, A.D. 2003c. VII. The Axial Forces in Rails, Track Buckling, and Pull-Aparts, In: *Fundamentals of Railway Track Engineering*. Simmons Boardman, Omaha, NE, USA. pp.209–249.
- Kerr, A.D. 2003d. X. Miscellaneous Track Problems and Analyses, In: *Fundamentals of Railway Track Engineering*. Simmons Boardman, Omaha, NE, USA. pp.318–336.
- Khachaturian, C., M.S. Dersch, J.R. Edwards and M. Trizotto Silva. 2022. Quantification of longitudinal fastener stiffness and the effect of fastening system loading demand.

Accepted. *Proceedings of the Institution of Mechanical Engineers, Part F: Journal of Rail and Rapid Transit*

- Khachaturian, C., M.S. Dersch, S. Liu and J.R. Edwards. in review. Effect of engineered composite sleeper compressive strength and modulus of elasticity on spike stress: a finite element investigation. *Proceedings of the Institution of Mechanical Engineers, Part F: Journal of Rail and Rapid Transit*
- Kish, A. 2011. On the fundamentals of track lateral resistance. In: *American Railway Engineering and Maintenance-of-Way-Association Annual Conference*, Minneapolis, MN, USA. 45 pages.
- Kish, A. 2013. Best practice guidelines for CWR neutral temperature management. In: *Proceedings of The American Railway Engineering and Maintenance-Of-Way Association Annual Conference*, AREMA, Indianapolis, IN, USA, pp. 1004–1028.
- Kish, A. and G. Samavedam. 1987. Longitudinal Force Measurement in Continuous Welded Rail from Beam Column Deflection Response. American Railway Engineering Association (AREA), Washington, D.C., USA, pp. 280–301.
- Lima, A. de O., J.R. Edwards, L.W. Chavez Quiroz, Y. Qian and M.S. Dersch. 2021. Load and response quantification of direct fixation fastening systems for heavy rail transit infrastructure. *Proceedings of the Institution of Mechanical Engineers, Part F: Journal of Rail and Rapid Transit*. DOI: 10.1177/0954409720987036.
- Lin, X., J.R. Edwards, M.S. Dersch, T.A. Roadcap and C. Ruppert. 2018. Load quantification of the wheel–rail interface of rail vehicles for the infrastructure of light rail, heavy rail, and commuter rail transit. *Proceedings of the Institution of Mechanical Engineers, Part F: Journal of Rail and Rapid Transit*, 232(2): 596–605 doi:10.1177/0954409716684266.
- Lombard, P. and L. Wildenboer. 1981. Concrete Sleepers and Fastenings on the South African Railways. *Die Siviele Ingenieur in Suid-Afrika*.
- Long, J. 2011. Lateral Load-Displacement Behavior for Single and Group Piles, In: *Analysis and Design of Deep Foundations*. University of Illinois, Urbana, IL, USA.
- LoPresti, J. 2018. Accelerated service testing of new and improved track components.
- Marquis, B., S. Liu and C. Stuart. 2020. Longitudinal rail load distribution: an analytical solution. In: *Proceedings Of The 2020 Joint Rail Conference*, American Society of Mechanical Engineers, St. Louis, MO, USA, pp. V001T08A010.
- Matias, S.R. and P.A. Ferreira. 2020. Railway slab track systems: review and research potentials. *Structure and Infrastructure Engineering*, 16(12): 1635–1653 doi:10.1080/15732479.2020.1719167.
- Matlock, H. 1970. Correlations for design of laterally loaded piles in soft clay. In: *2nd Annual Offshore Technology Conference Proceedings*, Houston, TX, USA.

- McHenry, M. and A. Klopp. 2017. Tie and fastener system loading environment simulation using NUCARS® multibody dynamic vehicle-track model. In: *Proceedings of the 25th International Symposium on Dynamics of Vehicles on Roads and Tracks*, Taylor & Francis Group, Rockhampton, Queensland, Australia, pp. 855–860.
- McHenry, M. and J. LoPresti. 2015. *Tie and Fastener System Gage Restraint Performance At FAST*. Association of American Railroads, Transportation Technology Center, Inc., TD-15-013. Pueblo, CO, USA.
- McHenry, M. and J. LoPresti. 2016. Field evaluation of sleeper and fastener designs for freight operations. In: *Proceedings of the 11th World Congress on Railway Research*, Milan, Italy.
- Norton, R. 2006. *Machine Design - An Integrated Approach*, Third ed. Prentice Hall, Upper Saddle River, NJ, USA.
- Otter, D.E., J.A. LoPresti and R.A. Sweeney. 2001. Longitudinal forces in bridges due to heavy haul freight operations. In: *Proceedings of the 7th International Heavy Haul Association Conference*, Brisbane, Australia, 4 pages.
- Quirós-Orozco, R.J. 2018. *Prestressed Concrete Railway Crosstie Support Variability and Its Effect on Flexural Demand*. Master's Thesis, University of Illinois at Urbana-Champaign, Department of Civil and Environmental Engineering, Urbana, IL, USA.
- Quirós-Orozco, R.J., J.R. Edwards, Y. Qian and M.S. Dersch. 2018. Quantification of loading environment and flexural demand of prestressed concrete crossties under shared corridor operating conditions. *Transportation Research Record: Journal of the Transportation Research Board*, 2672(10): 136–145 doi:10.1177/0361198118793500.
- Rakoczy, A.M., X. Shu, D.D. Davis and D. Li. 2016. Heavy point frog performance under passenger vehicles. In: *The Dynamics of Vehicles on Roads and Tracks*, Taylor & Francis Group, pp. 1329–1336.
- Read, D.M., A. Kish and J. LoPresti. 2005. Management of rail Longitudinal forces under heavy axle loads. In: *8th International Heavy Haul Association Conference*, pp. 659–665.
- Rhodes, D., J.S. Maree and P. Barthram. 2005. Track design for extreme traction and braking forces. In: *Proceedings of the 8th International Heavy Haul Association Conference*, Rio de Janeiro, Brazil.
- Roadcap, T., M. Dersch and J.R. Edwards. 2019a. Load environment and force transfer in railway fastening systems: A case study of the broken spike mystery. In: *Proceedings of the 2019 World Congress on Railway Research*, Tokyo, Japan.
- Roadcap, T., M.S. Dersch and J.R. Edwards. in review. *Mechanistic Investigation of Timber Crosstie Spike Fastener Failures – Phase I: The Magnitude of the Spike Failure Challenge*. US Department of Transportation, Federal Railroad Administration, DOT/FRA/ORD-xx/xx. Washington, DC, USA.

- Roadcap, T., B. Kerchof, M.S. Dersch, M. Trizotto and J.R. Edwards. 2019b. Field experience and academic inquiry to understand mechanisms of spike and screw failures in railroad fastening systems. In: *Proceedings of the 2019 AREMA Annual Conference with Railway Interchange*, AREMA, Minneapolis, MN.
- Sadeghi, J. and P. Barati. 2010. Evaluation of conventional methods in analysis and design of railway track system. *IJCE International Journal of Civil Engineers*, 8(1): 44–56.
- Samavedam, G., J. Gomes, A. Kish and A. Sluz. 1997. *Investigation on CWR Longitudinal Restraint Behavior in Winter Rail Break and Summer Destressing Operations*. US Department of Transportation. Washington, DC, USA.
- Sandhaas, C. 2011. *3D Material Model for Wood, Based on Continuum Damage Mechanics User Subroutine UMAT*. TU Delft, Stevin laboratory, 6-11–4. Delft, Netherlands.
- Sandhaas, C. 2012. *Mechanical Behaviour Of Timber Joints with Slotted-In Steel Plates*. Doctoral Thesis, Delft University of Technology, Delft, Netherlands.
- Shenton III, H.W. 1997. Analysis of crosstie track in lateral plane using new track equations. *American Society of Civil Engineers Journal of Transportation Engineering*, 123(3): 202–208 doi:10.1061/(ASCE)0733-947X(1997)123:3(202).
- Shurpali, A.A., J.R. Edwards, R.G. Kernes, D.A. Lange and C.P. Barkan. 2017. Improving the abrasion resistance of concrete to mitigate concrete crosstie rail seat deterioration (RSD). *American Society of Testing Materials International Materials Performance and Characterization*, 6(1): 521–534 doi:10.1520/MPC20170051.
- Talbot, A.N. 1918. Progress report of the special committee on stresses in track. In: *Proceedings of The American Railway Engineering Association (AREA)*, American Railway Engineering Association (AREA), Washington, DC, USA, pp. 875–1058.
- Transportation Safety Board of Canada (TSB). 2012. *Railway Investigation Report: Main Track Derailment*. Transportation Safety Board of Canada, R12E0008. Fabyan, Alberta, Canada.
- Trizotto, M., M.S. Dersch, J.R. Edwards and A. de O. Lima. 2021. Analytical elastic modelling of rail and fastener longitudinal response. *Transportation Research Record: Journal of the Transportation Research Board*. DOI: 10.1177/0361198120985848
- Tutten III, J. and L.E. Daniels. 2005. *Direct-Fixation Track Design, Part B - Final Research Report*. Transportation Research Board, Washington, D.C.
- Van Dyk, B.J. 2014. *Characterization of The Loading Environment for Shared-Use Railway Superstructure in North America*. Master's Thesis, University of Illinois at Urbana-Champaign, Department of Civil and Environmental Engineering, Urbana, IL, USA.
- Van Dyk, B.J., M.S. Dersch, J.R. Edwards, C. Ruppert Jr and C. Barkan. 2014. Load characterization techniques and overview of loading environment in North America.

- Transportation Research Record: Journal of the Transportation Research Board*, 2448: 80–86 doi:10.3141/2448-10.
- Van Dyk, B.J., J.R. Edwards, M.S. Dersch, C.J. Ruppert and C.P. Barkan. 2017. Evaluation of dynamic and impact wheel load factors and their application in design processes. *Proceedings of the Institution of Mechanical Engineers, Part F: Journal of Rail and Rapid Transit*, 231(1): 33–43.
- Van Dyk, B.J., J.R. Edwards, C.J. Ruppert Jr and C.P. Barkan. 2013. Considerations for mechanistic design of concrete sleepers and elastic fastening systems in North America. In: *Proceedings of the 10th International Heavy Haul Association Conference*, New Delhi, India.
- Van Dyk, B.J., A.J. Scheppe, J.R. Edwards, M.S. Dersch and C.P.L. Barkan. 2016. Methods for quantifying rail seat loads and a review of previous experimentation. *Proceedings of the Institution of Mechanical Engineers, Part F: Journal of Rail and Rapid Transit*, 230(3): 935–945.
- Van, M.A. 1997. *Stability of Continuous Welded Rail Track*. Doctoral Thesis, Technische Universiteit Delft, Delft, Netherlands.
- Wang, B.Z., C.P. Barkan and M. Rapik Saat. 2020. Quantitative analysis of changes in freight train derailment causes and rates. *Journal of Transportation Engineering, Part A: Systems*, 146(11): 04020127 doi:10.1061/JTEPBS.0000453.
- Webb, D.A., G.V. Webb, J.C. Gauntt, S. Smith and D.T. Connors. 2016. *The Tie Guide*. The Railway Tie Association (RTA), Fayetteville, GA, USA.
- Williams, B.A., D. Holder, J.R. Edwards, M.S. Dersch and C.P. Barkan. 2016. Quantification of the lateral forces in concrete sleeper fastening systems. *Proceedings of the Institution of Mechanical Engineers, Part F: Journal of Rail and Rapid Transit*, 230(7): 1714–1721 doi:10.1177/0954409715616997.
- Winkler, E. 1867. *Theory of Elasticity and Strength*. Dominicus, Prague.
- Wolf, G.P. 2014. Effects of wide gauge on derailment potential. In: *Proceedings Of 2014 Wheel Rail Interaction Heavy Haul Seminar*, Chicago, IL, USA. 4 pages.
- Wu, H. and B. Kerchof. 2014. Management of wheel/rail interface to prevent rail rollover derailments. *Proceedings of the Institution of Mechanical Engineers, Part F: Journal of Rail and Rapid Transit*, 228(6): 673–686 doi:10.1177/0954409714522222.
- Yu, H. and S. Liu. 2019. Finite element analysis of spike failure in elastic fastening systems for wood Ties. American Society of Mechanical Engineers Digital Collection.
- Zeman, J.C. 2010. *Hydraulic Mechanisms of Concrete-Tie Rail Seat Deterioration*. MS Thesis, University of Illinois at Urbana-Champaign, Department of Civil and Environmental Engineering, Urbana, IL, USA.

- Zeman, J.C., J.R. Edwards, D.A. Lange and C.P.L. Barkan. 2012. Hydraulic pressure cracking in rail seats of concrete crossties. *American Concrete Institute (ACI) Materials Journal*, 109(6): 639–646.
- Zhu, K., J.R. Edwards, Y. Qian and B. Andrawes. 2016. Finite element analysis of the effects of bolt condition on bolted rail joint stresses. *Transportation Research Record: Journal of the Transportation Research Board*, 2545: 36–45 doi:10.3141/2545-05.
- Zhu, K., Y. Qian, J.R. Edwards and B.O. Andrawes. 2017. Finite element analysis of rail-end bolt hole and fillet stress on bolted rail joints. *Transportation Research Record: Journal of the Transportation Research Board*, 2607: 33–42 doi:10.3141/2607-06.
- Zimmermann, H. 1941. *Die Berechnung Des Eisenbahnoberbaues (The Analysis of Railway Tracks)*, Third ed. Verlag W. Ernst & Sohn, Berlin, Germany.